Max Planck Graduate Center
mit der Johannes Gutenberg-Universität Mainz

MAX-PLANCK-GESELLSCHAFT

JG|U UNIVERSITÄTSmedizin. MAINZ

Surface-Functionalized Nanomaterials for a Drug-Delivery System in Cancer Immunotherapy

Dissertation

zur Erlangung des akademischen Grades eines

“Doctor rerum naturalium” (Dr. rer. nat.) der Fachbereiche:

Physik, Mathematik und Informatik,

Chemie, Pharmazie und Geowissenschaften,

Biologie und der Universitätsmedizin

vorgelegt von

Stefanie Ulrike Frick

Mainz, Juni 2014

Tag der mündlichen Prüfung:

Dekan:

1. Berichterstatter:
2. Berichterstatter:

Die vorliegende Dissertation wurde an der Hautklinik der Universitätsmedizin der Johannes Gutenberg-Universität in Mainz unter der Betreuung von [redacted] und am Max-Planck-Institut für Polymerforschung in Mainz unter der Betreuung von [redacted] in der Zeit vom Dezember 2010 bis Juni 2014 angefertigt.

Ich versichere, dass ich die vorliegende Dissertation selbstständig und ohne Benutzung anderer als der angegebenen Quellen und Hilfsmittel angefertigt habe.

Mainz, Juni 2014

I hereby declare that I wrote the dissertation submitted without any unauthorized external assistance and used only sources acknowledged in the work. All textual passages which are appropriated verbatim or paraphrased from published and unpublished texts as well as all information obtained from oral sources are duly indicated and listed in accordance with bibliographical rules. In carrying out this research, I complied with the rules of standard scientific practice as formulated in the statutes of Johannes Gutenberg-University Mainz to insure standard scientific practice.

Mainz, June 2014

Danksagung

Meiner Familie

Table of Content

List of Figures

List of Tables

Abstract

In cancer therapy there is a vast demand on novel cell type-specific drug delivery systems. High tunable engineered nanomaterials bear many characteristics that make them attractive as a drug carrier for improved immunotherapy. This thesis aims to disclose the biological interaction with as well as the uptake by primary human immune cells of chemically modified polystyrene nanoparticles and biologically functionalized hydroxyethyl starch nanocapsules.

In a first approach, polystyrene nanoparticles were studied as a model system for investigating the influence of chemical surface modifications on the uptake of nanoparticles by human dendritic cells and their immunogenicity. Fluorescently labeled sulfonate- and phosphonate-functionalized polystyrene nanoparticles were found to be taken up by human monocyte-derived immature and mature dendritic cells as measured by flow cytometry. Confocal laser scanning microscopy ascertained the intracellular nanoparticle uptake. The nanoparticle influence on dendritic cell maturation was addressed by the use of human immature monocyte-derived dendritic cells that can differentiate into mature dendritic cells upon activation. Both nanoparticles induced enhanced maturation of immature dendritic cells as depicted by upregulation of dendritic cell maturation markers as well as co-stimulatory molecules accompanied with elevated amounts of cytokines associated with dendritic cell activation compared to untreated dendritic cells. Sulfonate- as well as phosphonate-functionalized nanoparticles increased the T cell stimulatory potential of immature dendritic cells indicating a T helper type 1 cell response.

In a second approach, biodegradable hydroxyethyl starch nanocapsules were surface-functionalized with the cytokine IL-2 and their interaction with and uptake by IL-2 receptor-bearing T cells was assessed. The biological functionality of IL-2 linked to the capsule surface was confirmed on IL-2-dependent growing murine CTLL-2 cells. In order to investigate the uptake of IL-2-functionalized nanocapsules, primary human $CD4^+$ T cells were isolated from peripheral blood and activated for increased CD25 expression, which represents the IL-2 receptor alpha subunit and is decisive for internalization of the high affinity IL-2 receptor. IL-2-functionalized hydroxyethyl starch nanocapsules showed a significant uptake by $CD4^+CD25^{high}$ T cells compared to control capsules. Along capsule uptake IL-2-induced proliferation of $CD4^+CD25^{high}$ T cells was assessed with a proliferation dye by flow cytometry. In order to analyze the impact of different amounts of IL-2 linked to the nanocapsules, hydroxyethyl starch nanocapsules were surface-functionalized with half the amount of IL-2. Reduced amounts of IL-2 resulted in diminished $CD4^+CD25^{high}$ T cell proliferation and impaired uptake efficiency by $CD4^+CD25^{high}$ T cells. Moreover, IL-2-

functionalized hydroxyethyl starch nanocapsules were intravenously injected in mice and their biodistribution in spleen, liver and lymph nodes was measured. Elevated levels of nanocapsule-positive $CD4^+CD25^+$ T cells isolated from the lymph nodes were detected compared to control mice.

In summary, in this study polystyrene nanoparticles were analyzed for their chemical surface modification, whereas hydroxyethyl starch nanocapsules were even ligand-functionalized for a cell type-specific uptake. Studying IL-2-functionalized hydroxyethyl starch nanocapsules revealed a cell type-specific uptake by $CD4^+CD25^{high}$ T cells. This study provides substantial findings for the future development of IL-2-functionalized nanocapsules as a drug delivery system for $CD4^+CD25^{high}$ T cells in cancer immunotherapy.

Zusammenfassung

Zell-spezifische Tumortherapien für eine gezielte Verabreichung von Therapeutika rücken immer mehr in den Fokus intensiver Forschung. Dabei sind Polymer-basierte Nanopartikel, deren physikochemischen Eigenschaften leicht modifiziert werden können, von großem Interesse. In der vorliegenden Arbeit wurden die Interaktion und die Aufnahme chemisch modifizierter Polystyrolpartikel und biologisch funktionalisierter Hydroxyethylstärkekapseln analysiert.

In einem ersten Ansatz wurden Polystyrolpartikel als Modellsystem genutzt, um den Einfluss chemischer Oberflächenmodifikationen auf die Aufnahme in humane dendritische Zellen und deren immunmodulatorischen Eigenschaften zu untersuchen. Anhand durchflusszytometrischer Untersuchungen konnte die Aufnahme fluoreszenzmarkierter Sulfonat- und Phosphonat-funktionalisierter Polystyrolpartikel in humane dendritische Zellen gezeigt werden. Die intrazelluläre Aufnahme wurde mit Hilfe konfokaler Mikroskopie bestätigt. Unreife dendritische Zellen differenzieren durch Aktivierung zu reifen dendritischen Zellen. Ausgehend davon wurde der Einfluss der Nanopartikel auf die Reifung humaner dendritischer Zellen mittels Durchflusszytometrie erforscht. Sowohl Sulfonat- als auch Phosphonat-funktionalisierte Polystyrolpartikel induzierten eine Reifung unreifer dendritischer Zellen, die anhand einer erhöhten Expression von Oberflächenmolekülen, welche bei der Reifung und Stimulation dendritischer Zellen beteiligt sind, gemessen wurde. Außerdem zeigte sich in einer Kokultur mit allogenetischen T-Zellen, dass beide chemisch modifizierten Polystyrolpartikel eine erhöhte T-Zell-Stimulierung durch Nanopartikel-beladene dendritische Zellen hervorrufen, die auf eine Th1-Aktivierung hinweist.

In einem zweiten Ansatz wurde auf die Interaktion und die Aufnahme von bioabbaubaren Hydroxyethylstärkekapseln, die mit dem Zytokin IL-2 funktionalisiert wurden, durch IL-2-Rezeptor-tragende T-Zellen fokussiert. Die biologische Aktivität der IL-2-Kapseln wurde durch die Proliferation IL-2-abhängiger CTLL-2-Zellen bestätigt. Aufnahmestudien wurden mit primären humanen $CD4^+$-T-Zellen durchgeführt, die zuvor für eine erhöhte CD25-Expression aktiviert wurden. CD25 bildet die alpha-Untereinheit des IL-2-Rezeptors und ist für die Bildung des hochaffinen IL-2-Rezeptors essentiell. IL-2-funktionalisierte Hydroxyethylstärkekapseln zeigten eine signifikant erhöhte Aufnahme durch $CD4^+CD25^{high}$-T-Zellen im Vergleich zu nicht funktionalisierten Hydroxyethylstärkekapseln. Neben der Aufnahme wurde mittels Durchflusszytometrie eine verstärke Proliferation von $CD4^+CD25^{high}$-T-Zellen durch IL-2-funktionalisierte Stärkekapseln gemessen. Um die Wirkung unterschiedlicher Mengen des gebundenen IL-2 auf der Kapseloberfläche zu analysieren,

wurden weitere Hydroxyethylstärkekapseln, die mit der halben Menge an IL-2 auf der Oberfläche funktionalisiert wurden, untersucht und miteinander verglichen. Geringere Mengen an IL-2 auf der Kapseloberfläche deuteten eine reduzierte Aufnahme der Kapseln durch $CD4^{+}CD25^{high}$-T-Zellen an. IL-2-funktionalisierte Kapseln wurden weiterhin intravenös in Mäuse injiziert, um deren Verteilung in Milz, Leber und Lymphknoten zu untersuchen. Aus den Lymphknoten isolierte $CD4^{+}CD25^{+}$-T-Zellen zeigten eine verstärkte Assoziation mit IL-2-funktionalisierten Hydroxyethylstärkekapseln.

Insgesamt wurde in der vorliegenden Arbeit die Aufnahme in sowie die immunmodulatorischen Eigenschaften von Sulfonat- und Phosphonat-modifizierten Polystyrolpartikeln auf humane dendritische Zellen untersucht. Im Gegensatz zu den Polystyrolpartikeln wurden die Hydroxyethylstärkekapseln direkt mit einem biologischen Liganden für eine zell-spezifische Aufnahme modifiziert. Untersuchungen der IL-2-funktionalisierten Kapseln zeigten eine zell-spezifische Aufnahme und T-Zellproliferation. Diese Untersuchung trägt substantiell zur Weiterentwicklung von IL-2-funktionalisierten Kapseln für die gezielte Verabreichung von Therapeutika in $CD4^{+}CD25^{+}$-T-Zellen bei.

1 Introduction

The fundamental motivation of Paul Ehrlich – the founder of chemotherapy – was the postulation of chemical targeting ("Wir müssen chemisch zielen lernen.").[1] Based on his findings of specific receptors for antigens, Ehrlich constituted his "bullet concept" about drugs that directly interact with their desired target structure in or on a cell.[1] Although, the rational of improved cancer therapy came up in the early 20th century, cancer is still one of the most common causes of death in developed countries. This may especially be related to the fact that cancer is a very complex and heterogeneous disease.

Hanahan and Weinberg published six clear hallmarks of cancer, including sustained proliferative signaling, evading growth suppressors, resisting cell death, enabling replicative immortality, inducing angiogenesis and activating invasion and metastasis, all of them promoting sustained tumor progression.[2] Very early it became evident that two further hallmarks, deregulating cellular energetics and avoiding immune destruction, are appreciably essential for tumor formation and progression.[3] The ability of tumor cells to escape immunosurveillance and the tumor-promoting role of the immune system are the main obstacles why current immunotherapeutic approaches fail.[4] The two faces of the immune system in tumor immunity comprise cancer immunosurveillance and immune tolerance that are defined together as "cancer immunoediting".[4] Within the "three Es of cancer immunoediting", cancer cells are "eliminated" by the host immune system, followed by an "equilibrium" phase in which tumor cells are destroyed, but the tumor is not fully eliminated, and an "escape" phase during which mutated or altered tumor cells escape an immune attack.[4,5]

In addition, tumor microenvironments containing a high infiltrate of immune cells can largely vary between different tumor types but also patients with the same tumor burden can show tremendous heterogeneity.[6] The awareness of these facts paved the way towards personalized medicine.

1.1 Immune System

Immunity describes the feasibility of a host to protect itself against foreign microbes, including bacteria, fungi and viruses, that would harm the host and may cause diseases.[7] In general, the immune system can be classified into germline-encoded "innate immunity" and acquired antigen-specific "adaptive immunity". The interaction between innate and adaptive immunity is decisive for a host immune response.[7] Innate immunity is an immediate antigen-non-specific response against microbes and comprises humoral barriers (e.g. complement

system, inflammation) and cellular barriers (e.g. phagocytic cells, natural killer (NK) cells) for immediate host protection.[7-9] In contrast, adaptive immunity shows a slower response, but it generates a targeted and fierce response to pathogens with long-lived immunological memory, allowing for a rapid immune response after re-exposure of a specific antigen.[7] Professional antigen-presenting cells (APCs), so-called dendritic cells (DCs), constitute a connective bridge between innate and adaptive immunity.[7,10] Especially, Toll-like receptors (TLRs), so-called germline-encoded pattern-recognition receptors (PRRs), that are primarily expressed on myeloid cells, including macrophages and DCs, trigger “danger” signaling between innate and adaptive immunity.[11,12] TLRs discriminate between “self” and “non-self” by recognizing pathogen-associated molecular patterns (PAMPs) and damage-associated molecular patterns (DAMPs), including deoxyribonucleic acid (DNA), ribonucleic acid (RNA) and other components derived from bacteria.[11,12] Toll-like receptor 4 (TLR4), for instance, recognizes lipopolysaccharides (LPSs) that are present in the outer membrane of gram-negative bacteria.[13]

Immature dendritic cells (iDCs) bearing TLRs on their surface mature upon direct recognition of microbial and foreign antigens or indirectly by sensing an inflammation and induce an adaptive immune response by activating $CD4^+$ T helper lymphocytes, $CD8^+$ cytotoxic T lymphocytes (CTLs) and B lymphocytes.[14-16] Peripheral iDCs capture antigens via endocytic receptors, digest them into oligopeptides and present peptide antigens on major histocompatibility complex (MHC) class I and MHC class II molecules on the surface for induction of $CD8^+$ CTLs and $CD4^+$ T helper cells, respectively.[14,16] All nucleated cells express MHC class I molecules that present endogeneous antigens, whereas MHC class II molecules expressed by antigen-presenting cells enable presentation of phagocytosed exogeneous pathogens.[16] DCs feature the ability to additionally cross-present extracellular antigens on MHC class I molecules that is a prerequisite to activate $CD8^+$ T cells directed against extracellular antigens.[17] Following antigen processing, iDCs migrate to local lymph nodes and develop into terminal mature dendritic cells (mDCs) that trigger vital adaptive immunity.[14,16] DC maturation is pronounced by the loss of endocytic receptors, high surface expression of MHC molecules and upregulation of co-stimulatory molecules important for T cell activation.[9] Molecular changes during DC maturation are accompanied by morphological changes, including the loss of adhesive structures and cytoskeleton reorganization with an increased cell surface through extended “dendrites” and thus, procuring a more potent T cell activation.[9,10]

Each T lymphocyte bears unique T cell receptors (TCR) for specific antigen recognition that arose from somatic recombination and developmental selection in the thymus.[18] $CD4^+$ and

CD8$^+$ T cell activation and proliferation by DCs in secondary lymphoid organs depend on two signals: first, the recognition of the MHC-peptide complex by antigen-specific TCRs and second, the interaction of co-stimulatory molecules, like CD80 and CD86 present on the DC surface, with CD28 or cytotoxic T lymphocyte antigen 4 (CTLA-4) on T cells.[9,16] Differentiation and effector function of CD8$^+$ CTLs, which, besides NK cells, possess a pivotal role against virus infections and intracellular pathogens, require further APC-derived cytokine stimulation.[19,20] CD4$^+$ T cell activation by DCs may induce CD4$^+$ T helper cell differentiation into T helper type 1 (Th1) or T helper type 2 (Th2) cells depending on the stimulus and the kinetics of stimulation (Figure 1).[21] The cytokines interleukin-12 (IL-12) and IL-4 initiate a Th1 and Th2 response, respectively.[21,22] The former Th1 cells mainly produce the cytokine IFN-γ to activate macrophages for cell-mediated immunity and play an important role in anti-tumor immunity. The latter ones predominantly secret IL-4, IL-5 and IL-13 for humoral immunity through B cell activation.[22]

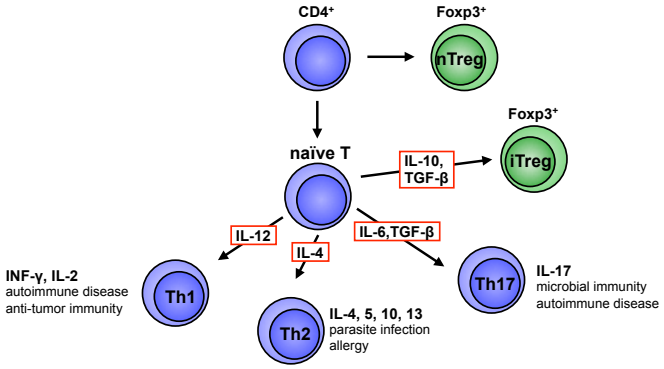

Figure 1. CD4$^+$ T cell differentiation. Naïve CD4$^+$ T cells can differentiate into distinct T effector cell types, including Th1, Th2 and Th17 cells, upon specific cytokine stimulation. In the presence of immunosuppressive cytokines T cells differentiate into induced regulatory T cells (iTregs). Natural Foxp3$^+$ regulatory T cells (nTregs) develop in the thymus. Adapted from Sakaguchi et al, 2008.[23]

Later discovered T helper type 17 (Th17) cells also induce cellular immunity against extracellular microbes and are characterized by their production of the inflammatory cytokines IL-17A, IL-17F and granulocyte-macrophage colony-stimulating factor (GM-CSF) and by their dependency on IL-6.[24] Besides T helper cells, CD4$^+$ T cells can develop into natural regulatory T cells (nTregs) in the thymus or differentiate into induced regulatory T cells (iTregs) in the periphery.[23]

1.2 Immune Tolerance

1.2.1 Central and Peripheral Tolerance

Central tolerance and control of immune responses in the periphery, with the former one taking place in the thymus and bone marrow and the latter one targeting peripheral autoreactive immune cells against self and innocuous antigens that escaped central tolerance, is primarily mediated by DCs and Tregs.[25,26]

Central tolerance regulates the elimination of autoreactive B and T cells containing genetically divers B cell receptors and TCRs that arose during V(D)J recombinations.[18,27] Within the thymus self-antigens are presented in MHC molecules by cortical and medullary epithelial cells as well as dendritic cells and upon low affinity of the TCR with self-MHC molecules T cells undergo a positive selection. T cells revealing strong interaction through the TCR with self-antigens and self-MHC molecules are deleted. However, some autoreactive T cells may escape this selection process, not all self-antigens are expressed in the thymus and moreover, T cells may be subjected to TCR editing and TCR revision and, thus, account for autoreactive T cells in the periphery.[18,27]

Among other cells, Tregs are vital regulators for balancing peripheral immune homeostasis.[28] In general, Tregs suppress the activation, differentiation and proliferation of T effector (Teff) cells either directly or via dendritic cells.[29] Treg-mediated suppression can be contact-dependent or cytokine-driven.[28] The complexity and diversity of immunosuppressive Tregs becomes apparent by the identification and description of diverse Treg subpopulations, including natural $CD4^+CD25^+Foxp3^+$ regulatory T cells (nTregs), interleukin-10-secreting type 1 regulatory T (Tr1) cells, induced regulatory T cells (iTregs) secreting transforming growth factor-β (TGF-β) or IL-10, TGF-β producing T helper type 3 cells, $CD8^+$ T suppressor cells and $CD4^-CD8^-$ T cells.[28,30]

Natural $CD4^+CD25^+Foxp3^+$ Tregs develop as mature T cells in the thymus and are indispensable for suppressing autoreactive Teff cells.[29] The transcription factor forkhead box P3 (Foxp3) is the master regulator for development and the suppressive activity of nTregs.[28,29] Foxp3 suppresses IL-2 production, but induces the expression of CD25 and CTLA-4, which is required for contact-dependent suppression of APCs and Teff cells by Tregs.[31,32] In mice, Foxp3 expression is exclusively restricted to regulatory T cells, whereas in humans also peripheral iTregs and activated Teff cells express Foxp3.[23]

Besides thymus-derived nTregs, especially iTregs and Tr1 cells that develop in the periphery contribute to immunological tolerance.[26,28] Both induced Treg populations predominantly trigger peripheral tolerance through the secretion of the immunosuppressive cytokines IL-10

and TGF-β.[26,33] IL-10-secreting iTregs can be induced upon stimulation of naïve $CD4^+$ T cells with immature dendritic cells.[34] Moreover, *in vivo* injection of antigen-primed immature DCs fosters IL-10 producing induced Tregs.[35]

Along their indispensable immunogenic properties as "the sentinels", dendritic cells can also force immunological tolerance by regulating constituents of the immune system in secondary lymphoid organs and in the periphery.[14,15,25,36] T cell activation and induction of antigen-specific T cell tolerance highly depends on the DC subset and the differentiation state of a dendritic cell.[25,37] Tolerance induction by DCs encompasses the silencing of differentiated antigen-specific T cells, induction of iTregs and activation and expansion of nTregs.[37,38]

1.2.2 Tumor-Associated Tolerance

Immune tolerance may prevent autoimmune diseases on the one hand, but may foster tumor progression on the other hand. [23,39] Tumor immune escape, involving mutations of the tumor cells, diminished antigen-presentation and the secretion of immunosuppressive cytokines by tumor cells, is one of the main obstacles for the failure of current immunotherapeutic approaches.[4]

Many tumor cells secret immunosuppressive and tumor-promoting cytokines, including TGF-β, IL-6, vascular endothelial growth factor (VEGF) and IL-10 that suppress DCs and T cells (Figure 2).[4,40,41] Increased IL-10 serum levels were found in many patients with different carcinomas, involving malignant melanoma.[42] Besides TGF-β, class-2 cytokine IL-10 is the major immunosuppressive cytokine for tolerance induction primarily by inhibition of differentiation and proliferation of T cells and induction of tolerogenic DCs and regulatory T cells.[26,37,41] Moreover, IL-10 can directly impair Th1 and Th2 cytokine production, like diminished IFN-γ and IL-2 secretion, and induce a state of anergy in activated T cells.[43]

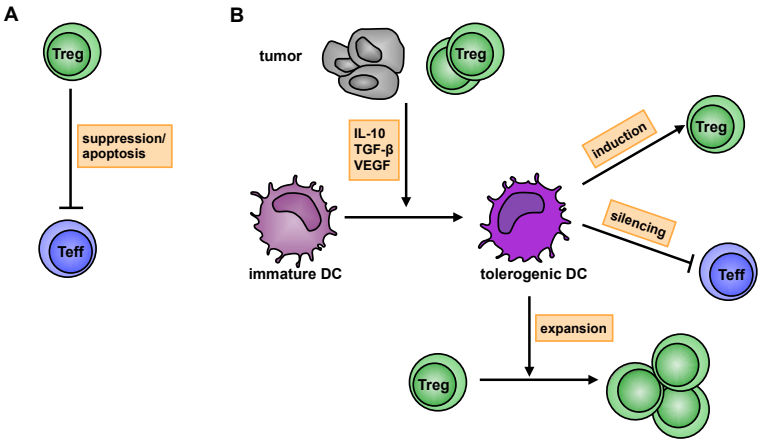

Figure 2. Tolerance induction in the tumor microenvironment. (A) Tregs directly induce suppression or apoptosis of Teff cells in the tumor microenvironment. (B) Besides, tolerogenic dendritic cells that are induced by immunosuppressive cytokines present in the tumor microenvironment may silence Teff cells. Additionally, tolerogenic DCs induce regulatory T cells and trigger the expansion of regulatory T cells. Adapted from Zou, 2006.[40]

Besides tumor cells, the anti-inflammatory cytokine IL-10 is produced by a variety of innate and adaptive immune cells, including Th2, Tregs, DCs and macrophages.[44,45] Expression of IL-10 by immune-stimulatory cells like Th1, Th2 and Th17 operates as a negative feedback loop to limit their action.[31,46] Additionally, Th2 cells were shown to be involved in aggressive tumors either by activation of B cells or by the production of IL-10.[6,47] Encountering IL-10 renders iDCs into a tolerogenic state exhibiting diminished capacity for $CD4^+$ Teff and $CD8^+$ CTL stimulation through reduced expression of MHC class II and co-stimulatory molecules (Figure 2).[48,49] Tolerogenic DCs mediate tolerance by inducing Teff cell anergy, deletion of autoreactive T cells and induction of iTregs (Figure 2).[36,50] Moreover, regulatory DCs express membrane-associated as well as soluble CD25 that may block IL-2 required for Teff cell proliferation.[51]

In the tumor microenvironment myeloid-derived suppressor cells (MDSCs), including immature macrophages and dendritic cells, additionally regulate immune responses by promoting clonal expansion of nTregs and iTregs by secretion of IL-10 and TGF-β for suppression of $CD8^+$ and $CD4^+$ T cells.[12,52] Additionally, MDSCs were found to exert their suppressive function by inhibiting T effector cell proliferation through elevated expression of arginase 1 and inducible nitric oxide synthase (iNOS), the production of radical oxygen species (ROS) and may inhibit Teff cell recruitment to the tumor site.[53,54]

Diverse attempts aim to reduce or deplete Tregs in the tumor microenvironment as augmented numbers of Tregs in tumor tissues were associated with poor prognosis.[40,55] Depletion of $Foxp3^+$ Tregs using depletion of regulatory T cells (DEREG) mice in a B16 melanoma mouse model showed a promising increase of $CD8^+$ CTLs resulting in partial

tumor regression.[56] Moreover, generation of a recombinant fusion protein, the so-called Denileukin diftitox (ONTAK), composed of human IL-2 cytokine and diphtheria toxin, caused inhibition of protein synthesis and cell death in high affinity IL-2 receptor expressing cells *in vitro*.[57] *In vivo* studies on melanoma patients with ONTAK, which was FDA (Food and Drug Administration) approved in 1999 for treatment of cutaneous T cell lymphoma (CTCL), showed a considerable decrease of $CD4^+CD25^+$ Tregs in the blood accompanied with an increase of melanoma-specific Teff cells.[58-60] This approach further points to a clinical benefit from depleting Tregs in carcinomas.

1.3 The Two Faces of the Cytokine IL-2 in Immunity and Immune Regulation

The cytokine interleukin-2 (IL-2) has a pivotal role in the thymic development of nTregs and maintenance of peripheral immune tolerance and concurrently, establishes T cell-mediated immunity by acting as a growth factor for Teff cells.[61] The former role of IL-2 was implemented in IL-2/IL-2R deficient mice disclosing autoimmunity through the inability to produce $CD4^+CD25^+Foxp3^+$ Tregs.[62] Besides Treg development, IL-2 sustains peripheral tolerance by inducing elevated levels of Foxp3 expression.[63]

The 15 kDa cytokine IL-2 is primarily secreted by antigen-activated Teff cells upon TCR stimulation and CD28 co-stimulation and regulates its own production by an autoregulatory negative feedback loop via signal transducer and activator of transcription 5 (STAT5) activation.[62] $CD8^+$ T cells, NK T cells, activated DCs and mast cells secrete only diminished amounts of IL-2.[64] The high-affinity trimeric IL-2 receptor particularly found on $CD4^+CD25^+Foxp3^+$ Tregs and transiently on activated $CD4^+$ and $CD8^+$ T cells is composed of three subunits, IL-2Rα (CD25), IL-2Rβ (CD122), and the common gamma chain γc (CD132).[62,63] IL-2 binds to the IL-2Rα subunit and thereby, initiates the association with the two other subunits giving rise to the high-affinity quaternary IL-2/IL-2R complex.[62] The cytokine-receptor complex is internalized and while CD25 recycles back to the membrane, IL-2 and the other subunits are directed to lysosomal degradation.[62,65,66] IL-2 can also interact with the intermediate-affinity receptor IL-2Rβ/γc complex that is predominantly expressed on memory T cells and NK cells.[63,67] IL-2 signaling requires IL-2Rβ and γc expression to retain immune homeostasis and autoimmunity.[68,69] Mice that are deficient for either IL-2Rα or IL-2 show similar phenotypes like mice depleted of IL-2Rβ with a partial influence on T and B cell development, but substantial effects on autoimmunity.[70,71] The studies emphasize the importance of IL-2 signaling for Treg development and homeostasis and their function through the high-affinity IL-2R complex.[72] Expression of IL-2R α and β chain is regulated by IL-2 in a positive feedback loop.[62,73] In addition, IL-2 plays a vital role in the early Th1 and

Th2 cell differentiation by promoting IL-12Rβ2 expression and inducing IL-4Rα expression, respectively.[73] In contrast, the T cell growth factor IL-2 inhibits the differentiation of Th17 cells by decreasing the expression levels of IL-6Rβ, whose signaling is mandatory for Th17 induction via STAT3.[63,64]

Treg cells constitutively express elevated levels of IL-2Rα *in vivo* that is indispensable for the formation of the high-affinity trimeric IL-2R rendering them more sensitive for IL-2 signaling.[74,75] Although CD25 expression is not a unique marker for human Tregs, as Teff cells augment expression of the α chain upon activation, targeting of Tregs can be procured via CD25 in different ways.[62,74] Boyman et al. first described the proliferative potential of the anti-mouse IL-2 monoclonal antibody (mAb) S4B6 building stable immune complexes with endogenous IL-2 for pronounced Teff cell proliferation. However, the anti-mouse IL-2 mAb JES6-1 together with IL-2 causes elevated Treg proliferation.[76,77] This effect is due to different binding sites of the two antibodies on IL-2, with the former one mimicking the way IL-2Rα interacts with IL-2, accompanied with varied expression levels of the IL-2Rα, β, and γc chain on different cell populations.[63] The latter one predominantly binds IL-2 on its interaction site with CD122 and thus, favors proliferation of $CD25^+$ expressing cells.[63] As indicated before, Tregs are more susceptible for IL-2 interaction compared to activated $CD4^+$ Teff cells.[74] Several studies are now concentrating on applying high-dose IL-2 treatment for cancer immunotherapy versus low-dose IL-2 treatment for autoimmune diseases.[78-81] Both approaches, high- versus low-dose IL-2 treatment are aiming to compensate the imbalance of Teff and Tregs and target Teff cells and Tregs, respectively.[82]

1.4 Immunotherapeutic Approaches Against Cancer

Surgery followed by chemotherapy or radiotherapy is still the standard treatment against many carcinomas with patient-suffering side effects and limited success particularly in the long run. Growing evidence supports a major role of the immune system in tumor formation, progression and regression and thus, current cancer therapies are primarily directed to the host immune system.[6,52,83]

There are two main routes to tune the immune system that can also be combined for therapy; either by activating an immune response through vaccination or by inhibiting the immunosuppressive branch of the immune system.[84] An effective immune response can be achieved by blocking distinct immune checkpoints.[85] The FDA-approved ipilimumab antibody directed against cytotoxic T-lymphocyte-associated antigen 4 (CTLA-4), which is expressed on T cells and dampens T effector cell activation, blocks the CTLA-4 inhibitory signal on T effector cells.[85,86] Concomitantly, blockade of CTLA-4 on Tregs impairs their suppressive

function.[85] Currently, ipilimumab is used in cancer patients suffering from melanoma resulting in an improvement of the clinical outcome and further clinical trials with ipilimumab against other tumor types are undertaken.[86] In general, antibodies for cancer therapy can function immunomodulatory or label tumor cells for recognition by immune cells.[87] Another way for boosting an immune response represents virus-based vaccines.[88] Virus-based cancer vaccines, which can foster the expression of tumor-associated antigens (TAAs) in antigen-presenting cells, concomitantly act as a danger signal due to their natural immunogenicity.[86,88] However, tumor therapy can also be performed as passive immunization through the adoptive cell transfer of naturally occurring, *ex vivo* expanded T cells into tumor patients.[89] These TAA-specific T cells can also be genetically engineered for an improved efficacy against the tumor.[89]

As DCs play a vital role in immunity, many investigations are focusing on the *ex vivo* activation and reinjection of TAA-presenting DCs into the patient.[90,91] DC-based immunotherapies are already in clinical trials and the first DC vaccine, sipuleucel-T, against metastatic prostate cancer, was approved by the FDA in 2010.[86,92] For this therapeutic approach antigen-presenting DCs are isolated from the patient, stimulated with a fusion protein of prostatic acid phosphatase, a protein that is overexpressed in prostate cancer, and GM-CSF, and reintroduced into the patient.[92] Although this therapeutic approach shows auspicious improvement in disease pattern, the tumor is not eradicated and the cost-intensive and laborious *ex vivo* manipulation of the cells is a clear drawback.[93]

1.5 Engineered Nanomaterials in Immunotherapy

Next generation of vaccines aim to target particular cells *in vivo* for cell type-specific activation, expansion or drug delivery with diminished side effects, reduced drug load, drug protection and improved efficacy.[94,95] Augmented research in biomedical engineering devoted on the generation of metabolizable nanomaterials as a drug delivery system aiming a cell type-specific targeting *in vivo*.[95,96] Many parameters, including shape, size and zeta potential, may highly affect the biological properties of nanoparticles, including biodistribution, cellular uptake and immunogenicity.

Distinct nanomaterials may interact with serum proteins generating a protein corona on the nanoparticle surface and thereby, can impact solubility and nanoparticle uptake into cells.[97,98] The hydrophilic polymer poly(ethylene glycol) (PEG) is frequently used to increase the solubility and circulation time of proteins or nanomaterials and simultaneously diminishes opsonization by plasma proteins.[99,100] Additionally, shielding nanomaterials with PEG is supposed to reduce possible immunogenicity of the nanomaterial.[101] As PEG is not

biodegradable, biodegradable substitutes for PEG with similar biological properties are investigated. Hydroxyethyl starch (HES) is commonly used as a plasma volume expander and reveals similar properties compared with PEG, yet is biodegradable.[102] Previous studies revealed that dsDNA (double-stranded DNA) can be stably encapsulated and is still functionally active in starch capsules and beyond that, HES capsules are largely inert regarding unspecific uptake.[103,104]

The size of nanoparticles (NPs) can be adjusted depending on the aimed targeting structure *in vivo*. Smaller NPs with an optimal size below 100 nm, but exceeding a size of 10 nm to avoid clearance from circulation, show elevated accumulation in tumors due to the enhanced permeability and retention (EPR) effect, whereas larger NPs, between 100 and 200 nm, are generated for elongated circulation times in the body.[94,100] Tumors with a size above 1 to 2 mm require vasculature to receive nutrients and oxygen, however, these newly formed tumor vessels show a leaky and immature state.[105] Thus, macromolecules may accumulate in the tumor and may be entrapped in the tumor due to an insufficient lymphatic drainage.[105] The aforementioned heterogeneity of different tumor types and differences between cancer patients affect the EPR effect and accessibility of nanomaterials into tumors decisively. Dealing with the EPR effect, nanoparticles can be used as a delivery system for immunomodulatory compounds into the tumor microenvironment.[106]

Augmented investigations on different targeting strategies for nanomaterials are in progress: NP accumulation in the tumor can be enhanced based on the EPR effect and specific targeting of tumor cells or immune cells can be mediated by antibodies, small proteins, peptides or small molecules interacting with receptors or proteins present on the target cell.[94,107] Stephan et al. circumvented *in vivo* targeting by directly labeling the cells with nanomaterials *ex vivo*.[108] They linked the nanomaterial to the surface of T cells via free thiol groups present on the cell surface and applied the engineered T cells in an adoptive T cell transfer.[108]

Ligand-mediated targeting of drugs and polymer-based nanomaterials to tumor cells or immune cells disclose many advantages, including selective toxicity and lower drug load, compared to nanomaterials that are not targeted to specific cells.[94,107] Additionally, encapsulation of drugs into NPs allows application of poorly soluble agents, protects the drug from degradation, increases the blood half-life and enables administration of more than one pharmaceutical simultaneously.[94] The receptor DEC-205, specifically detected with the mouse monoclonal antibody NLDC-145, is a membrane glycoprotein that is highly expressed on thymic and intestinal epithelia and on dendritic cells, but is marginally expressed on other organs.[109-111] Several approaches utilizing antigen-loaded NPs for DC targeting, which take

advantage of the exclusive c-type lectin receptor DEC-205 and CD11c on the surface of dendritic cells, featured already promising results for induction of $CD4^+$ and $CD8^+$ T cell immunity in mouse models.[112-114]

Following cell type-specific targeting, a subsequent challenge of NPs as a drug delivery system is the intracellular release of the cargo. Intracellular degradation of NP shell or cargo release can be achieved, for instance, by the integration of an acid-cleavable crosslinker that reveals faster hydrolyzation at lysosomal pH (pH 5.0).[115,116] This pH-dependent release makes use of a roughly neutral pH in the bloodstream (pH 7.4) and cytoplasm (pH 7.2), a lightly acidic pH in early endosomes and an acidic pH in late endosomes.[117]

In 2010, the first clinical trial for the delivery of small interfering RNA (siRNA) to solid tumors via targeted cyclodextrin-based nanoparticles in cancer patients was published.[118] This first human phase I clinical trial for targeted polymer-based drug delivery systems will most likely pave the way for generation of other NP-based therapeutics.

1.6 Motivation

Current cancer therapies are focusing on immunotherapy in order to boost an active durable response of the immune system against the tumor that may even counter drug resistance of tumor cells or tumor stem cells in the long run.[119] Dendritic cells (DCs) represent the key players of the immune system by means of their ability to monitor lymphocyte activation and expansion, including T cells and B cells, and their extensive body distribution in the lymphoid tissue, blood and peripheral tissue.[14,90] Thus, DCs constitute the target of many immunotherapeutic approaches against cancer.[92] Immature DCs with a profound endocytic and phagocytic potential capture antigens, process them and present peptides on their surface for lymphocyte activation and expansion.[14,16] Upon antigen loading, DCs migrate to secondary lymphoid tissues and develop into mature DCs that are characterized by high expression of the co-stimulatory molecules CD40, CD80 (B7-1) and CD86 (B7-2), the maturation marker CD83 and the chemokine receptor C-C chemokine receptor type 7 (CCR7) (Figure 3A).[14] However, if DCs are not fully activated or in the presence of immunosuppressive cytokines, DCs may develop into tolerogenic DCs bearing immunosuppressive properties.[25,36]

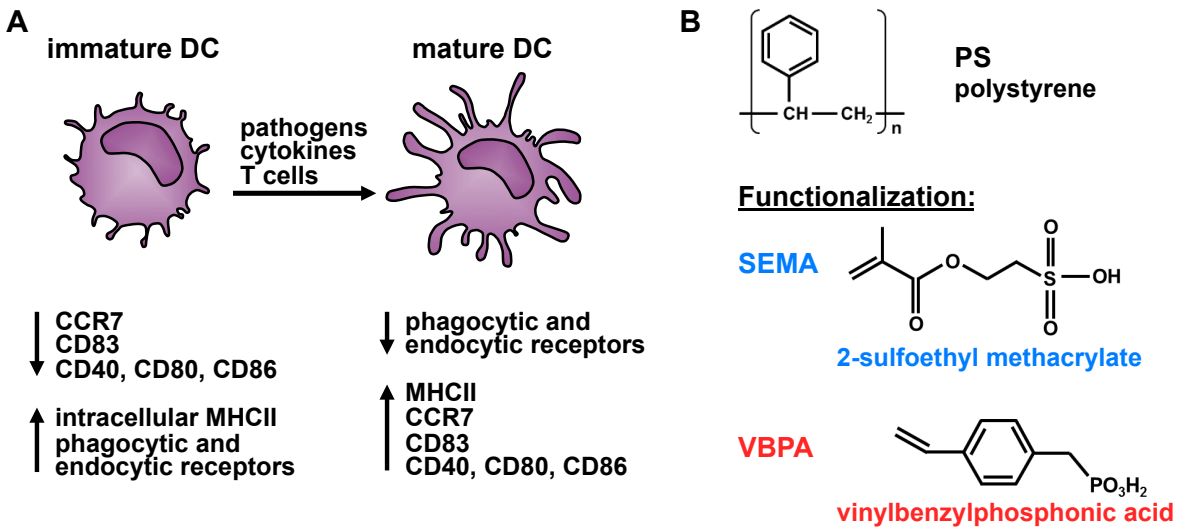

Figure 3. Influence of polystyrene NPs on DC maturation. (A) Immature DCs (iDCs) are characterized by low expression of the cell surface markers CCR7, CD83, CD40, CD80 and CD86, but show high expression of phagocytic and endocytic receptors. In contrast, mature DCs (mDCs) that develop upon pathogen, cytokine or T cell encountering, reveal a reduced phagocytic and endocytic potential. They show high expression of MHCII molecules, CCR7, CD83, CD40, CD80 and CD86. Adapted from Banchereau et al., 1998.[14] (B) In the present study the uptake and immunogenicity of polystyrene nanoparticles that were either SEMA (2-sulfoethyl methacrylate)- or VBPA (vinylbenzylphosphonic acid)-functionalized was analyzed.

Nanomaterials that are highly tunable regarding size, charge, surface functionalization and drug load are currently investigated as an attractive drug delivery system to DCs.[114] Besides antigen delivery to DCs, a major demand on nanomaterials is to induce terminal DC maturation for a proper T cell stimulation. DC maturation can either be induced by additional administration of adjuvants or the nanomaterial may induce DC maturation per se.[114]

In the present study the uptake and immunogenicity of SEMA (2-sulfoethyl methacrylate)- and VBPA (vinylbenzylphosphonic acid)-functionalized polystyrene nanoparticles (NPs) were addressed (Figure 3B). Due to their high stability and narrow size distribution, polystyrene NPs constitute a good model system to assess nanoparticle characteristics for therapeutic approaches. Surface charge and functionalization of NPs were previously described to highly impact the ability of nanomaterials to foster improved NP uptake and induce DC maturation.[120,121]

A major limitation of current therapies against carcinomas is the invasion into or formation of immunosuppressive $CD4^+CD25^+Foxp3^+$ Tregs, iTregs and tolerogenic DCs in the tumor microenvironment that dampen a proper immune response against the tumor.[4,40,84] Tregs may directly suppress T effector (Teff) cells or function via tolerogenic DCs.[29] They are characterized by high surface expression of CD25, the alpha subunit of the IL-2 receptor (Figure 4). In addition, activated $CD4^+$ T effector cells reveal elevated CD25 expression levels, but recent investigations ascertained that Tregs are more prone to encounter IL-

2.[74,122] Thus, the cytokine IL-2, which is FDA-approved for immunotherapy and known to be internalized by the IL-2 receptor complex composed of IL-2Rα, β and γc, was used for Treg targeting (Figure 4).[62,73]

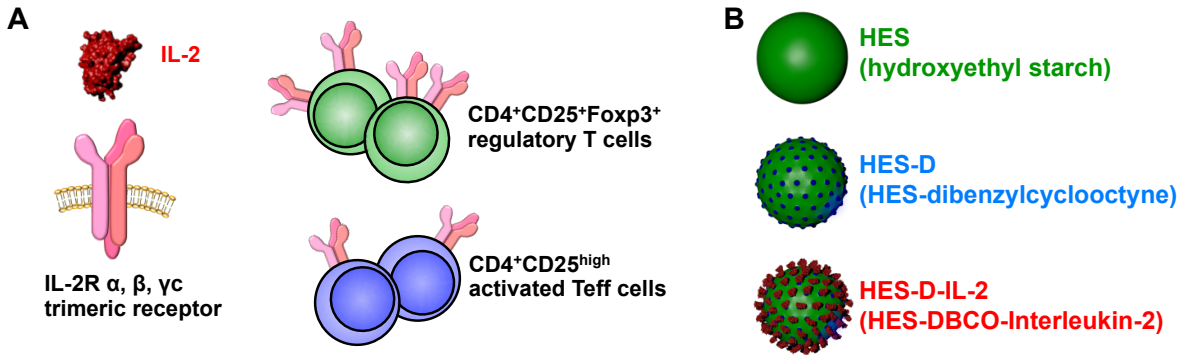

Figure 4. IL-2-functionalized nanocapsules for targeting $CD4^+CD25^+$ regulatory T cells. (A) The cytokine IL-2 interacts through high affinity with the trimeric IL-2 receptor (IL-2R) complex composed of IL-2Rα, β and γc chain. $CD4^+CD25^+Foxp3^+$ regulatory T cells (Tregs) and activated $CD4^+CD25^{high}$ T effector cells are characterized by high expression of CD25 on their surface. (B) In the present study, hydroxyethyl starch (HES) capsules were surface-functionalized with dibenzylcyclooctyne (DBCO) for linking IL-2 to the capsule surface via click chemistry. HES-D-IL-2 capsules were analyzed for their uptake by $CD4^+CD25^{high}$ T cells.

Hydroxyethyl starch (HES) nanocapsules (NCs) were surface-functionalized with dibenzylcyclooctyne (DBCO), HES-D, for coupling IL-2 to the surface via click chemistry (HES-D-IL-2) (Figure 4). The biologic functionality of IL-2 bound to HES capsules to induce T cell proliferation and their uptake by $CD4^+CD25^{high}$ T cells was investigated in the present study. Engineering NCs that can be loaded with small molecules or siRNA for specific Treg targeting may enable Treg silencing or deletion in the tumor microenvironment in the long run.

2 Results

2.1 SEMA- and VBPA-Functionalized Polystyrene Nanoparticles

Polystyrene nanoparticles (NPs) function as a suitable model system to study nanomaterial properties. Size, charge and surface functionalization of polystyrene NPs can easily be altered in order to address the influence of different NP parameters on uptake, toxicity and immunogenicity. Since polystyrene is not biodegradable, polystyrene can be substituted for biodegradable polymers in future studies.

The results about unfunctionalized and surface-functionalized polystyrene NPs were already published in a peer-reviewed journal and are the basis for the first part of the results and discussion of the present study.[123]

2.1.1 Characterization of SEMA- and VBPA-Functionalized Nanoparticles

Polystyrene nanoparticles were generated by miniemulsion polymerization from the monomer styrene. Synthesis and characterization of the presented polystyrene NPs were kindly performed by [redacted] (Max Planck Institute for Polymer Research, Mainz, Germany). Unfunctionalized polystyrene (PS) and 2-sulfoethyl methacrylate (SEMA)- and vinylbenzylphosphonic acid (VBPA)-functionalized polystyrene NPs had a particle size between 175 and 227 nm with a small relative size distribution (rSD) as measured by dynamic light scattering (DLS) (Table 1). Besides DLS, measured size and size distribution was confirmed by scanning electron microscopy (SEM) (Figure 5).

Table 1. Physico-chemical analysis of unfunctionalized PS and SEMA- and VBPA-functionalized polystyrene NPs. From Frick et al., 2012.[123]

Sample	D_z [nm]	rSD [%]	Zeta potential [mV]	SD [mV]	Functional groups per nm^2	PMI amount, [mg per $g_{polymer}$]
PS	175	14	-4	0.3	-	0.37
SEMA	245	15	-15	1.2	1.03	0.21
VBPA	227	12	-32	2.3	1.49	0.42

As NPs had to be dried on a silica wafer for SEM imaging, the actual size of NPs obtained by SEM is slightly reduced compared to the values measured by DLS. SEM images further confirmed monodisperse NPs with a small size distribution. Characterization of the polystyrene NPs exhibited a relatively neutral zeta potential for unfunctionalized PS NPs (-4 mV), whereas SEMA and VBPA NPs revealed a lower zeta potential of -15 mV and -32 mV, respectively (Table 1). SEMA-functionalized polystyrene NPs contained 1.03 functional

groups per nm^2 surface, whereas 1.49 VBPA groups per nm^2 NP surface were present on VBPA-functionalized NPs. For NP detection in biological applications, the fluorescent perylene dye *N*-(2,6-diisopropylphenyl)perylene-3,4-dicarbonacidimid (PMI) was incorporated into the particles. As the amount of PMI, assessed via spectroscopy, varied between the different NPs, fluorescence intensity had to be adjusted in subsequent biological assays.

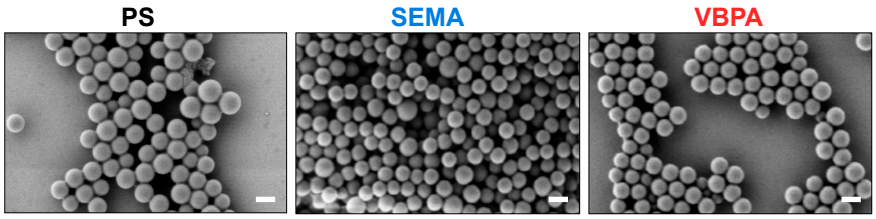

Figure 5. Scanning electron microscopy of unfunctionalized PS and SEMA- and VBPA-functionalized polystyrene NPs. Scale bar represents 200 µm. From Frick et al., 2012.[123]

2.1.2 Uptake of SEMA and VBPA Nanoparticles by Dendritic Cells

As professional antigen-presenting cells, dendritic cells (DCs) bridge innate and adaptive immunity and thus, play a vital role during immune responses.[7,10] Immature dendritic cells (iDCs) with high endocytic potential take up antigens, process them and present antigen-loaded MHC molecules on the DC surface for T cell activation.[14] Activated iDCs migrate to secondary lymphoid organs and develop into mature dendritic cells (mDCs) that activate T cells. DC maturation can be induced by pathogens, interaction with other immune cells and distinct cytokines.[14]

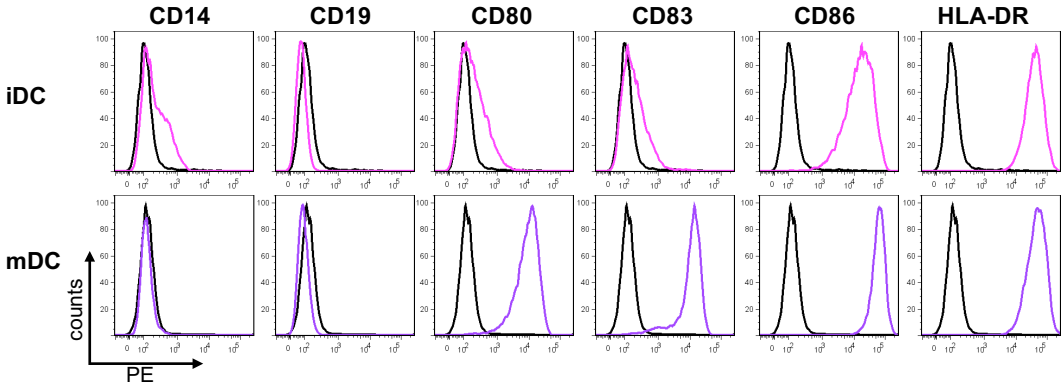

Figure 6. Phenotypic characterization of DCs. Precursors of DCs were isolated from human PBMCs and cultured with specific cytokines for 5/6 and 7/8 days for generation of iDCs (upper row) and mDCs (lower row), respectively. Before applying DCs in experimental setups, cells were characterized for the expression of the cell surface markers CD14, CD19, CD80, CD83, CD86 and HLA-DR by using flow cytometry analysis and the expression level was plotted against the counted cells (y-axis). Representative histograms from one experiment are depicted. Black histograms indicate isotype controls, whereas pink (iDCs) and purple (mDCs) lines depict the expression of the respective cell surface marker on the DCs.

In order to determine the uptake of the investigated NPs by iDCs and mDCs, monocyte-derived DCs were generated from human peripheral blood mononuclear cells (PBMCs) by stimulating adherent monocytes with the cytokines IL-4 and GM-CSF. Human iDCs were harvested on day five or six of culture and analyzed for their cell surface marker expression profile by flow cytometry (Figure 6). In general, CD80 and CD83 were barely expressed, whereas CD86 and human leukocyte antigen (HLA)-DR were highly expressed on iDCs (Figure 6, pink lines) compared to isotype stained control cells (Figure 6, black lines). To exclude the presence of macrophages and B cells in the cell suspension, the cells were additionally stained for CD14 and CD19, respectively. Only residual amounts of $CD14^+$ and $CD19^+$ PBMCs were detected. For generation of mDCs, iDCs were further cultured for two days with additional cytokine stimulation, including IL-1β, tumor necrosis factor alpha (TNF-α), IL-6 and prostaglandin E2 (PGE_2). Monocyte-derived mDCs showed elevated expression levels of the co-stimulatory molecules CD80 and CD86, the maturation marker CD83 and HLA-DR (Figure 6, purple lines). Compared to iDCs, the expression level of CD86 was even increased after maturation. Macrophages and B cells were not detectable in the mDC culture as the cells were negative for CD14 and CD19, respectively.

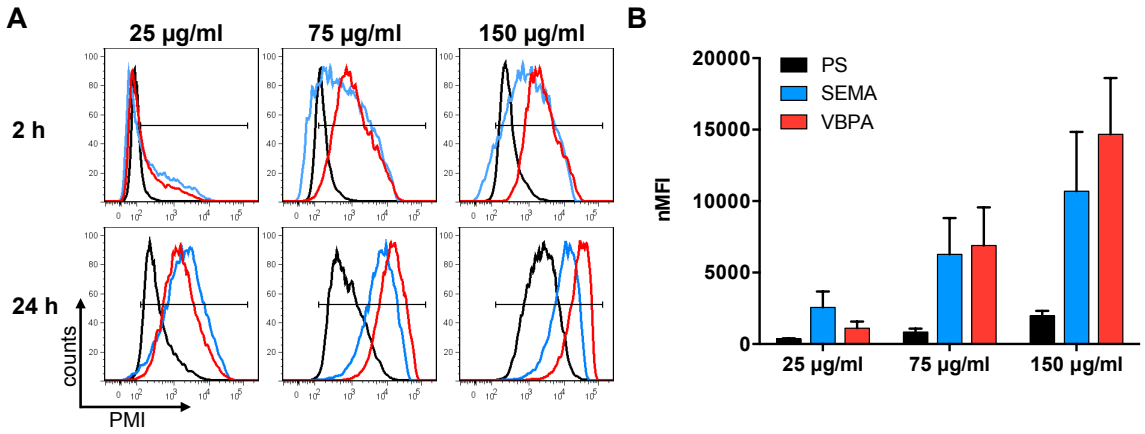

Figure 7. Flow cytometry analysis of PS, SEMA and VBPA nanoparticle uptake by iDCs. Human iDCs were incubated with control PS (black), SEMA (blue) and VBPA (red) nanoparticles at concentrations of 25, 75 and 150 µg/ml for 2 and 24 h. (A) Histograms of one representative experiment show the amount of PMI-positive cells compared to unstained iDCs and mean fluorescence intensity (MFI) by plotting the expression level (x-axis) against the counted cells (y-axis). Untreated iDCs were taken as control for gating (black line). (B) Normalized MFI (nMFI) values of PS, SEMA and VBPA nanoparticle uptake for 24 h by iDCs from three independent experiments are shown (mean ± SD). Adapted from Frick et al., 2012.[123]

Control PS, SEMA and VBPA NPs were applied on iDCs at a concentration of 25, 75 and 150 µg/ml and uptake was assessed 2 and 24 h after addition by flow cytometry. Untreated control iDCs were taken as a negative control for gating. Flow cytometry analysis depicted that all tested NPs show a gradual uptake by iDCs with increasing time and elevated concentrations illustrated by a histogram shift on the x-axis to the right (Figure 7A). A

histogram shift on the x-axis indicates that even NP-positive iDCs may continue taking up NPs so that the amount of NPs per cell increases. Fluorescence intensity is expressed as mean fluorescence intensity (MFI) of the NP-dye PMI demonstrating the amount of fluorescent dye of positive cells. VBPA NPs featured the fastest and highest uptake meaning that even 2 h after addition of 75 µg/ml VBPA NPs all iDCs were positive for the fluorescent dye PMI and the VBPA histograms showed the highest intensity for PMI (Figure 7A, red histograms). Similar results were obtained for SEMA NPs, but the uptake was slower compared with VBPA NPs (Figure 7A). 24 h after NP addition, all iDCs were positive for SEMA NPs at the lowest concentration used. Unfunctionalized PS NPs showed least uptake by iDCs regarding the percentage of PMI-positive cells and the MFI values. After 24 h incubation, iDCs were measured positive for all NPs at the highest NP concentration used. For comparison of the MFI values between the different NPs, the MFI values were normalized to SEMA NPs revealing the lowest amount of the fluorescent dye PMI. A summary of the normalized mean fluorescence intensities (nMFIs) depicted tremendous differences between control PS NPs and functionalized NPs with a lower uptake of unfunctionalized PS NPs by iDCs (Figure 7B). As the focus of the study was aimed at SEMA and VBPA NPs, PS NPs were not included in further investigations. Additionally, vast differences in the amount of NPs per cell may influence immunogenicity that will also be addressed in the ongoing study.

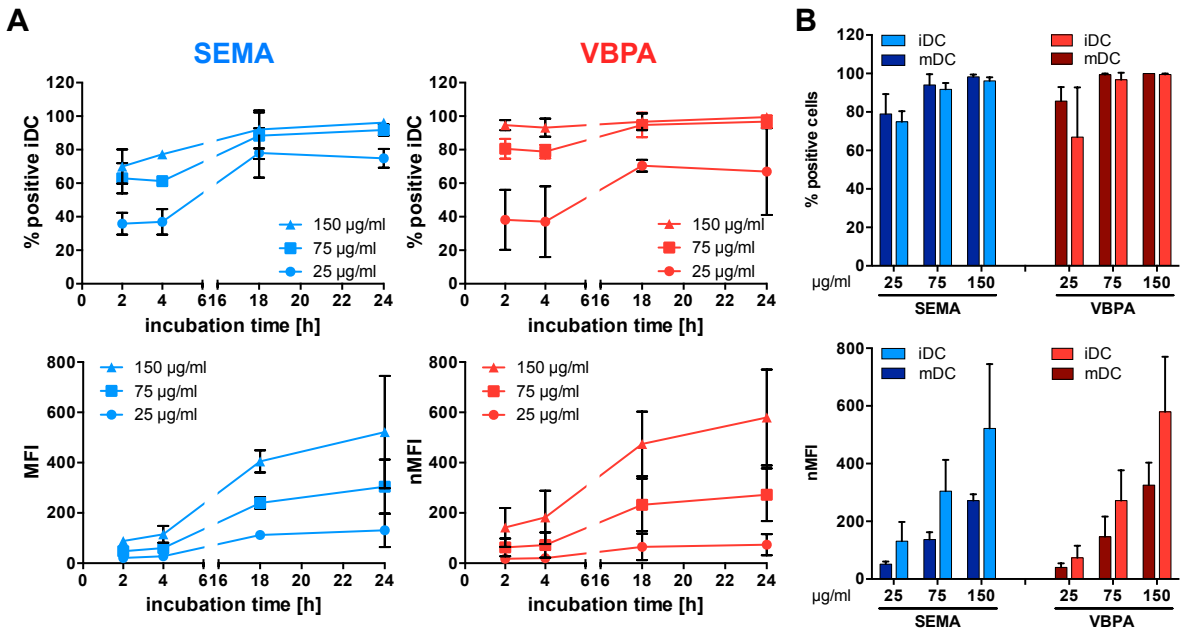

Figure 8. SEMA and VBPA polystyrene nanoparticle uptake by iDCs. (A) Immature DCs were incubated with 25, 75 and 150 µg/ml SEMA (left graph) and VBPA (right graph) for 24 h. Uptake of PMI-labeled particles by iDCs was determined 2, 4, 18 and 24 h after addition by flow cytometry. Upper graphs show the percentages of NP-positive cells; lower figures depict the mean fluorescence intensity (MFI) of PMI of all iDCs. MFI values for VBPA NPs were normalized (nMFI) to the reduced-PMI amount in SEMA particles. (B) Comparison of SEMA and VBPA nanoparticle uptake by iDCs and mDCs at a concentration of 25, 75 and 150 µg/ml after 24 h incubation by flow cytometry analysis. The upper graph shows the percentage of PMI-labeled NP-positive cells. The lower graph contains the normalized mean fluorescence intensities (nMFIs) of iDCs and mDCs. Summaries of three independent experiments are represented as mean ± SD. Adapted from Frick et al., 2012.[123]

The kinetics of SEMA and VBPA uptake by iDCs and mDCs was performed for 24 h at concentrations of 25, 75 and 150 µg/ml. Both NPs showed a gradual increase in the percentage of NP-positive cells with increased concentrations at later time points (Figure 8A, upper row). At the two higher concentrations, 75 and 150 µg/ml, more than 90% of iDCs were detected positive for the NP-dye PMI 18 h after NP addition. Comparing SEMA and VBPA uptake by iDCs, VBPA NPs were found to be taken up faster as even after 2 h incubation almost 80% of iDCs were NP-positive at a concentration of 75 and 150 µg/ml, whereas the same concentrations and incubation time resulted in less than 70% SEMA-positive iDCs. A summary comparing SEMA and VBPA uptake by iDCs and mDCs 24 h after NP addition revealed marginal differences between both particles regarding percentages of positive cells (Figure 8B). Additionally, comparing the amount of NP-positive cells between iDCs and mDCs only negligible differences in the percentages of SEMA- and VBPA-positive cells were observed. MFI analysis also showed that later time points and increasing NP concentrations were positively correlated with NP uptake by iDCs (Figure 8A, lower row). Comparing SEMA and VBPA NP uptake by iDCs regarding the MFI values, VBPA NPs indicated a slightly increased uptake by iDCs than SEMA NPs. Similar results were obtained

for mDCs, but the overall uptake of SEMA and VBPA NPs per mDC was lower compared to iDCs (Figure 8B). Direct comparison between iDC and mDC NP uptake illustrated that the percentage of NP-positive cells was similar, but the nMFI values were considerably increased in iDCs compared with mDCs.

Altogether, SEMA and VBPA NPs revealed a dose- and time-dependent uptake by iDCs and mDCs. Comparing the two NPs, VBPA uptake was slightly increased to SEMA NP uptake. Additionally, total iDC uptake was superior to the measured uptake of SEMA and VBPA NPs by mDCs.

Both NPs, SEMA- and VBPA-functionalized polystyrene, showed no significant increase of Annexin V-positive cells compared to untreated iDCs and mDCs as determined via flow cytometry.[123] This result indicates that the investigated nanoparticles did not exhibit a cytotoxic effect on DCs *in vitro*.

2.1.3 Confocal Laser Scanning Microscopy Analysis

In addition to flow cytometry analysis, confocal laser scanning microscopy (cLSM) was conducted to examine whether the NP-positive cells detected by flow cytometry had internalized the NPs or whether the NPs were simply associated with the cell membrane.

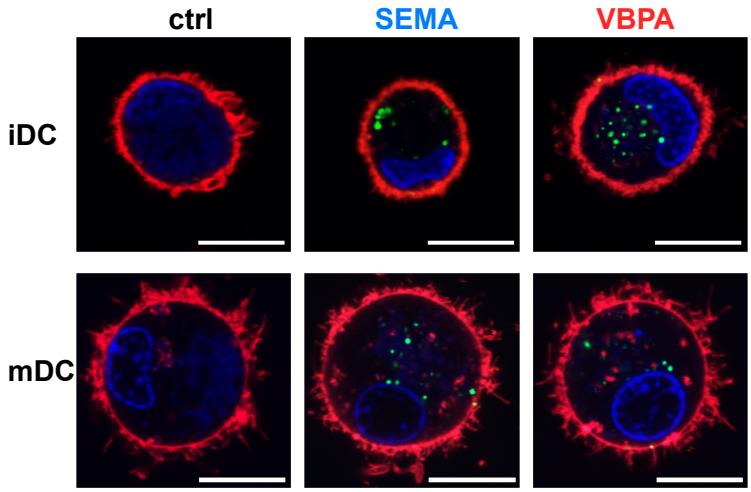

Figure 9. Confocal laser scanning microscopy images of SEMA- and VBPA-treated iDCs and mDCs. Monocyte-derived iDCs and mDCs were treated with 75 µg/ml SEMA and VBPA polystyrene NPs for 24 h. Untreated iDCs and mDCs were taken as control. Cell membrane (red) and cell nucleus (blue) were stained prior to microscopy with CellMask™ Orange Plasma membrane stain and DRAQ5®, respectively. Nanoparticles (green) were detected based on the incorporated fluorescent dye PMI. Scale bar corresponds to 10 µm. From Frick et al., 2012.[123]

Human iDCs and mDCs were treated with 75 µg/ml SEMA and VBPA NPs for 24 h before microscopy was performed. After removal of excessive amounts of unbound NPs from the cell culture supernatant, cell membranes were stained with CellMask™ Orange and cell

nuclei with DRAQ5®. CLSM analysis confirmed intracellular localization of SEMA and VBPA NPs in iDCs and mDCs (Figure 9). The association of polystyrene NPs with the cell membrane was hardly detected indicating that PMI-positive cells measured by flow cytometry depicted NP-loaded DCs. CLSM analysis further indicated a reduced NP uptake of both SEMA and VBPA by mDCs compared to iDCs. Additionally, VBPA uptake per cell was slightly increased against SEMA uptake by cLSM analysis. This result was in accordance with flow cytometry analysis of NP uptake, which depicted an elevated NP uptake by iDCs compared to mDCs and a slightly increased internalization of VBPA-functionalized NPs compared with SEMA NPs.

2.1.4 Nanoparticle-Induced Dendritic Cell Maturation

To determine the immunogenic potential of both SEMA and VBPA polystyrene NPs, DC maturation was assessed after NP addition. Monocyte-derived iDCs were stimulated with SEMA and VBPA nanoparticles for 24 h, unbound NPs in the supernatant were washed out and the cells were further cultured for two days. The expression pattern of cell surface molecules associated with DC maturation (CD83), T cell activation (CD80, CD86, B7-DC and B7-H2) and CCR7, which is associated with DC migration to lymph nodes, was examined by flow cytometry.[9,14] Untreated iDCs and mDCs served as control groups.

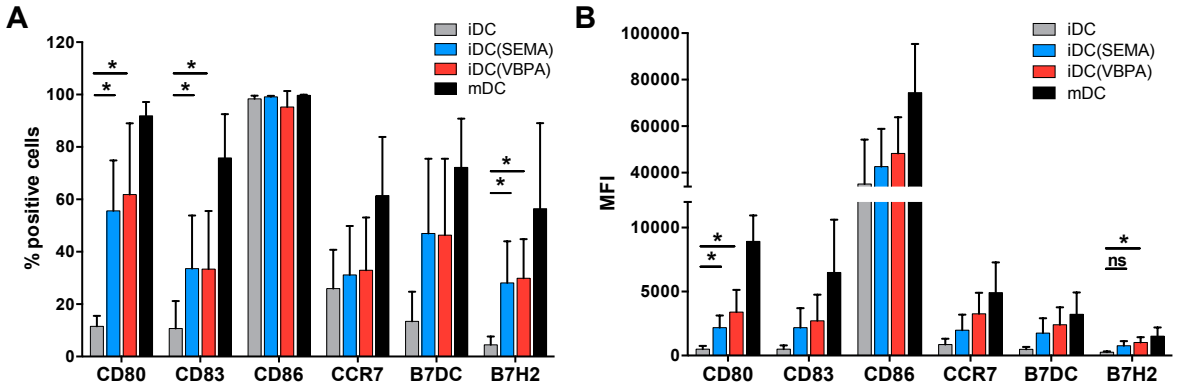

Figure 10. Phenotypic characterization of NP-loaded iDCs by flow cytometry analysis. Human iDCs were treated with SEMA and VBPA polystyrene NPs at a concentration of 75 µg/ml for 24 h. NPs in the supernatant were washed out and after two further days of culture, iDCs were analyzed for their expression of distinct cell surface markers, including CD80, CD83, CD86, CCR7, B7-DC and B7-H2. Untreated iDCs and mDCs were taken as controls. Percentage of positive cells (A) and mean fluorescence intensity (MFI) (B) of the appropriate marker molecule are represented. Pooled data from four independent experiments are illustrated (mean ± SD; ns = not significant; * $p < 0.05$). From Frick et al., 2012.[123]

The overall frequency of CD80, CD83, CCR7, B7-DC and B7-H2 positive iDCs was tremendously lower compared with mDCs (Figure 10A). Only the amount of CD86 positive iDCs and mDCs was comparable. Compared to untreated iDCs, NP-loaded iDCs exhibited a

significantly increased expression of CD80, CD83 and B7-H2. The percentages of CD80, CD83 and B7-H2 positive iDCs treated with NPs was at an intermediate level between the measured percentages of iDCs and mDCs. Additionally, SEMA and VBPA NP treatment increased the amount of CCR7 and B7-DC positive iDCs. Irrespectively of their treatment nearly all iDCs and mDCs were measured positive for the cell surface marker CD86. Moreover, mean fluorescence intensity of each cell surface marker molecule was disclosed by flow cytometry. According to the percentage of positive cells, MFI values of CD80 expression were significantly increased after NP treatment compared to unstimulated iDCs (Figure 10B). The expression level of B7-H2 was also elevated on NP-loaded iDCs, but only VBPA NPs showed a significant increase. The other analyzed cell surface markers, including CD83, CD86, CCR7 and B7-DC, were increased on NP-treated iDCs compared to untreated iDCs as well. Altogether, the analyzed cell surface markers that are involved in co-stimulation, migration and iDC maturation were increased on NP-treated iDCs, but the expression levels were still lower as measured on fully matured DCs.

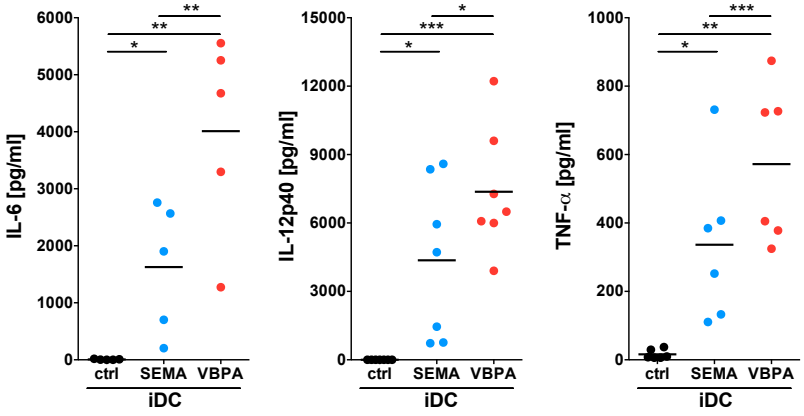

Figure 11. Cytokine profile of SEMA- and VBPA-treated iDCs. Human iDCs were cultured with SEMA and VBPA polystyrene NPs at 75 µg/ml for 24 h. Culture supernatants were analyzed for the amount of the cytokines IL-6, IL-12p40 and TNF-α by ELISA measurements. Data from five to seven independent experiments are shown (mean ± SD; * $p < 0.05$; ** $p < 0.01$; *** $p < 0.001$). From Frick et al., 2012.[123]

Besides cell surface marker analysis, cytokines that are involved in iDC maturation and T cell activation were measured after NP treatment by an enzyme-linked immunosorbent assay (ELISA). Monocyte-derived iDCs (d5) were cultured with 75 µg/ml SEMA and VBPA NPs for 24 h before the supernatants were analyzed for the presence of the cytokines IL-6, IL-10, IL-12p40, IL-12p70 and TNF-α. The amounts of IL-6, IL-12p40 and TNF-α were significantly increased in the supernatants of SEMA- and VBPA-treated iDCs compared with untreated control iDCs (Figure 11). Surprisingly, comparing the amount of secreted cytokines of SEMA- and VBPA-treated iDCs, the supernatants of VBPA-treated iDCs contained significantly elevated levels of IL-6, IL-12p40 and TNF-α. The cytokines IL-10 and IL-12p70 were not

detected in the supernatants of iDCs and mDCs irrespectively of the treatment. As *in vitro* DC maturation is induced by the addition of the cytokines IL-1β, TNF-α, IL-6 and PGE_2, the cytokine levels present in mDC supernatants were not comparable to the supernatants of NP-treated iDCs and thus, control mDC supernatants were not analyzed by ELISA.

Many factors, including foreign antigens or components form bacteria, can induce DC maturation.[13,14] Endotoxin, which is a lipopolysaccharide (LPS) derived from the outer membrane of gram-negative bacteria, can be present on reusable labwares or even raw materials. To determine the amount of endotoxin in the nanoparticle suspension, a Limulus Amebocyte Lysate (LAL) PYROGENT™ Plus Single Test (sensitivity of 0.06 endotoxin units per ml (EU/ml)) was executed. By using this assay no endotoxin was measurable, indicating that the endotoxin level was below 0.06 EU/ml or the NP sample was completely endotoxin-free.

Analysis of the expression pattern of cell surface markers and the production of cytokines that are involved in DC maturation induced by SEMA and VBPA NPs revealed a DC phenotype pointing towards an mDC phenotype.

2.1.5 Pronounced $CD4^+$ T Cell Proliferation Through SEMA and VBPA Nanoparticle-Loaded Immature Dendritic Cells

Mature DCs are known to induce $CD4^+$ T cell activation with T cell differentiation into T helper type 1 (Th1) or T helper type 2 (Th2) cells and T cell proliferation.[21,22] The former T helper cell type is characterized by the secretion of the cytokine IFN-γ, whereas the latter T helper cell type is known to produce the cytokines IL-5 and IL-13.[21,22]

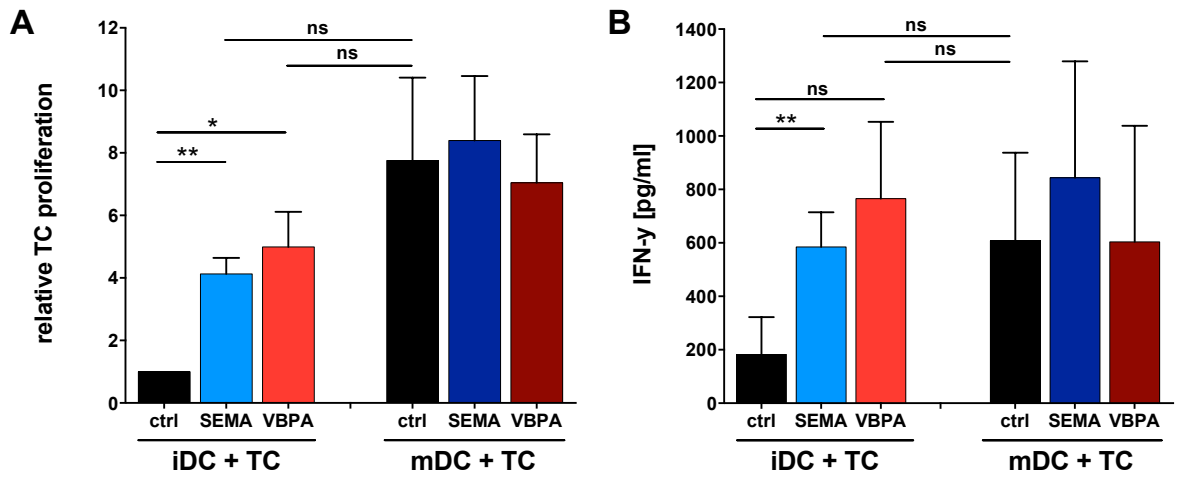

Figure 12. Mixed leukocyte reaction of NP-loaded DCs and allogeneic T cells. Human iDCs were incubated with 75 µg/ml SEMA and VBPA NPs for 24 h. (A) After two further days of iDC culture or mDC induction, DCs were co-cultured with allogeneic T cells and T cell proliferation was measured by addition of [^{3}H]-thymidine for 16 h. Triplicates of each assay were normalized to untreated control iDCs. Pooled data from triplicates of four independent experiments are shown (mean ± SEM). (B) NP-loaded DCs were co-cultured with allogeneic T cells and the amount of secreted IFN-γ was measured after three days of co-culture by ELISA. Mean ± SD of three independent experiments are shown (ns = not significant; * $p < 0.05$; ** $p < 0.01$). From Frick et al., 2012.[123]

In order to address the T cell stimulatory potential of SEMA- and VBPA-treated iDCs and mDCs, the proliferation of allogeneic CD4$^+$ T cells was measured in a mixed leukocyte reaction (MLR). For this purpose, iDCs (d5) were stimulated with SEMA- and VBPA-functionalized NPs for 24 h, followed by the removal of soluble NPs in the supernatant and either iDCs were maintained immature or mDCs were induced. Allogeneic T cells were co-cultured with NP-loaded iDCs and mDCs and proliferation was determined in a [^{3}H]-thymidine proliferation assay. Untreated iDCs and mDCs were taken as controls. SEMA- and VBPA-loaded iDCs induced a significantly higher T cell proliferation compared to control iDCs (Figure 12A). In contrast, T cell proliferation triggered by untreated mDCs was not significantly increased compared to the T cell proliferation induced by NP-treated iDCs. NP-loaded iDCs that were matured into mDCs showed no differences in the T cell stimulatory capacity compared to control mDCs.

Besides T cell proliferation, the amounts of T helper cell cytokines present in the co-culture supernatants were measured by ELISA. In general, control mDCs showed an elevated IFN-γ production compared to iDCs (Figure 12B). The amount of IFN-γ was strongly increased in MLRs of allogeneic T cells co-cultured with SEMA- and VBPA-treated iDCs compared to control iDCs. The increased IFN-γ production of SEMA- or VBPA-loaded iDCs was comparable with the amount of IFN-γ secreted by untreated mDCs. Results of co-cultures of allogeneic T cells and NP-loaded mDCs did not differ from the control mDC co-cultures. The

Th2 cytokines IL-5 and IL-13 were not increased in co-cultures of allogeneic T cells and NP-loaded DCs compared with untreated control DCs (data not shown).

In summary, SEMA- and VBPA-loaded iDCs induced strong proliferation of allogeneic T cells with increased levels of the Th1 cytokine IFN-γ.

2.2 IL-2-Functionalized Hydroxyethyl Starch Nanocapsules

In addition to sulfonate- and phosphonate-functionalized polystyrene NPs, functionalized starch capsules were investigated for their uptake by specific immune cells. Biodegradable starch nanocapsules (NCs) were already shown to be highly stable with reduced leakage of incorporated molecules.[103] Additionally, the unspecific uptake of starch NCs was reported to be minor, rendering the capsules as a promising approach for cell type-specific targeting.[104]

2.2.1 Characterization of Hydroxyethyl Starch Nanocapsules

Synthesis, functionalization and physico-chemical analysis of hydroxyethyl starch (HES) NCs was kindly performed by [redacted] (Max Planck Institute for Polymer Research, Mainz, Germany). HES NCs were surface-functionalized with the cytokine IL-2 to render the capsules capable for cell type-specific uptake by IL-2 receptor (IL-2R)-bearing cells. For protein conjugation, an amine group (NH_2) was introduced on the HES NC surface, followed by linking dibenzylcyclooctyne (DBCO)-NHS ester to the reactive amine groups via NHS ester chemistry. Azide-functionalized IL-2 was conjugated to the capsule surface by copper-free click chemistry.

In the present study, unfunctionalized HES NCs and DBCO-functionalized HES NCs were taken as controls and referred to as “HES” and “HES-D” NCs, respectively. IL-2-functionalized HES-D NCs were termed “HES-D-IL-2” NCs. The size of HES NCs was determined by dynamic light scattering (DLS) detecting a capsule size between 210 and 225 nm (Table 2). A size distribution between 28% and 31%, expressed as relative standard deviation (rSD), showed a rather homogeneous size distribution. Measuring the zeta potential of all three analyzed NCs revealed negative zeta potentials between -16 and -6 mV. To render the HES NCs detectable in biological investigations, the fluorescent dye sulforhodamine 101 (SR101) was incorporated into the capsule core during inverse miniemulsion polymerization. As depicted in Table 2, HES capsules contained unequal amounts of SR101 which requires to be considered for later investigations.

Table 2. Physico-chemical analysis of unfunctionalized and surface-functionalized hydroxyethyl starch nanocapsules.

Sample	D_z [nm]	rSD [%]	Zeta potential [mV]	Relative fluorescence intensity
HES	210	28	-12	0.7
HES-D	210	28	-16	1
HES-D-IL-2	225	31	-6	0.31

2.2.2 IL-2-Induced Proliferation of CTLL-2 Cells

In order to examine the biological activity of azide-functionalized IL-2 (IL-2-N_3) and IL-2 linked to the surface of HES-D capsules, both IL-2-N_3 and HES-D-IL-2 capsules were applied on the murine cytotoxic T cell line CTLL-2.

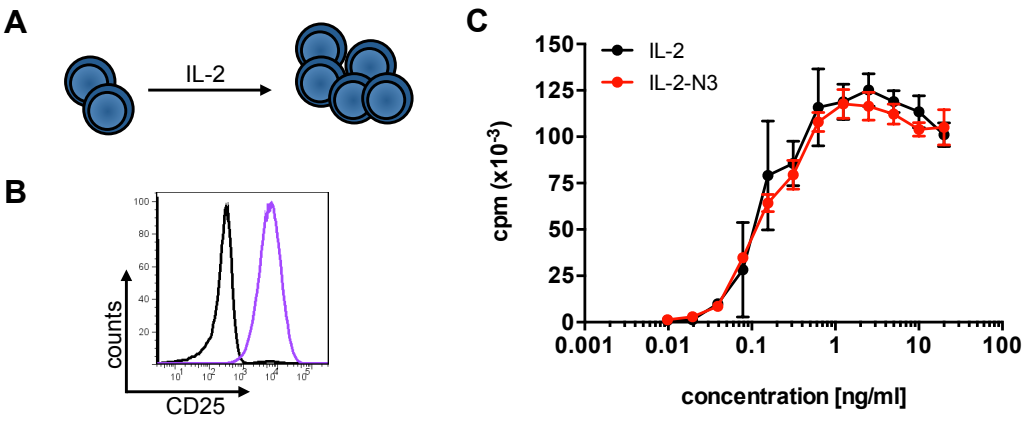

Figure 13. IL-2-dependent CTLL-2 proliferation. (A) Schematic figure of CTLL-2 cells growing IL-2-dependently. (B) Expression of CD25, the alpha subunit of IL-2R, on CTLL-2 cells was analyzed by flow cytometry. Cells were stained with anti-CD25-APC mAb. CD25 expression (purple) was compared to isotype control (black) and CD25 expression was plotted against the number of counted cells. (C) Different concentrations of IL-2 (1:2 dilutions; starting with 20 ng/ml) were used for CTLL-2 stimulation. Unfunctionalized IL-2 (black) was compared to azide-functionalized IL-2 (IL-2-N_3) (red). Proliferation was assessed by a [^{3}H]-thymidine assay measuring counts per minute (cpm). One representative experiment depicts the mean ± SD from pooled data of measured triplicates.

Cloned CTLL-2 cells are derived from a C57BL/6 mouse and grow IL-2-dependently (Figure 13A). To determine the expression level of the alpha subunit (CD25) of the IL-2R on CTLL-2 cells, the murine tumor cell line was stained with anti-mouse-CD25 mAbs and analyzed by flow cytometry. All measured CTLL-2 cells were found to express CD25 homogeneously on their cell surface (Figure 13B).

As the azide-functionalization of IL-2 may change the quaternary arrangement of the cytokine, IL-2-N_3 was titrated on CTLL-2 cells against wild-type IL-2 and proliferation was measured in a [^{3}H]-thymidine proliferation assay. The CTLL-2 proliferation assay verified that

the azide-functionalized IL-2 was still biologically active by detecting comparable CTLL-2 proliferation induced by azide-functionalized and unfunctionalized IL-2 (Figure 13C). The EC_{50} value of IL-2 stimulation describes the concentration of cytokine that is required to attain the half-maximal response of CTLL-2 proliferation. Unfunctionalized IL-2 and IL-2-N_3 exhibited similar EC_{50} values of 0.082 ng/ml and 0.117 ng/ml, respectively.

Prior to testing the biological activity of IL-2 linked to the HES capsule surface the amount of IL-2 in the HES-D-IL-2 capsule suspension was measured by ELISA. Since the HES-D-IL-2 NCs were dialyzed against 0.9% NaCl saline and centrifuged twice after IL-2 linkage, the two supernatants obtained during purification were additionally analyzed for the amount of soluble IL-2.

Table 3. ELISA quantification of IL-2 linked to HES capsules and soluble IL-2 present in the supernatant.

Sample	IL-2 [ng/ml]
HES-D-IL-2	2022
HES-D-IL-2 SN1	646100
HES-D-IL-2 SN2	22.8

ELISA measurements depicted 2022 ng/ml IL-2 in the capsule suspension (Table 3). As ELISA measurements are based on a sandwich array, not all IL-2 molecules bound to the capsule surface may be accessible for ELISA measurements. The actual amount of IL-2 on the capsule surface is most probably higher. The first supernatant, HES-D-IL-2 SN1, received during HES-D-IL-2 purification contained 646100 ng/ml IL-2, whereas the second supernatant, HES-D-IL-2 SN2, showed a considerably diminished amount of IL-2 with 22.8 ng/ml IL-2. This reduction in the amount of soluble IL-2 present in the second supernatant (HES-D-IL-2 SN2) already indicated reduced levels of soluble IL-2 in the HES-D-IL-2 NC supernatant, excluding a significant effect of soluble IL-2 in the following experiments.

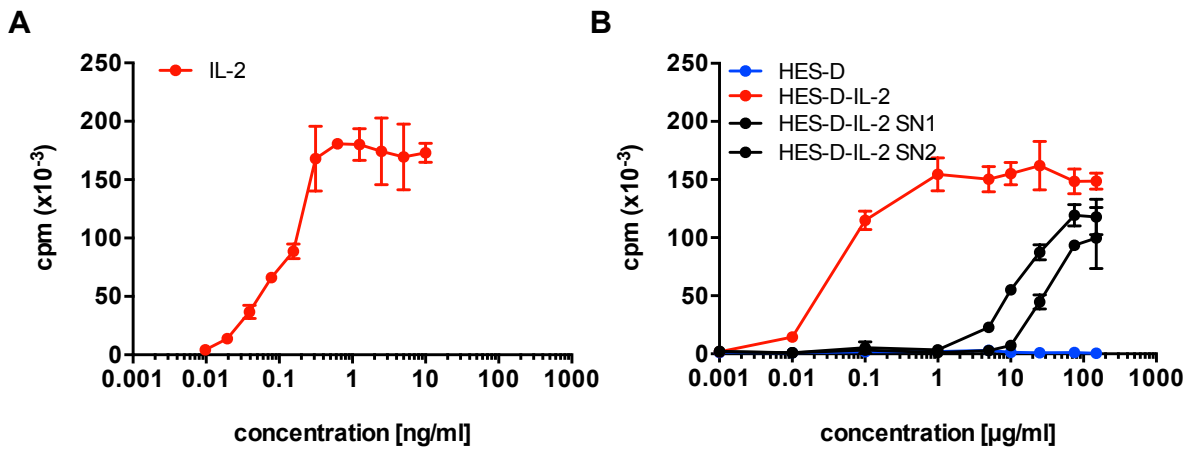

Figure 14. CTLL-2 proliferation assay with HES-D-IL-2 nanocapsules. CTLL-2 proliferation was determined by a [^{3}H]-thymidine assay measuring thymidine incorporation as counts per minute (cpm). One representative experiment of triplicates is shown (mean ± SD). (A) Unfunctionalized IL-2 was titrated on CTLL-2 cells for control (1:2 dilutions; starting from 10 ng/ml). (B) CTLL-2 cells were treated with different concentrations of HES-D-IL-2 NCs. HES-D capsules served as a control. The two supernatants (HES-D-IL-2 SN1 and HES-D-IL-2 SN2) obtained during HES-D-IL-2 purification after dialysis were additionally titrated on CTLL-2 cells comparable to the NC volume used for HES-D-IL-2 titration.

In addition to IL-2-N_3, the biological activity of HES-D-IL-2 NCs was determined on CTLL-2 cells to exclude steric hindrance of IL-2 for interacting with IL-2R or alteration of IL-2 confirmation after NC linkage. CTLL-2 cells were stimulated with different concentrations of HES-D-IL-2 and HES-D NCs for 48 h before the cells were exposed to [^{3}H]-thymidine for 16 h and proliferation was measured. For control, unfunctionalized IL-2 was titrated on CTLL-2 cells as well. The supernatants that were obtained during centrifugation after dialysis were also incubated with CTLL-2 cells with the same volume as HES-D-IL-2 NCs. Analysis of unfunctionalized IL-2 demonstrated proliferation of CTLL-2 cells with an EC_{50} value of 0.096 ng/ml (Figure 14A). Titration of HES-D-IL-2 NCs on CTLL-2 cells induced proper proliferation of CTLL-2 cells with an EC_{50} value of 0.041 µg/ml (Figure 14B). Applying a concentration of approximately 1 µg/ml HES-D-IL-2 NCs resulted already in the maximal stimulation of CTLL-2 cells. The two supernatants derived from HES-D-IL-2 purification, HES-D-IL-2 SN1 and HES-D-IL-2 SN2, also induced CTLL-2 proliferation, but at a much lower level compared to the IL-2-functionalized NCs.

Altogether, titration of IL-2-N_3 and HES-D-IL-2 NCs on CTLL-2 cells induced consistent CTLL-2 proliferation indicating that the azide-functionalized IL-2 and IL-2 linked to the capsule surface were still biologically functional.

2.2.3 HES-D-IL-2 Nanocapsule Uptake by $CD4^+CD25^{high}$ T Cells

Only 1-2% cells of peripheral blood mononuclear cells (PBMCs) represent $CD4^+CD25^+Foxp3^+$ Tregs.[124] In order to perform uptake kinetics with different NC concentrations, higher cell numbers were required than the amount of Tregs that can be obtained from buffy coats. Thus, for uptake studies of HES-D-IL-2 NCs by T cells, primary human $CD4^+$ T cells were isolated from PBMCs and activated for elevated expression of IL-2Rα subunit CD25.

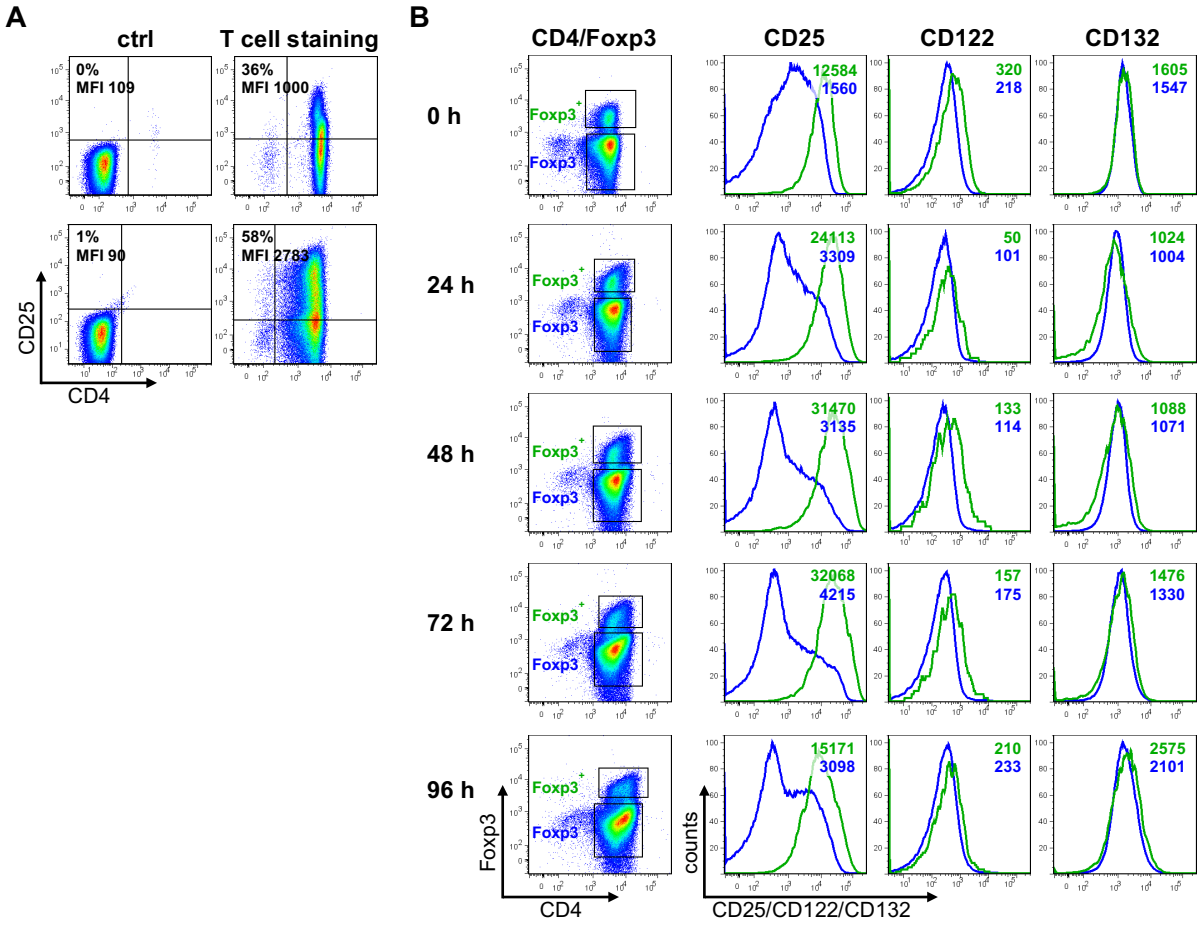

Figure 15. Activation of isolated $CD4^+$ T cells from PBMCs. $CD4^+$ T cells were isolated from PBMCs and stimulated with anti-CD3 and anti-CD28 mAbs for 16 h and analyzed by flow cytometry. (A) CD25 expression on $CD4^+$ T cells directly after isolation (upper row) and after stimulation with anti-CD3 and anti-CD28 mAbs for 16 h (lower row). CD25 detection (y-axis) was plotted against $CD4^+$ T cells (x-axis). Isotype stained T cells were taken as control for gating. (B) Following anti-CD3 and anti-CD28 mAb stimulation, $CD4^+CD25^{high}$ T cells were cultured for 96 h with 50 U/ml IL-2. Expression of CD25, CD122 and CD132 was analyzed every 24 h. For this purpose, $CD4^+$ T cells were gated for $Foxp3^+$ (green) and $Foxp3^-$ (blue) cells. Detection of the distinct cell surface markers (x-axis) was plotted against the amount of measured cells (y-axis) and the assessed mean fluorescence intensity values were included in the plots.

Isolation of $CD4^+$ T cells from PBMCs was performed using anti-human-CD4 microbeads and T cells were stimulated for 16 h with anti-CD3 and anti-CD28 mAbs. The level of CD25 expression was measured before and after CD3/CD28 stimulation by flow cytometry. Post isolation, 36% of $CD4^+$ T cells expressed CD25 at a MFI value of 1000 (Figure 15A). In contrast, anti-CD3 and anti-CD28 mAb stimulation increased the amount of $CD4^+CD25^+$ double positive T cells to 58% with an MFI of 2783. Activated $CD4^+CD25^{high}$ T cells were cultured with 50 U/ml IL-2 for another four days and expression levels of the three subunits of IL-2R, comprising CD25, CD122 and CD132, were analyzed every 24 h by flow cytometry. Additionally, the cells were stained intracellular for the transcription factor Foxp3, primarily expressed in Tregs, but also at low levels in activated $CD4^+$ Teff cells in humans.[23] Activated $CD4^+CD25^{high}$ T cells were discriminated between $CD4^+Foxp3^-$ and $CD4^+Foxp3^+$ T cells and histograms for expression of CD25, CD122 and CD132 were compared. Prior to IL-2 stimulation (0 h) $CD4^+Foxp3^+$ T cells showed higher CD25 expression (MFI 12584) than $CD4^+Foxp3^-$ T cells (MFI 1560) (Figure 15B). In both T cell populations CD25 expression increased to an expression peak at 72 h after IL-2 stimulation with $CD4^+Foxp3^-$ T cells exhibiting an MFI value of 4215 and $CD4^+Foxp3^+$ T cells featuring an MFI value of 32068. Expression of CD25 slightly decreased in both populations 96 h after IL-2 stimulation compared to 72 h. Expression of CD122 by $CD4^+Foxp3^-$ and $CD4^+Foxp3^+$ T cells was not as inducible as CD25 by IL-2 stimulation (Figure 15B). CD132 was constitutively and equally expressed before and 96 h after IL-2 stimulation on both $CD4^+Foxp3^-$ and $CD4^+Foxp3^+$ T cell populations.

The analysis of IL-2R expression on CD3/CD28 activated $CD4^+CD25^{high}$ T cells cultured with IL-2 revealed that CD25 expression was highly inducible over time, whereas CD122 and CD132 were constitutively expressed.

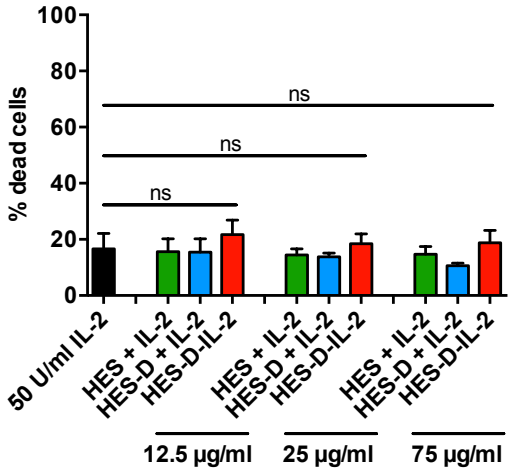

Figure 16. $CD4^+CD25^{high}$ T cell viability measured by flow cytometry. $CD4^+CD25^{high}$ T cells were treated with 12.5, 25 and 75 µg/ml HES-D-IL-2 for 72 h and dead cells were measured using the Viability Dye eFluor® 780. Control nanocapsules, HES and HES-D, supplemented with 50 U/ml IL-2 were additionally examined. Untreated $CD4^+CD25^{high}$ T cells cultured with 50 U/ml IL-2 were taken as control. Mean ± SD values of three independent experiments are presented (ns = not significant).

Before applying nanomaterials on *in vitro* and *in vivo* investigations, possible cytotoxicity of the nanomaterial has to be excluded. Hence, $CD4^+$ T cells, that were anti-CD3 and anti-CD28 mAb stimulated 16 h for inducing $CD4^+CD25^{high}$ T cells, were stimulated with different concentrations of HES-D-IL-2 NCs for 24 h and 72 h and the amount of dead cells was assessed with the Viability Dye eFluor® 780 by flow cytometry. IL-2-functionalized HES NCs induced no significant increase of dead $CD4^+CD25^{high}$ T cells as analyzed at 24 h (data not shown) and at 72 h after NC addition compared to control cells stimulated with IL-2 alone (Figure 16). Unfunctionalized HES and HES-D NCs supplemented with soluble IL-2 were additionally applied on $CD4^+CD25^{high}$ T cells, but the amount of dead cells was not significantly increased compared to IL-2-treated $CD4^+CD25^{high}$ T cells.

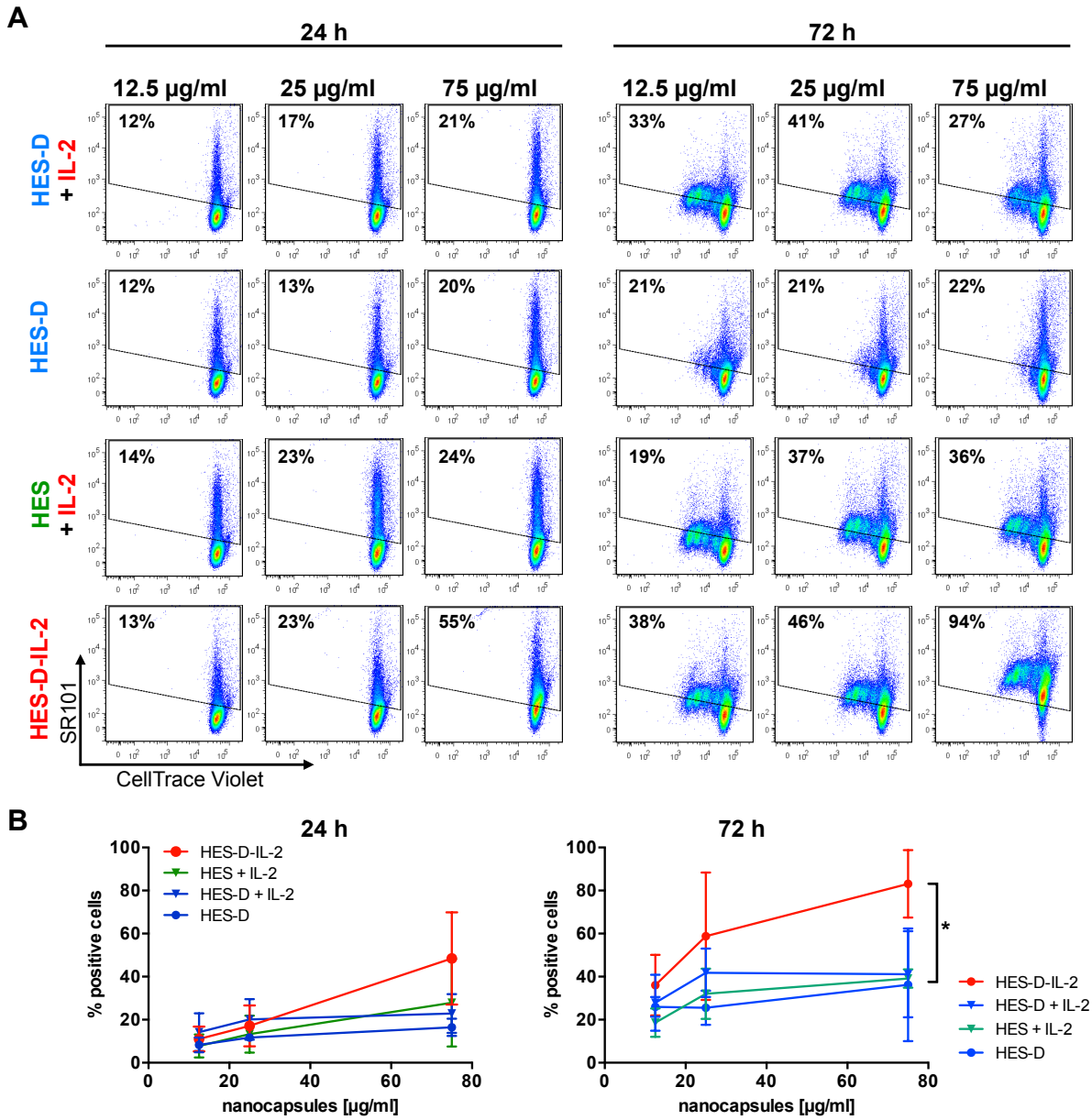

Figure 17. Uptake of HES nanocapsules by $CD4^{+}CD25^{high}$ T cells assessed by flow cytometry. $CD4^{+}CD25^{high}$ T cells were stimulated with HES-D, HES and HES-D-IL-2 at 12.5, 25 and 75 µg/ml for 24 and 72 h. Control capsules (HES, HES-D) were applied together with 50 U/ml IL-2. HES-D NCs were additionally administered alone. (A) Measured CellTrace™ Violet intensity was plotted against the NC-dye SR101. The gating strategy for measuring the amount of NC-positive cells was based on untreated T cells stimulated with 50 U/ml IL-2. Percentages of capsule-positive cells are indicated in the plots. (B) Summary of three independent experiments shows the NC uptake at different concentrations after 24 and 72 h (mean ± SD; * $p < 0.05$).

For uptake studies of HES-D-IL-2 NCs by T cells, isolated $CD4^{+}$ T cells were stained with the proliferation dye CellTrace™ Violet to examine IL-2-induced T cell proliferation in flow cytometry simultaneously to the uptake measurements. CellTrace™ Violet penetrates intact cell membranes and is not ejected upon cell division due to its covalent linkage to intracellular proteins.[125] Hence, the CellTrace™ Violet stain is diluted with each division cycle

of the mother cell. Anti-CD3 and anti-CD28 mAb activated $CD4^+CD25^{high}$ T cells were stimulated with 12.5, 25 and 75 µg/ml HES-D-IL-2 NCs for 96 h and every 24 h cell samples were taken for flow cytometry analysis. In Figure 17A representative dot plots of one experiment are depicted illustrating the measured amount of NC-positive T cells (y-axis) against proliferation (x-axis) 24 h and 72 h after NC addition. HES-D-IL-2 NCs showed a gradual association with or uptake by $CD4^+CD25^{high}$ T cells with 55% positive cells at a concentration of 75 µg/ml 24 h after NC addition (Figure 17A). Assessing NC uptake 72 h after NC addition, confirmed a dose- and time-dependent increase of HES-D-IL-2 NC-positive cells. At the highest concentration applied, almost all cells (94%) were detected positive for the HES-D-IL-2 NC-dye SR101. In contrast, control NCs that were administered together with soluble IL-2 (HES + IL-2, HES-D + IL-2) or alone (HES-D) resulted in less than 40% NC-positive $CD4^+CD25^{high}$ T cells at the highest concentration used 24 h and 72 h after NC addition. Proliferation of $CD4^+CD25^{high}$ T cells, which readout is seen by a shift of the stained T cell population on the x-axis from the right to left, was only visible 72 h after T cell culture (Figure 17A). Control NCs applied together with soluble IL-2 and HES-D-IL-2 NCs showed comparable T cell proliferation, whereas control HES-D NCs lacking soluble IL-2 did not induce $CD4^+CD25^{high}$ T cell proliferation.

Pooled data of three independent experiments were summarized in Figure 17B. 24 h after NC addition (75 µg/ml) only a moderate increase between HES-D-IL-2 NCs and control HES NCs in NC-positive cells was detected. However, 72 h after NC addition, at a concentration of 75 µg/ml HES-D-IL-2 NCs caused a significantly increased amount of NC-positive cells compared to controls, including HES-D + IL-2, HES + IL-2 and HES-D. The difference between IL-2-functionalized HES capsules and control NCs regarding the amount of NC-positive $CD4^+CD25^{high}$ T cells was most obvious at elevated concentrations.

Altogether, stimulation of $CD4^+CD25^{high}$ T cells with HES-D-IL-2 NCs showed a time- and dose-dependent increase in NC-positive cells peaking at a concentration of 75 mg/ml 72 h after NC addition. Additionally, HES-D-IL-2 capsules were found to induce profound proliferation of primary $CD4^+CD25^{high}$ T cells.

2.2.4 Confocal Laser Scanning Microscopy of HES-D-IL-2 Nanocapsule Uptake by $CD4^+CD25^{high}$ T Cells

By use of flow cytometry for analyzing the amount of NC-positive cells, it cannot be discriminated between intracellular located NCs and NCs associated with the cell membrane. Therefore, confocal laser scanning microscopy (cLSM) was conducted to investigate cellular distribution of NCs and to confirm the results obtained by flow cytometry.

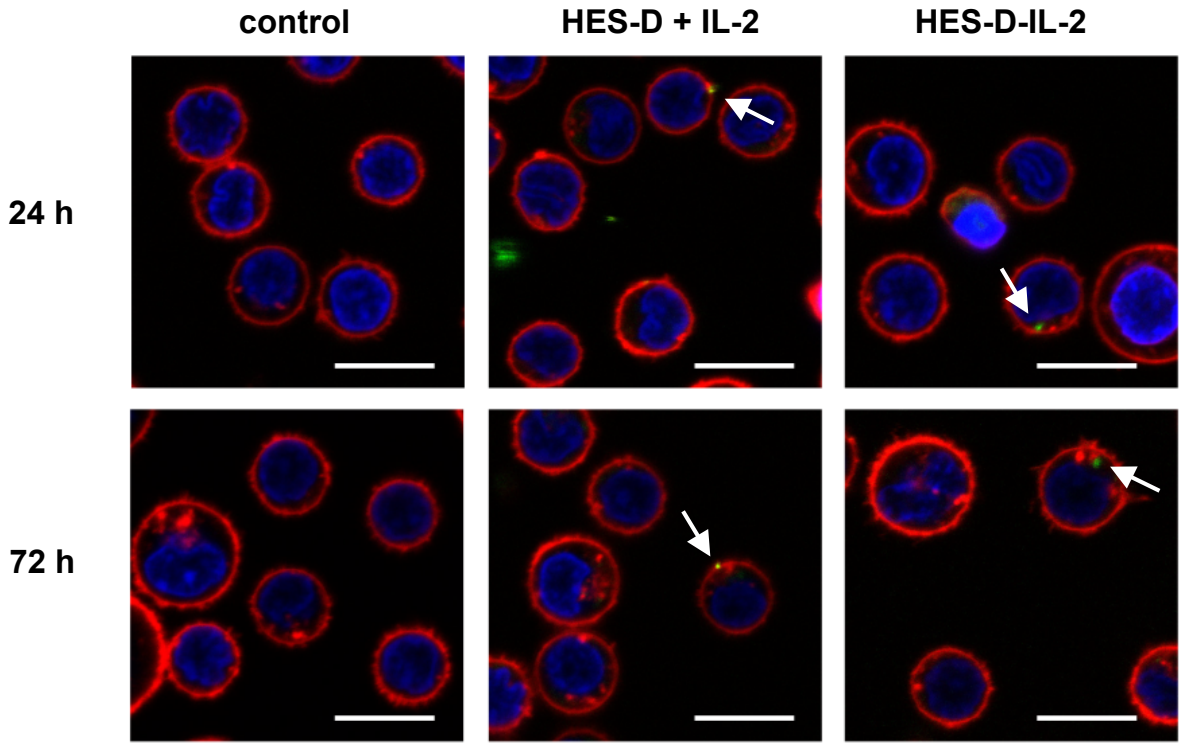

Figure 18. Confocal laser scanning microscopy of NC-treated $CD4^+CD25^{high}$ T cells. PBMC-derived $CD4^+CD25^{high}$ T cells were stimulated with 75 µg/ml HES-D-IL-2 for 24 and 72 h. Control HES-D nanocapsules were applied together with 50 U/ml soluble IL-2. Cell nuclei (blue) and cell membrane (red) were stained with Hoechst and CellMask™ Deep Red Plasma membrane stain, respectively. Nanocapsules (green) were detectable by the incorporated fluorescent dye SR101. White arrows indicate nanocapsules. Scale bar represents 10 µm.

Activated $CD4^+CD25^{high}$ T cells were incubated with 75 µg/ml HES-D-IL-2 or HES-D NCs supplemented with soluble IL-2 and cLSM was performed 24 h and 72 h after NC addition. Untreated $CD4^+CD25^{high}$ T cells served as controls. Before microscopy, cell membranes and nuclei were stained with CellMask™ Deep Red Plasma membrane stain and Hoechst 33342 nucleic acid stain, respectively. HES-D-IL-2 NCs (green) were predominantly found to be located intracellular in $CD4^+CD25^{high}$ T cells, whereas HES-D NCs (green) supplemented with soluble IL-2 were repeatedly associated with the cell membranes as indicated by the white arrows (Figure 18). The overall detection signal of nanocapsules was not very strong.

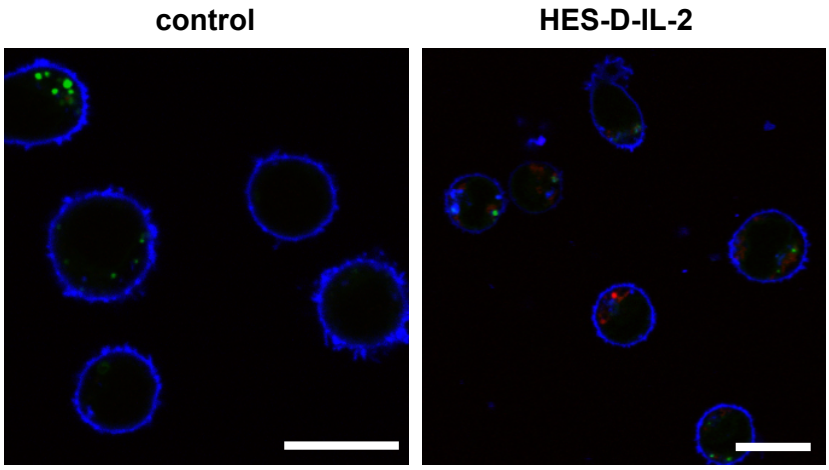

Figure 19. Confocal laser scanning microscopy of lysosome-stained $CD4^+CD25^{high}$ T cells. $CD4^+CD25^{high}$ T cells were stimulated with 75 µg/ml HES-D-IL-2 NCs for 24 h. $CD4^+CD25^{high}$ T cells stimulated with 50 U/ml IL-2 were taken as control. Cell membrane (blue) and lysosomes (green) were stained with CellMask™ Deep Red Plasma membrane stain and LysoTracker® Green, respectively. Nanocapsules (red) were detected through the incorporated fluorescent dye SR101. Scale bar represents 10 µm.

In addition to HES-D-IL-2 NC uptake analyzed by cLSM, the intracellular localization of NCs was investigated more closely by additionally staining lysosomes with LysoTracker®. Untreated $CD4^+CD25^{high}$ T cells were taken as controls. The finding that intracellular HES-D-IL-2 NCs (red) were not co-localized with lysosomes (green) indicated that the internalized capsules were not entrapped in lysosomes 24 h after NC addition (Figure 19).

All in all, cLSM analysis confirmed the internalization of HES-D-IL-2 NCs by $CD4^+CD25^{high}$ T cells. Co-staining of lysosomes indicated that HES-D-IL-2 capsules were not localized in lysosomal vesicles.

2.2.5 High versus Low Amounts of IL-2 Bound to Hydroxyethyl Starch Nanocapsules

IL-2 targeting highly depends on the expression level of the IL-2R, in particular on CD25, as CD25 is required for the high affinity IL-2R.[62,63] The high-affinity trimeric IL-2 receptor is primarily expressed on $CD4^+CD25^+Foxp3^+$ Tregs and transiently on activated $CD4^+$ and $CD8^+$ T cells.[62,63] Thus, Tregs were found to be more susceptible to low-doses of IL-2 compared to activated $CD4^+$ Teff cells.[62,74] In the present study, the amount of IL-2 linked to the HES-D NC surface was varied by coupling half the amount of IL-2 compared to the level of IL-2 used for HES-D-IL-2 NC synthesis to determine the influence of different IL-2 levels for cell type-specific uptake and proliferation induction.

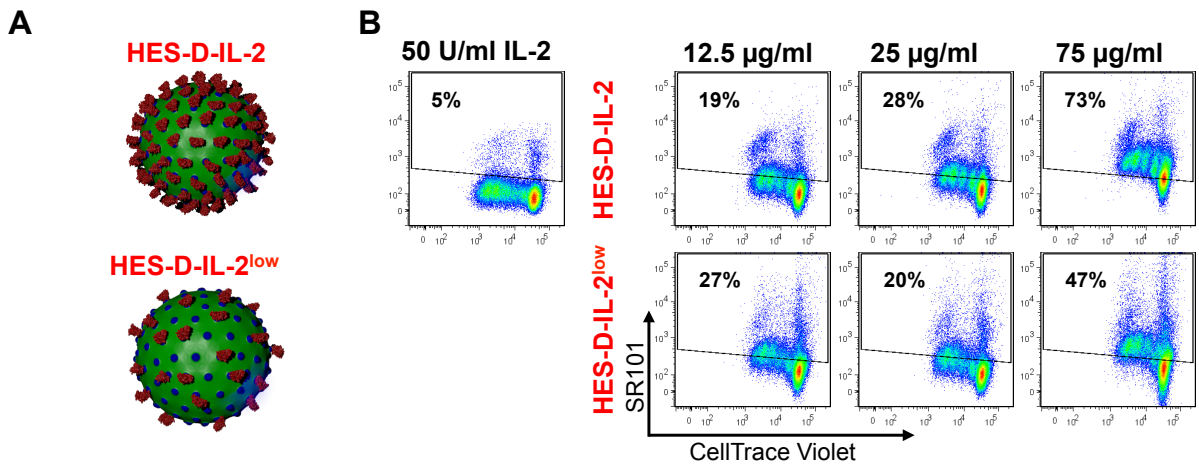

Figure 20. High versus low amounts of IL-2 linked to HES nanocapsules. (A) Schematic figure of HES-D-IL-2 and HES-D-IL-2^{low} exhibiting different amounts of IL-2 on the capsule surface. HES-D-IL-2^{low} NCs were coupled with half the amount of IL-2 compared to HES-D-IL-2 capsules. (B) CD4^{+}CD25^{high} T cells were stimulated with HES-D-IL-2 and HES-D-IL-2^{low} at 12.5, 25 and 75 µg/ml for 72 h and NC uptake was assessed by flow cytometry. Untreated T cells cultured with 50 U/ml IL-2 served as controls. For uptake analysis, CellTrace™ Violet positive cells were plotted against the NC-dye SR101. Percentages of capsule-positive cells are depicted in each plot.

HES-D NCs that were functionalized with half the amount of IL-2 compared to HES-D-IL-2 NCs were termed "HES-D-IL-2^{low}" NCs (Figure 20A) (kindly synthesized by [redacted]). ELISA measurements of HES-D-IL-2^{low} NCs revealed a relative IL-2 concentration of 968 ng/ml, whereas HES-D-IL-2 capsules had a relative IL-2 concentration of about 2022 ng/ml. Both IL-2-functionalized HES capsules showed similar physico-chemical properties including equal amounts of the fluorescent dye SR101 (data not shown).

CellTrace™ Violet-stained CD4^{+}CD25^{high} T cells were stimulated with HES-D-IL-2 and HES-D-IL-2^{low} NCs for 72 h at 12.5, 25 and 75 µg/ml and analyzed by flow cytometry for NC uptake. Untreated control CD4^{+}CD25^{high} T cells stimulated with IL-2 alone were taken as controls. HES-D-IL-2 NCs showed a gradual uptake by activated CD4^{+}CD25^{high} T cells with 73% NC-positive cells at a concentration of 75 µg/ml (Figure 20B). In contrast, HES-D-IL-2^{low} NC treatment (75 µg/ml) of activated CD4^{+}CD25^{high} T cells resulted in 47% NC-positive cells. The differences between HES-D-IL-2 and HES-D-IL-2^{low} NC uptake by activated T cells were very remarkable with HES-D-IL-2^{low} NCs revealing a decreased uptake by CD4^{+}CD25^{high} T cells compared to HES-D-IL-2 NCs. However, after application of low NC concentrations (12.5 µg/ml) no pronounced differences in the uptake between HES-D-IL-2^{low} and HES-D-IL-2 were detected.

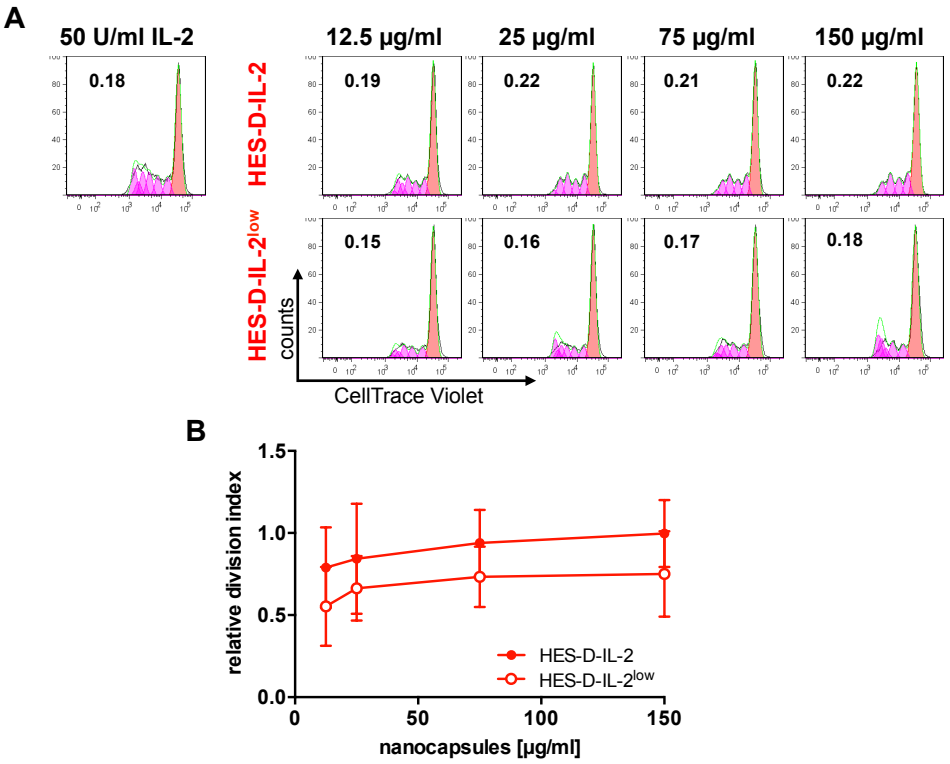

Figure 21. Proliferation-inducible potential of HES-D-IL-2 versus HES-D-IL-2^{low} nanocapsules. (A) CD4^{+}CD25^{high} T cells were stimulated with HES-D-IL-2 and HES-D-IL-2^{low} at 12.5, 25, 75 and 150 µg/ml for 72 h and proliferation was determined by measuring the dilution of the proliferation dye CellTrace™ Violet with flow cytometry. Representative histograms of HES-D-IL-2- and HES-D-IL-2^{low}-induced CD4^{+}CD25^{high} T cell proliferation at 72 h after capsule addition. Dilution of the proliferation dye CellTrace™ Violet (x-axis) expressed as division index is depicted in each histogram graph. Untreated cells cultured with 50 U/ml IL-2 were taken as control. (B) The division index of each sample was accounted by FlowJo and normalized to the division index of 50 U/ml IL-2 stimulated control cells. Mean ± SD from three independent experiments are shown.

In addition to NC uptake, the potential of HES-D-IL-2 and HES-D-IL-2^{low} NCs to induce T cell stimulation was addressed. Therefore, both IL-2-functionalized NCs were titrated on CTLL-2 cells and proliferation was measured in a [^{3}H]-thymidine assay. At lower NC concentrations HES-D-IL-2 NC-induced CTLL-2 proliferation was slightly increased compared to HES-D-IL-2^{low} NC-induced CTLL-2 proliferation (data not shown). Unfunctionalized control HES-D NCs did not induce CTLL-2 proliferation.

Besides CTLL-2 cell proliferation, proliferation of primary activated CD4^{+}CD25^{high} T cells was examined. For this purpose activated CD4^{+}CD25^{high} T cells were treated with HES-D-IL-2 and HES-D-IL-2^{low} NCs at various concentrations and proliferation was assessed based on the proliferation dye CellTrace™ Violet. The division index describing the average division number of all measured cells in each sample was quantified with FlowJo software.[126] Representative proliferation histograms underlined the higher proliferative potential of CD4^{+}CD25^{high} T cells by HES-D-IL-2 NC stimulation compared to HES-D-IL-2^{low} NCs (Figure 21A). Comparing division indices, that were normalized to control cells stimulated with

soluble IL-2 alone, showed that the relative division indices of HES-D-IL-2 NCs were slightly higher compared to HES-D-IL-2^{low} NCs (Figure 21A and B). However, both NCs induced a slight increase in T cell proliferation with elevated concentrations.

Altogether, the differences between HES-D-IL-2 and HES-D-IL-2^{low} NC uptake by CD4^{+}CD25^{high} T cells were most apparent at higher concentrations. IL-2-dependent proliferation of CTLL-2 cells and primary CD4^{+}CD25^{high} T cells revealed differences between HES-D-IL-2 and HES-D-IL-2^{low} NCs at lower concentration.

2.2.6 Cell Type-Specific Uptake of HES-D-IL-2 Nanocapsules *In Vivo*

So far the insights into the functionality of IL-2-functionalized HES NCs for cell type-specific targeting of CD4^{+}CD25^{high} T cells were derived from *in vitro* investigations. In order to determine the distribution of HES NCs that were labeled with the fluorescent dye SR101 into distinct organs and to address the cell type-specific uptake *in vivo*, HES-D-IL-2 nanocapsules were administered in mice.

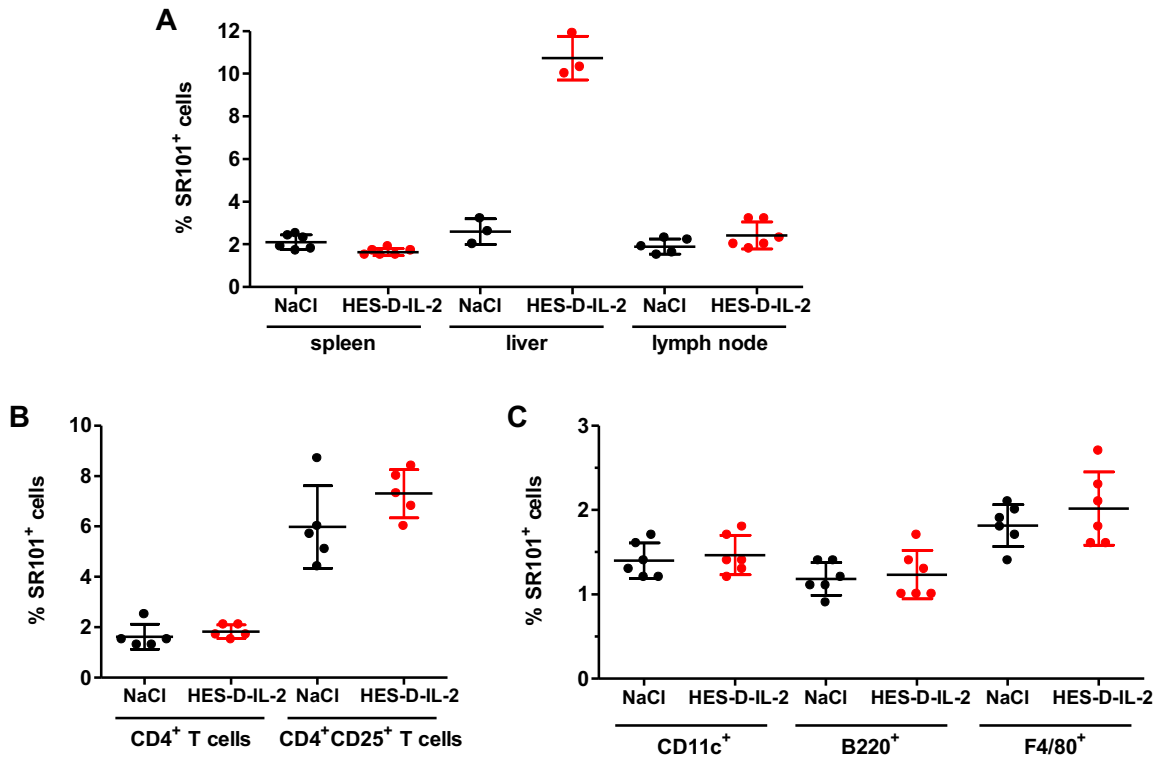

Figure 22. Application of HES-D-IL-2 nanocapsules *in vivo*. HES-D-IL-2 nanocapsules were intravenously injected into C57BL/6 mice, followed by euthanizing the mice 24 h post injection for organ extraction, and flow cytometry analysis. NaCl treated mice were taken as controls. Mean ± SD from three to six mice are shown. (A) Splenocytes, liver cells and lymph node cells were isolated and examined for percentage of SR101-labeled HES-D-IL-2 NC-positive cells. (B) Additionally, lymph node cells were stained with anti-CD4 mAbs alone and with anti-CD4 mAbs together with anti-CD25 mAbs. (C) Lymph node cells were stained for cell surface markers of antigen-presenting cells, including CD11c, B220, F4/80, and analyzed for the amount of SR101-positive cells. Mean ± SD values of three to five different mice are presented.

C57BL/6 mice were intravenously injected with 300 µg HES-D-IL-2 NCs and the presence of NCs was measured in lymph nodes, the spleen and liver 24 h after NC administration. HES-D-IL-2 NC injection corresponds to approximately $1.5x10^{12}$ NCs/mouse. Injection of 0.9% NaCl solution into mice served as negative control. Flow cytometry analysis of unstained splenocytes from HES-D-IL-2 NC-treated mice showed no cell uptake of NCs (Figure 22A). On the contrary, around 10% of liver cells were detected positive for the NC-dye SR101. Unstained lymphocytes were analyzed for detection of NC-positive cells as well, but only a slight increase in the total amount of NC-positive cells was detectable (Figure 22A). Lymph node cells were analyzed in more detail by staining various cell surface molecules. Gating for $CD4^+$ T cells revealed a minor increase in NC-positive cells, whereas gating on $CD4^+CD25^+$ T cells showed a higher increase of NC-positive cells (Figure 22B). To exclude the possibility that antigen-presenting cells take up the administered capsules, lymph node-derived DCs, macrophages and B cells were additionally analyzed. $CD11c^+$ DCs and $B220^+$ B cells

featured no increase in NC-positive cells, while F4/80$^+$ macrophages depicted a slight shift of NC-positive cells (Figure 22C).

Cell type-specific uptake *in vivo* was not as decisive as *in vitro* investigations, but showed slight HES-D-IL-2 NC uptake by CD4$^+$CD25$^+$ T lymphocytes. Further studies with a higher number of mice are required to shed light on HES-D-IL-2 NC uptake by T cells *in vivo*. Additionally, using murine models of inflammation or mice, which were polyclonally stimulated for enhanced T cell activation, may enable better assessment of NC-specific uptake by CD4$^+$CD25$^+$ T cells.

3 Discussion

3.1 SEMA and VBPA Polystyrene Nanoparticle-Induced Immunity

Intensive research is currently dedicated to the generation of engineered nanomaterials as a drug delivery system in cancer immunotherapy.[95,96] Various characteristics, including surface functionalization, size and zeta potential, may highly affect the biological properties of nanoparticles with regard to biodistribution, cellular uptake and immunogenicity.[100,127-129] Polystyrene nanoparticles generated by miniemulsion polymerization serve as a good model system to determine the influence of physico-chemical properties on the uptake and immunogenicity of the particles due to their high stability and their minor size distribution. Thus, in the present study the uptake and immunogenicity of sulfonate- and phosphonate-functionalized polystyrene nanoparticles was assessed by use of human monocyte-derived dendritic cells.

3.1.1 Time- and Dose-Dependent Uptake of Polystyrene Nanoparticles

All three analyzed polystyrene nanoparticles (NPs) were internalized by immature dendritic cells (iDCs) and mature dendritic cells (mDCs). Rejman et al. already reported that polystyrene NPs with a size below 500 nm are internalized energy-dependently. Moreover, NPs that are sized below 200 nm were found to be engulfed via clathrin-coated pits, whereas increasing NP size leads to a caveolae-mediated uptake.[130]

In the present study, unfunctionalized polystyrene (PS) NPs that reveal a slightly diminished size of 175 nm featured a slower uptake by iDCs compared with SEMA- and VBPA-functionalized polystyrene NPs (Figure 7). Moreover, regarding mean fluorescence intensity (MFI) values, unfunctionalized PS NP uptake per cell was tremendously decreased. Previous investigations described a size-dependent uptake of polystyrene nanoparticles with a diminished particle size to be positively correlated with increased uptake by DCs.[120,130] The uptake of polystyrene NPs by hepatocytes was also size-dependent with NPs exhibiting a size of 20 nm showed an enhanced uptake compared to 200 nm sized NPs.[131] Foged at al. additionally discovered that uptake can be regulated by altering NP surface charge as positively charged NPs exhibit elevated interactions with DCs.[120] Unfunctionalized PS NPs possessed a lower size and a more neutral zeta potential than the negatively charged SEMA and VBPA NPs and thus, should foster a better uptake with regard to current literature. Therefore, the reduced uptake of PS NPs by DCs is most likely due to the lacking surface functionalization, as the functionalization was the only characteristic, besides size and zeta potential, that distinguished unfunctionalized PS NPs from SEMA and VBPA NPs. Due to the

fact that unfunctionalized PS NPs showed a considerable lower degree of internalization per DC, they were not included in subsequent investigations. Tremendous differences in the amount of NPs per cell may influence immunogenicity.

Uptake studies of SEMA and VBPA NPs by iDCs revealed a dose- and time-dependent uptake as assessed by flow cytometry. At the two highest concentrations used (75 and 150 µg/ml), almost all cells were positive for the NP-dye PMI 18 h after NP addition. In contrast, MFI analysis showed that even 18 h after NP addition iDCs still continued taking up SEMA and VBPA NPs per cells indicating that the uptake capacity of iDCs was not saturated yet. Comparing iDC with mDC uptake depicted only marginal differences in the amount of NP-positive cells (Figure 8A). In contrast, MFI measurements displayed a considerable difference between iDC and mDC internalization of SEMA- and VBPA-functionalized NPs (Figure 8B). Additionally, confocal laser scanning microscopy (cLSM) analysis indicated a slightly reduced abundance of SEMA and VBPA NPs in mDCs compared to iDCs (Figure 9). This difference between iDC and mDC NP uptake may be due to the fact that iDCs are characteristic for their high endocytic capacity and antigen presentation, whereas mDCs feature a pronounced T cell stimulatory potential.[9,14] DC maturation is accompanied with a diminished ability of mDCs for endocytosis that results from their downregulation of endocytic receptors.[9,14] Various studies assessed NP uptake by iDCs, whereas only few investigations concentrated on the simultaneous determination of NP uptake by mDCs. However, Bartneck et al. depicted that NP charge primarily influences NP uptake by DCs.[132] Within that study positively charged gold NPs showed an enhanced uptake by mDCs with a higher percentage of NP-positive cells compared to iDCs, whereas treatment with negatively charged gold NPs resulted in an increased amount of NP-positive iDCs compared to mDCs.[132]

Between the two functionalized NPs, VBPA polystyrene NPs showed a slight increase in NP internalization by iDCs at higher concentrations compared to SEMA NPs as confirmed by flow cytometry and cLSM analysis (Figure 8 and Figure 9). This discrepancy may be caused by the different surface functionalization, but has to be addressed in future investigations.

In general, the polystyrene NP uptake presented here and in previous studies showed that many factors influence particle uptake by human cells. The awareness that NP size and surface charge highly affect internalization allows tuning the particles more attractively for improved uptake.[94,100] Besides reduced size, it was found that a more positive zeta potential is positively correlated with an increased tumor targeting and uptake.[94,120] However, amino-functionalized polystyrene NPs cause higher cytotoxic effects on HeLa cells and NIH 3T3 fibroblasts than carboxy-functionalized NPs.[133] Other studies confirmed that highly cationic

NPs are cytotoxic by causing cell membrane damage and thus, disclose that a compromise between increased uptake and cytotoxicity has to be found.[133,134]

In conclusion, the present study depicted a time- and dose-dependent uptake of SEMA and VBPA NPs by human monocyte-derived immature and mature DCs. Comparing NP uptake by iDCs and mDCs, iDCs revealed a slightly elevated uptake with a higher amount of NPs per cell. This may be due to the increased endocytic potential of iDCs in comparison with mDCs, but has to be elucidated in more detail in future studies.

3.1.2 SEMA and VBPA Nanoparticle-Induced DC Maturation Resulting in Th1 Response

Regarding the immunostimulatory effect of nanomaterials, various studies did not observe NP uptake by immune cells to be associated with induction of an immune response, whereas others found NP-induced DC maturation resulting in pronounced T cell activation.[135-137]

In the present study, it became apparent that the functionalized nanoparticles triggered DC maturation and induction of a Th1 response. SEMA- and VBPA-induced DC maturation was an intermediate state between immature and mature DCs. The expression of the co-stimulatory cell surface markers CD80 and B7-H2 as well as of the maturation marker CD83 were significantly increased in SEMA- and VBPA-treated iDCs compared with untreated control cells (Figure 10). CD80, CD86 and B7-H2 regulate T cell activation through CD28 and CTLA-4 present on the T cell surface.[16] CD28 is constitutively expressed on T cells, whereas CTLA-4 is induced upon T cell activation for counteracting CD28 T cell stimulation.[138,139] B7-H2, known as CD275 and inducible co-stimulator (ICOS) ligand, interacts with ICOS present on T cells mediating co-stimulatory T cell activation.[139] In addition to cell surface marker analysis, SEMA- and VBPA-induced DC maturation was accompanied by a significant increase in the cytokines IL-6, IL-12p40 and TNF-α post NP treatment (Figure 11). Activated DCs are known to produce IL-6, IL-12 and TNF.[140] Moreover, IL-6 and TNF-α, amongst GM-CSF, IL-4, IL-1β and PEG_2, are applied on iDCs for induction of DC maturation *in vitro*.[141] IL-12 is primarily expressed by activated DCs and moreover, is known to trigger Th1 differentiation and proliferation.[142,143] As aforementioned, the lipopolysaccharide (LPS) endotoxin of the bacterial cell wall induces DC maturation.[14] However, the detected DC maturation by polystyrene particles is most likely not related to endotoxin as the LAL test revealed no endotoxin levels higher than 0.06 EU/ml in the NP suspension.

In addition to phenotypic analysis of NP-treated DCs, the effector function of matured DCs to induce T cell proliferation was assessed. Indeed, SEMA- and VBPA-matured DCs induced

vast T cell proliferation associated with IFN-γ production, indicating a Th1 response. The Th1 cytokine IFN-γ mediates cellular immunity resulting in the killing of intracellular parasites.[22]

Collectively, cell surface marker analysis accompanied with measured cytokine production depicted SEMA and VBPA NP-induced iDC maturation. NP-induced iDC maturation was not as potent as cytokine-induced iDC maturation into terminally differentiated mDCs *in vitro* as the matured phenotype of NP-induced DCs was between iDCs and mDCs. However, the degree of NP-induced DC maturation can also be a matter of NP concentration and incubation time. Analysis of the effector function of NP-loaded DCs further underlined the potential of SEMA and VBPA NPs to trigger DC maturation. NP-loaded DCs induced a pronounced T cell proliferation compared to control iDCs with elevated levels of IFN-γ production indicating a Th1 immune response.

Several NPs were shown to disclose adjuvant properties by the induction of DC maturation.[135,136] Poly(lactic-co-glycolic acid) (PLGA) nanoparticles induced DC maturation with elevated expression levels of CD40, CD86 and CD80 on the DC surface.[135] Additionally, poly(γ-glutamic acid) NPs induced DC maturation and the investigators assigned the immunomodulatory potential of the particles to be Toll-like receptor TLR2- and TLR4-dependent.[144] Seong and Matzinger postulated that besides defined pathogen-associated molecular patterns (PAMPs) hydrophobic regions of molecules may act as a “danger signal” and induce an immune response through TLR signaling.[128] As polystyrene particles are very hydrophobic, in general, and SEMA and VBPA functionalization further fostered a hydrophobic potential, the hydrophobicity of the particles may represent an explanation for detected DC maturation. Previous investigations further demonstrated fullerene NP-induced DC maturation to be accompanied with a Th1 immune response.[136] Conway et al. even found that the application route and the size of poly-lactide-co-glycolide NPs are decisive for the induced T helper cell type differentiation.[145] Within that study microparticle treatment resulted in a Th1 response, whereas nanoparticles sized between 200 and 600 nm caused a Th2 response.[145] Other studies even further engineered nanoparticles with cationized proteins to shift an exclusive Th1 response towards a stronger Th2 response accompanied by a Th1 response.[146] The exact way by which SEMA and VBPA particles induce DC maturation resulting in T cell proliferation with an indicated Th1 response has to be addressed in future studies.

DCs are the most potent antigen-presenting cells that link innate with adaptive immunity and thus, are highly investigated for DC-based cancer immunotherapies.[147] The DC-based immunotherapy sipuleucel-T, which was FDA-approved in 2010, is based on *ex vivo* loading of DCs with tumor-peptides, DC activation and reintroduction into the patient to mount an

improved immune response against prostate cancer.[86,92] Although this therapeutic approach results in clinical improvement, *ex vivo* manipulation of DCs possesses many practical limitations. By the use of nanoparticles, DCs can be directly targeted *in vivo* either actively through distinct surface receptors or passively through their high endocytic potential to delivery tumor-antigens and induce DC activation. Thus, depending on the aim of application, NPs acting as an adjuvant by mounting an immune response may be beneficial.[114,121] Especially, by using NPs as a drug delivery system for DC-based immunotherapies, DC activation plays a major role.[148,149] Some investigations even focus on NPs that show high immunogenicity or they modulate the nanomaterials for higher immunogenicity. Sokolova et al. functionalized calcium phosphate nanoparticles with TLR ligands for peptide delivery to DCs triggering an enhanced DC maturation.[150] Another study engineered polystyrene particles as artificial antigen-presenting cells that prime antigen-specific $CD4^+$ T cells.[151]

3.2 HES-D-IL-2 Nanocapsules for $CD4^+CD25^{high}$ T cell Targeting

Hydroxyethyl starch is used as a safe volume expander in clinics, but cytotoxicity of its polymeric form was analyzed in the present study.[152] Due to its biological inert behavior, hydroxyethyl starch (HES) was taken for nanocapsule (NC) generation by the miniemulsion process. In order to address cell type-specific NC targeting, the small cytokine IL-2 served as a targeting ligand. The cytokine predominantly interacts with the high affinity IL-2 receptor (IL-2R), composed of IL-2Rα (CD25), IL-2Rβ (CD122), and the common gamma chain γc (CD132), which is highly expressed by Tregs and transiently by activated Teff cells.[62,63]

IL-2 highlights many advantages compared to antibodies that are frequently used as a targeting ligand for nanomaterials.[94] Antibodies are glycoproteins with a molecular weight of 150 kDa and a hydrodynamic radius of 15-20 nm compared to IL-2 with a molecular weight of 15 kDa.[94] Antibodies detect appropriate antigens via two dimeric regions ($F(ab')_2$ fragment) on the tip of the Y-shape structured antibody and thus, these regions have to be accessible. Since antibodies are composed of two heavy and two light chains hold together by disulfide bonds, they are susceptible to environmental changes for degradation.[94] Additionally, the base of the Y-shaped structure, the so-called Fc fragment, is immunogenic by binding to Fc receptors present on immune cells and interacts with proteins from the complement system.[94] Above all, the anti-Tac antibody directed against IL-2R is not internalized by the IL-2R-expressing leukemia cell line HUT-102B2.[153] Therefore, using anti-CD25 mAbs for IL-2R-mediated internalization of the nanomaterial, the distinct mAb has to be extensively investigated for internalization by Tregs.

3.2.1 Biologically Functional IL-2 on HES-D-IL-2 Nanocapsules

As copper was shown to exert cellular toxicity, a copper-free click reaction was performed in the present study for linking IL-2 to the surface of HES capsules. [154] In this study, so-called "click-chemistry" that already showed promising results in previous investigations and can be performed under mild conditions was used for conjugation of IL-2 ligands to NC surfaces.[104,155,156] For this purpose, HES NCs were surface functionalized with dibenzylcyclooctyne (DBCO) containing an alkyne group and concomitantly, IL-2 was azide-functionalized. In an azide-alkyne cycloaddition, IL-2 was linked to the HES NC surface. As there are no reactive azide or terminal alkyne groups in nature, the click reaction is very specific.[157] Recent investigations even described *in situ* click reactions by using an azide-functionalized antibody against tumor cells and a DBCO labeled nanomaterial.[158] The DBCO-functionalized NPs carrying cytostatic drugs reacted with the antibody bound to tumor cells, the complex got internalized and tumor lysis was induced.[158]

In the present study, the cytokine IL-2 was directly linked to HES nanocapsules (NCs) as targeting moiety. The cytokine IL-2 holds three sulfhydryl groups at position Cys-58, Cys-105, and Cys-125 with an intramolecular disulfide bond between Cys-58 and Cys-105.[159] Using sulfhydryl groups, which are present in the amino acid sequence of the protein, for linkage to the capsule surface via disulfide bonds, may disrupt the three-dimensional structure of the protein. Thus, in the present study, IL-2 was azide-functionalized at its N-terminus via NHS ester reaction chemistry. Following DBCO-functionalization of HES capsules, IL-2 was "clicked" to HES capsules for obtaining HES-D-IL-2 capsules. Both, azide-functionalization of IL-2 and DBCO-functionalization of the NCs, were accompanied by the introduction of a PEG spacer to avoid interaction forces between the particle surface and targeting ligand for maintenance of the three-dimensional protein structure.

IL-2-N_3 as well as HES-D-IL-2 capsules featured a pronounced IL-2-dependent CTLL-2 proliferation indicating that the three-dimensional protein structure was conserved after azide-functionalization and HES capsule linkage (Figure 13 and Figure 14). Control HES-D capsules revealed no CTLL-2 proliferation demonstrating that CTLL-2 proliferation cannot be induced by the mere presence of HES NCs and thus, proliferation must be caused by IL-2. Analysis of the supernatants, HES-D-IL-2 SN1 and HES-D-IL-2 SN2, obtained during HES-D-IL-2 purification clarified that the amount of IL-2 present in the capsule supernatants was largely reduced and that the second centrifugation step further decreased the amount of soluble IL-2 (Figure 15B). This clearly indicates that the HES-D-IL-2-induced CTLL-2 proliferation primarily results from IL-2 linked to the capsule surface rather than being caused by soluble IL-2.

3.2.2 HES-D-IL-2 Nanocapsule Internalization by Human $CD4^+CD25^{high}$ T Cells

Total $CD4^+$ T cells isolated from peripheral blood mononuclear cells (PBMCs) revealed only a low percentage of $CD25^+$ T cells. Anti-CD3 and anti-CD28 mAb stimulation of $CD4^+$ T cells induced increased CD25 expression as determined by flow cytometry (Figure 15). This is in accordance with literature as CD25 expression can be increased upon T cell activation.[62,160] The γc subunit of the IL-2R is known to be constitutively expressed on lymphoid cells, involving all T cells, whereas IL-2Rα and IL-2Rβ are only upregulated on $CD4^+$ T cells upon activation.[161] In the present study, CD25 expression was induced by stimulation with anti-CD3 and anti-CD28 mAbs, followed by IL-2 stimulation peaking after 72 h, in particular on $CD4^+Foxp3^+$ T cells. CD122 was expressed on anti-CD3 and anti-CD28 mAb stimulated T cells, but was not further increased by IL-2 stimulation. The expression of all three IL-2R subunits is mandatory for an optimal internalization of IL-2 by the high-affinity IL-2R.[62,63] Analysis of cell viability after NC treatment showed no significant increase in dead cells as measured by flow cytometry (Figure 16). Thus, HES capsules did not induce toxicity in primary T cells at the concentrations examined 72 h after NC addition. Uptake studies of HES-D-IL-2 by $CD4^+CD25^{high}$ T cells showed no increase in NC-positive T cells at early time points (24 h) and lower concentrations (12.5 and 25 µg/ml) compared to control capsules (Figure 17). However, application of a higher HES-D-IL-2 NC concentration showed an elevated amount of NC-positive cells 24 h after NC addition. Interestingly, 72 h after NC addition, HES-D-IL-2 NCs revealed a significant uptake by $CD4^+CD25^{high}$ T cells at 75 µg/ml compared to control capsules. Considering that IL-2 alone is internalized by the IL-2R at high frequencies within one hour, the uptake of IL-2-functionalized hydroxyethyl starch capsules was rather slow.[66,153,162] However, with respect to the increased size of HES-D-IL-2 NCs compared to unfunctionalized IL-2, uptake by T cells featuring a low endocytic potential may be retarded. Therefore, it may take some time until enough capsules are accumulated intracellularly for proper fluorescence detection. Along with the low endocytic potential of T cells, CD25, which is essential for the high affinity IL-2R, has to be upregulated for internalization of the IL-2/IL-2R complex.[62,160] Here, CD25 expression achieved highest expression level 72 h after IL-2 stimulation of anti-CD3 and anti-CD28 stimulated $CD4^+$ T cells. Altogether, $CD4^+$ T cells show a much slower and decreased internalization of IL-2-functionalized capsules compared to unfunctionalized IL-2, but with respect to the aforementioned points, this observation was highly expected.

In the present study, DBCO-functionalized HES NCs were taken as control. Considering the fact that also minor surface functionalization may alter the uptake of capsules, HES-D NCs represented not an optimal negative control for uptake. Surface functionalization of HES-D

with a mutated IL-2 protein, which is deficient for IL-2R binding, IL-2 internalization and signal induction, would have been an ideal negative control for uptake studies. As previous studies reported NP uptake to be cell cycle-dependent, HES and HES-D NCs supplemented with soluble IL-2 were additionally applied as a negative control for uptake.[163] In fact, HES-D NCs supplemented with soluble IL-2 showed a slight increase in uptake by $CD4^+CD25^{high}$ T cells compared to HES-D capsules applied alone (Figure 17). Besides the different surface functionalization between HES, HES-D and HES-D-IL-2, that may alter the cell uptake in an IL-2-independent manner, the difference on the amount of fluorescent dye per capsule constitutes another drawback for taking HES and HES-D NCs as negative controls. As HES-D-IL-2 capsules contain half and one third of the amounts of the fluorescent dye SR101 incorporated in HES and HES-D, respectively, the actual abundance of HES-D-IL-2 NC-positive cells may have been much higher than measured. Thus, HES and HES-D capsules used as controls for the present study display no ideal controls for HES-D-IL-2 NC uptake studies and may have scaled down the uptake efficiency of HES-D-IL-2 NCs.

Regarding $CD4^+CD25^{high}$ T cell proliferation, 24 h after T cell stimulation no dilution of the proliferation dye CellTrace™ Violet was detectable (Figure 17). 48 h after HES + IL-2, HES-D + IL-2 and HES-D-IL-2 addition a moderate T cell proliferation was visible (data not shown), but 72 h after addition a pronounced $CD4^+CD25^{high}$ T cell proliferation was measured. Considering the high potential of HES-D-IL-2 NCs to induce T cell proliferation, the capsule dye gets diluted with each cell division. Thus, the higher the T cell proliferation, the higher the NC-dye SR101 gets diluted and a lower percentage of SR101-positive cells may be measured. The question whether HES-D-IL-2 NC internalization by $CD4^+CD25^{high}$ T cells is mandatory for T cell proliferation remains elusive. Previous studies inhibiting IL-2 internalization through the high-affinity IL-2R resulted in inhibition of proliferation.[164] Within that study an antibody directed against the IL-2Rα chain did not abrogate IL-2 binding to the high-affinity IL-2R, but when cross-linked with a second antibody endocytosis was inhibited causing growth inhibition.[164] This study clearly indicates that IL-2 internalization is a prerequisite for induction of T cell proliferation.

CLSM analysis verified the internalization of HES-D-IL-2 nanocapsules, whereas HES-D NCs showed a pronounced cell membrane association with less intracellularly located capsules compared to HES-D-IL-2 NCs (Figure 18). Membrane-associated HES-D capsules may explain the high amount of SR101-positive T cells measured by flow cytometry. For real quantitative uptake studies, particles associated with cell membranes should be excluded during flow cytometry analysis. One technique for getting rid of cell membrane associated particles is to perform an acid washing step prior to flow cytometry analysis.[165,166] Another

way to eliminate the fluorescence signal of loosely attached particles at the membrane is to quench the fluorescent dye of extracellular particles by adding trypan blue.[167,168]

If nanomaterials are aimed to serve as a drug delivery system, their endosomal or lysosomal release has to be elucidated. Electron microscopy studies revealed that internalized IL-2 is directed to lysosomal vesicles upon receptor-mediated endocytosis.[162] However, lysosome staining combined with HES-D-IL-2 NC detection by cLSM depicted no co-localization in $CD4^+CD25^{high}$ T cells (Figure 19). This result may either indicate that HES-D-IL-2 NCs escaped from endosomal or lysosomal vesicles or that the capsules are taken up by an endosome-independent pathway. For a long time, it was supposed that receptor-mediated endocytosis is exclusively triggered by clathrin-mediated endocytosis, which vesicles are targeted for lysosomal degradation.[169,170] However, IL-2R internalization was found to be dynamin- and RhoA-dependent, but clathrin-independent.[171]

In order to elucidate the internalization of IL-2-labeled NCs in more detail, real-time microscopy may be performed in future studies. Another approach to address whether NCs reveal endosomal or lysosomal escape is to perform a red blood cell hemolysis assay.[172] In this technique nanomaterials are incubated with red blood cells, whose lipid bilayer resembles endosome and lysosome vesicles, at pH levels present in early endosome (pH 6.8), late endosome (pH 6.2) and lysosome (pH 5.6) and hemoglobin release is measured.[172] Further, a third technique to examine the route of internalization and intracellular localization is to apply capsules together with small inhibitors specific for a specific uptake pathway.[130,173]

3.2.3 High versus Low Amounts of IL-2 Linked to Hydroxyethyl Starch Nanocapsules

Regulatory T cells mediate immune tolerance by suppression of Teff cells and the secretion of immunosuppressive cytokines that can induce tolerogenic DCs and regulatory T cells in a positive feedback loop. Many investigations are devoted to diminish or deplete Tregs in the tumor microenvironment as increased Treg numbers were associated with poor clinical outcome.[40,55]

The aim of linking different amounts of IL-2 to the surface of NCs is to target different T cell populations. CD25 expression is not exclusively attributed to $CD4^+CD25^+Foxp3^+$ Tregs as activated Teff cells show elevated CD25 expression as well.[29,62,160] However, $CD4^+CD25^+Foxp3^+$ Tregs reveal higher sensitivity towards IL-2 than activated $CD4^+$ T cells.[74,75] Due to their higher sensitivity and increased expression of CD25, Tregs can be targeted via low-dose IL-2 stimulation, whereas Teff cells require high-dose IL-2 levels.[74,82] High-dose IL-2 treatment is primarily used for tumor therapy.[78,81] In contrast, low-dose IL-2 administration is investigated for treatment of autoimmune diseases for a prolonged and

increased Treg activation.[79,80,174] Generating low-dose and high-dose IL-2-functionalized capsules may enable a more specific targeting of $CD4^+CD25^+Foxp3^+$ Tregs and $CD4^+$ Teff cells, respectively.

In the present study, HES-D-IL-2 NC uptake by T cells was increased compared with HES-D-IL-2^{low} capsules that were functionalized with half the amount of IL-2 (Figure 20). As HES-D-IL-2 and HES-D-IL-2^{low} NCs revealed similar fluorescence intensities per capsule, the increase of SR101-positive cells was directly comparable. Further experiments have to be performed in future studies to determine whether the elevated uptake of HES-D-IL-2 NC by $CD4^+CD25^{high}$ T cells is significant.

Analyzing the potential of HES-D-IL-2 and HES-D-IL-2^{low} NCs to induce CTLL-2 proliferation depicted a slightly better CTLL-2 proliferation by HES-D-IL-2 NCs (data not shown). This difference was visible at lower NC concentrations but lessened at higher concentrations. In contrast, HES-D-IL-2 revealed a much better proliferative potential on primary $CD4^+CD25^{high}$ T cells compared with HES-D-IL-2^{low} NCs with regard to the relative division index. As the proliferative potential of primary T cells is very donor-dependent the division index was normalized to control T cells cultured with IL-2 alone. The division index of HES-D-IL-2 NCs at the highest concentration used was comparable to IL-2-stimulated control T cells, whereas HES-D-IL-2^{low} NCs did not reach control T cell proliferation even at a concentration of 150 µg/ml. Altogether, the differences between HES-D-IL-2 and HES-D-IL-2^{low} NCs were not as tremendous as expected particularly taking into account that half the amount of IL-2 was used for HES-D-IL-2^{low} NC functionalization compared to HES-D-IL-2. It may therefore be desirable to link less than half of the amount of IL-2 to the surface of HES-D-IL-2^{low} NCs.

In order to determine whether HES-D-IL-2^{low} NCs bearing half the amount of IL-2 on their surface are preferentially taken up by Tregs than activated Teff cells, non-activated total $CD4^+$ T cells from PBMCs should be incubated with HES-D-IL-2 and HES-D-IL-2^{low} NCs for internalization and the cells should additionally be stained for CD25 and Foxp3 during flow cytometry allowing discrimination between $CD25^{high}$ and $CD25^{low}$ T cells.

Only few previous investigations concentrated on the coupling of different amounts of targeting ligand to the surface of nanomaterials.[94] Bandyopadhyay et al. showed that increasing amounts of anti-DEC-205 antibodies on the surface of biodegradable poly(lactic-co-glycolic acid) (PLGA) NPs caused elevated IL-10 production by DCs and T cells that is due to cross-linking of DEC-205 receptors on the surface of DCs.[175] However, differences in uptake of NPs that were surface-functionalized with two distinct amounts of anti-DEC-205 antibodies by DCs were not measured.[175]

3.2.4 Application of HES-D-IL-2 Nanocapsules *In Vivo*

Small nanomaterials below a size of 10 nm may be cleared from circulation very early, whereas larger particles exceeding a size of 100 nm are not suited for tumor targeting by the enhanced permeability and retention effect (EPR) except for nanomaterials that are transported into the tumor microenvironment via cells.[100] In comparison, nanomaterials with a size between 100 and 200 nm are most suitable for sustained circulation and efficient uptake by cells.[100] Besides size, many factors may influence the *in vivo* distribution of nanomaterials. Thus, *in vivo* distribution, organ accessibility and cell type-specific uptake of a distinct nanomaterial has to be determined.

In the present study, mice were intravenously injected with HES-D-IL-2 NCs and NaCl solution for control, euthanized 24 h after injection and liver, spleen and lymph node cells were analyzed by flow cytometry. Isolated splenocytes showed no NC-positive cells, whereas liver cells showed an increase of NC-positive cells of around 10% compared to NaCl control-treated mice (Figure 22). Diverse nanomaterials show rapid blood clearance and accumulation in the liver.[176] However, Allen et al. found that PEGylation of liposomes diminishes accumulation in the liver and spleen, whereas blood circulation and uptake into skin, gut, bone marrow and lymph nodes is increased.[177] The IL-2-functionalized HES NCs used in the present study already possessed nine PEG groups; four PEG molecules between IL-2 and the azide group and another five PEG groups were located between DBCO and the capsule surface. It remains elusive whether the liver accumulation of HES-D-IL-2 may be higher without PEG groups. Unstained lymph node cells showed a moderate increase in HES-D-IL-2 NC-positive cells compared to the NaCl treated control group. The difference between control and HES-D-IL-2 NC-treated lymph node cells was even higher when gated on $CD4^+CD25^+$ T cells indicating a specific uptake of HES-D-IL-2 NCs by $CD4^+CD25^+$ T cells. In contrast, antigen-presenting cells, including $CD11c^+$ dendritic cells and $B220^+$ B cells, showed no elevated uptake of HES-D-IL-2 NCs. $F4/80^+$ macrophages indicated a slight uptake by lymphocytes, but this increase was lower as compared to $CD4^+CD25^+$ T cells.

The obtained results look very promising, but have to be validated by further investigations, including the analysis of shorter and longer incubation times than 24 h. Additionally, it is imperative to perform detailed pharmacokinetic studies revealing the NC amount present in the blood over time.

Previous nanotechnology approaches for cancer immunotherapy considered IL-2 in the light of T cell stimulation. Due to the short half-life of IL-2 in serum and high-dose IL-2 administration causing severe side effects, nanoparticles were utilized as an IL-2 delivery system to foster T cell stimulation.[106,178,179] Steenblock et al. generated biodegradable

poly(lactic-co-glycolide) (PLGA) with a sustained IL-2 release for $CD8^+$ T cell expansion.[178] Another investigation reported IL-2 loaded polyplexes to function as a therapeutic approach against melanoma through a pivotal $CD4^+$, $CD8^+$ T cell and NK cell activation and expansion.[179] Moreover, Park et al. generated liposomal polymeric gels capable of delivering both hydrophobic and hydrophilic cargos into the B16 melanoma tumor microenvironment.[106] Simultaneous delivery of IL-2 and an inhibitor of the immunosuppressive cytokine transforming growth factor alpha (TGF-α) resulted in tumor growth retention through enhanced NK infiltration into the tumor and $CD8^+$ T cell activation at the tumor site.[106]

Few investigations already concentrated on targeting T cells via nanomaterials. For instance, Dinauer et al. coupled anti-CD3 antibodies to the surface of gelatin nanoparticles for receptor-mediated endocytosis by the human T cell line Jurkat and primary human T cells.[180] Within that approach anti-CD3 antibodies were linked to the particle surface via NeutrAvidin®-biotin interaction.[180] Zheng et al. first described *in vivo* targeting of adoptively transferred T cells via IL-2 in lymphodepleted mice.[181] They genetically fused IL-2 to an Immunoglobulin G (IgG) backbone and linked IL-2 to the liposome surface via thiol-maleimide coupling.[181]

4 Conclusion and Outlook

Many current immunotherapeutic approaches against cancer fail due to the immunosuppressive arm of the immune system that is primarily mediated by regulatory T cells and tolerogenic dendritic cells (DCs).[4,40,84] Thus, immunotherapies that diminish immunosuppression in the tumor microenvironment may be given in combination with immunotherapeutic approaches that boost an immune response against the tumor. Engineered nanoparticles may provide a drug delivery system for immune cells to alter activation and function of immunosuppressive cells or cells that trigger an immune response. Therapeutic agents that may be encapsulated into the particles can be directly addressed to specific cells resulting in reduced side effects, improved cargo protection and prolonged circulation of the therapeutic agent.

SEMA and VBPA polystyrene nanoparticles (NPs) revealed immunogenic properties by inducing DC maturation accompanied with a pronounced T cell proliferation indicating a Th1 response. The functionalized polystyrene NPs may either serve as adjuvants administered in combination with therapeutic approaches that trigger an antigen-specific immune response or the NPs may be further functionalized, for instance, with a tumor-specific antigen. However, polystyrene is not biodegradable and has to be excreted. Thus, polystyrene NPs are rather designated as a good model system for studying nanomaterials.

On the other hand, hydroxyethyl starch (HES) nanocapsules (NCs) are biodegradable. HES is already used in clinics as a volume expander and is therefore approved by the Food and Drug Administration (FDA). The present study displayed HES NCs as promising nanomaterials for a targeted drug delivery system. To confirm this finding further questions have to be addressed in future studies.

Firstly, although the increased uptake of HES-D-IL-2 NCs by $CD4^{+}CD25^{high}$ T cells already indicated a cell type-specific uptake, the CD25-driven internalization of IL-2-functionalized HES NCs has to be confirmed in onward investigations. Co-staining of CD25 while measuring NC uptake by flow cytometry may assess this question. Moreover, applying anti-CD25 antibodies (PC-61, daclizumab/basiliximab) with increasing NC concentrations for measuring NC uptake by flow cytometry may show whether CD25-dependent uptake can be decreased or inhibited by blocking CD25 on the surface of T cells.[55,182] Another possibility to verify CD25-dependent uptake of HES-D-IL-2 NCs would be to compare NC uptake between naïve CD25-negative T cells and CD25-positive Tregs.

Secondly, the release of the capsule content should be investigated, for instance, by the incorporation of a CellTracker™ that stains the cytoplasm or other cellular compartments if

released form the NCs.[183] If the HES capsule shell is not disrupted intracellularly, other chemical modifications have to be introduced into the capsule shell to render the capsules acid-labile or redox-sensitive.

Thirdly, the cargo, for instance siRNA, encapsulated by HES NCs should still be intact after encapsulation. In previous investigations, Baier at al. reported the encapsulation of dsDNA into HES NCs with subsequent polymerase chain reaction showing that dsDNA is not degraded during miniemulsion polymerization.[103] For the purpose of testing the stability of degradation-sensitive siRNA after encapsulation, fluorescence resonance energy transfer (FRET) with dye-labeled siRNA can be analyzed by fluorescence microscopy.[184] Within this FRET approach both siRNA strands are labeled with a fluorescent dye, a donor dye and an acceptor dye. The emission spectrum of the donor dye comprises the excitation spectrum of the acceptor dye and if both dyes are in close proximity the acceptor dye is excited through the donor dye.[185]

The last question that has to be addressed relates to the NC distribution and its effect on tumor burden. Melanoma only accounts for approximately 5% of skin cancer, but due to its aggressive behavior it causes most skin cancer deaths. Besides the demand for more efficient therapeutic approaches, melanoma represents a good model for studying cancer therapy due to its good visualization on the skin of mice. Thus, therapeutic efficacy of cell type-specific nanocapsules containing small molecules or siRNA should be investigated in mouse models for human and murine melanoma.[186] This can either be achieved by using a *BRaf*^{V600E}*-Pten*-driven induced spontaneous melanoma model or induced B16 melanoma model for murine melanoma models or by injection of human melanoma cell lines into the skin of immunocompromised mice.[187]

As listed above, various investigations have to be performed to shed further light on the ability of HES-D-IL-2 NCs for cancer immunotherapy.

Immunosuppressive regulatory T cells (Tregs) and tolerogenic DCs constitute the main obstacle to mount an effective immune response. DCs can be targeted via the receptor DEC-205 and in combination with anti-IL-10R antibodies tolerogenic DCs may be addressed. As depicted above, Treg targeting may be achieved via low-dose IL-2 functionalization of nanocapsules. Both cell types were shown to produce elevated amounts of the immunosuppressive cytokine IL-10 and besides, many tumor cells were shown to produce IL-10.[43] IL-10 signals through the immunosuppressive transcription factor STAT3, which induces IL-10 expression in a positive feedback loop.[188] Thus, inhibiting IL-10 cytokine expression or STAT3 signaling in tolerogenic DCs and Tregs may mount a more effective immune response.

Considering targeted HES NCs as a drug delivery system, small molecules for inhibiting STAT3 or siRNA against IL-10 or IL-10 receptor will be encapsulated into HES nanocapsules that bear a hydrophilic core. Knockdown of the immunosuppressive cytokine IL-10 in immature DCs was reported to induce an elevated Th1 response through increased CD40 expression and elevated IL-12 levels.[189] Others also reported an IL-10 silencing in DCs to be associated with increased IL-12 production resulting in an improved antigen-dependent cytotoxic T lymphocyte (CTL) response.[190] Besides IL-10/IL-10R silencing by siRNA, targeting STAT3 inhibitors to Tregs and tolerogenic DCs may support a proper immune response.

Many passively targeted nanomaterials, most notably liposomes, for cancer therapy are already FDA-approved.[191] The most prominent example is Doxil that are pegylated liposomes loaded with the chemotherapeutic agent doxorubicin.[192] Actively targeted nanocarriers are still highly examined in preclinical investigations, but only engineered antibodies and small proteins have been approved for clinical application, including the aforementioned Ontak that is composed of IL-2 genetically fused to diphtheria toxin.[191] However, various liposomal or polymer-based nanomaterials as drug delivery systems to tumors are in clinical trials. For instance, the compound CALAA-01, which is a transferrin-targeted cyclodextrin-based nanoparticle carrying siRNA, is already in a Phase I clinical trial.[191]

A major advantage of nanomaterials as a drug delivery system is that nanoparticles are highly tunable meaning that both the cargo as well as the targeting moiety can more or less easily be exchanged. In conclusion, nanoparticle research may be constantly approaching the *leitmotiv* of Paul Ehrlich to establish the ability to “aim chemically” (“we have to learn how to aim chemically”).[1]

5 Experimental Part

5.1 Nanomaterial Synthesis and Characterization

5.1.1 Miniemulsion Polymerization – Direct and Indirect Miniemulsion

An emulsion is a heterogeneous suspension of two or more immiscible liquids in which one liquid forms small droplets (dispersed phase) in the other liquid (continuous phase).[193] Compared to macroemulsion and microemulsion, a miniemulsion contains stable droplets with a reduced polydispersity.

Coping with miniemulsion polymerization, it can be distinguished between the direct (oil-in-water) and indirect (water-in-oil) miniemulsion process.[194] In the miniemulsion process small droplets with a size between 50 and 500 nm can be generated by high shear force, for instance, by applying ultrasonication or high-pressure homogenization. The dispersed phase, the continuous phase, a surfactant and a co-stabilizing reagent are mixed and exposed to high shear force in a first step.[194] In a second step, polymerization is initiated in each single droplet.[193]

The interphase between small droplets and the continuous phase has to be stabilized in order to prevent coalescence and Ostwald ripening as the droplets are highly deformable after dispersion.[194] Coalescence is the fusion of two droplets caused by collision, whereas Ostwald ripening describes the diffusion of a monomer from a small droplet to a larger droplet and thus, larger droplets grow.[194] Ostwald ripening may occur if the dispersed phase is sparingly soluble in the continuous phase or if the particle concentration is too high. If the emulsion is standing or stored for too long, “aging” may also be caused through Ostwald ripening.

Amphiphilic surfactants in the continuous phase reduce the surface tension of small droplets and cover the droplet and later the particle surface.[194] Both, surfactants and co-stabilizers can act as an emulsifier by reducing electrostatic and/or steric forces. In the present study, the water-soluble Lutensol AT50 and sodium dodecyl sulfate (SDS) and the oil-soluble blockcopolymer poly((ethylene-*co*-butylene)-*b*-(ethylene oxide)) (P(E/B-*b*-EO)) were used as surfactants in the miniemulsion polymerization. Lutensol AT50 is a poly(ethylene oxide) (PEO) hexadecyl ether with an PEO block of about 50 units. The hydrophobic reagent hexadecane, which was used as a hydrophobic agent for particle synthesis, is largely employed to increase the droplet stability by antagonizing Ostwald ripening and further allows reduced addition of surfactant. Additionally, the amount of surfactant can impact the droplet size and thus, allows for selective bioengineering of nanomaterials in the

miniemulsion process.[195] A fluorescent dye can either be incorporated into the shell or core of particles or capsules in order to facilitate fluorescence detection in biological investigations.

In the direct miniemulsion (oil-in-water) a hydrophobic monomer (e.g. styrene) is mixed with an oil-soluble initiator (e.g. 2,2'-azobis(2-methylbutyronitrile) (V59)), a hydrophobic agent (e.g. hexadecane) and a fluorescent dye (e.g. the perylene dye). Following stirring the styrene mixture is mixed with a surfactant (e.g. Lutensol AT50) in water for the generation of sub-microscopic polystyrene particles. Exposure of the particles to ultrasonication under cooling conditions results in small nanoparticles with a homogeneous size distribution. Polymerization is then initiated by heating the mixture. Compared to the direct miniemulsion, a major advantage of inverse (water-in-oil) miniemulsion polymerization is the ability to generate nanocapsules with a hydrophilic core.[194] In the indirect or inverse miniemulsion (water-in-oil) process a hydrophilic monomer (e.g. hydroxyethyl starch) is mixed with a fluorescent dye (e.g. sulforhodamine 101). Besides, an oil-soluble surfactant (e.g. poly((ethylene-*co*-butylene)-*b*-(ethylene oxide))) is mixed with a co-stabilizer (e.g. cyclohexane) and afterwards, mixed with the monomer suspension. Homogenization is initiated by ultrasonication and polymerization is achieved by addition of a crosslinker (e.g. 2,4-toluene diisocyanate) mixed with a co-stabilizer (e.g. cyclohexane) and a surfactant (e.g. poly((ethylene-*co*-butylene)-*b*-(ethylene oxide))).

5.1.1.1 Generation of SEMA- and VBPA-Functionalized Polystyrene Nanoparticles

The functionalized polystyrene nanoparticles were synthesized and characterized by [redacted] (Max Planck Institute for Polymer Research, Mainz, Germany) and already described in previous investigations.[123,196,197] In brief, the unfunctionalized and surface-functionalized polystyrene nanoparticles (NPs) were synthesized via radical-free co-polymerization in a direct (oil-in-water) miniemulsion polymerization.[198] Polystyrene NPs were engineered from the monomer styrene. However, the functionalized polystyrene NPs additionally contained the co-monomer 2-sulfoethyl methacrylate (SEMA) or vinylbenzylphosphonic acid (VBPA). Hexadecane was added as a co-stabilizer and the oil-soluble initiator 2,2'-Azobis(2-methylbutyronitrile) (V59) was taken for initiation of polymerization. Lutensol AT50 was used as a non-ionic surfactant. For detection of nanoparticles in biological systems, the fluorescent perylene dye *N*-(2,6-diisopropylphenyl)perylene-3,4-dicarbonacidimid (PMI) was incorporated into the particles. After stirring the mixture, the droplets were homogenized by ultrasonication under cooling conditions. Due to heating, polymerization was initiated and the mixture was further stirred. Polystyrene NPs were washed with demineralized water in six centrifugation steps for removal of free surfactant.

5.1.1.2 Preparation of HES-D-IL-2 Nanocapsules

Synthesis and characterization of hydroxyethyl starch (HES) nanocapsules (NCs) were kindly performed by [redacted] (Max Planck Institute for Polymer Research, Mainz, Germany) and the capsules were already previously described.[103,104] In contrast to polystyrene NPs, HES NCs were synthetized by an inverse (water-in-oil) miniemulsion polymerization (Figure 23). A HES solution was mixed with the fluorescent dye sulforhodamine 101 (SR101) to allow detection of the labeled NCs by flow cytometry and microscopy. Alongside, the oil-soluble surfactant poly((ethylene-*co*-butylene)-*b*-(ethylene oxide)) (P(E/B-*b*-EO)) was dissolved in cyclohexane, mixed with the HES-SR101 suspension and stirred. Homogenization was conducted via ultrasonication under cooling conditions. The crosslinker 2,4-toluene diisocyanate (TDI) was mixed with cyclohexane and the blockcopolymer P(E/B-*b*-EO) and added to the droplet suspension for crosslinking of HES. In detail, the hydroxyl groups of HES reacted with the isocyanate groups in TDI. Following polymerization and continuous stirring of the dispersion, the generated NCs were harvested by centrifugation and redispersed in cyclohexane. The HES dispersion was further mixed with TDI and stirred for introduction of amino groups (NH_2) on the capsule surface. Following NH2 functionalization the HES capsules were transferred in an aqueous phase by mixing the capsule dispersion with a sodium dodecyl sulfate (SDS) aqueous solution. Afterwards, the capsules were redispersed in a sonication bath, centrifuged, redispersed in H_2O and dialyzed for removal of soluble SDS. In the present study, these unfunctionalized HES NCs served as a negative control.

For the purpose of ligand linkage to the capsule surface, HES NCs were mixed with dibenzylcyclooctyne (DBCO)-PEG5-NHS ester and afterwards, unbound DBCO was removed by two centrifugation steps. DBCO-functionalized HES capsules, HES-D, were additionally implemented as a negative control in the present study.

Alongside, human Interleukin-2 (IL-2) (from Cell Sciences) was azide-functionalized with NHS-PEG4-azide through NHS ester chemistry (IL-2-N_3). IL-2-N_3 molecules were then linked to HES-D capsules via click reaction obtaining HES-D-IL-2 capsules. Additionally, IL-2-functionalized HES nanocapsules were generated with half the amount of IL-2 used for IL-2 functionalization and are referred to as HES-D-IL-2^{low} capsules. In principle, the copper-free click reaction, the so-called azide-alkyne cycloaddition, is based on a ring opening from an alkyne to a double bond (triazole). Following click reaction, the capsules were again dialyzed, centrifuged twice and redispersed in a 0.9% NaCl solution.

During NC synthesis the amount of NH_2 groups present on the capsule surface was measured by polyelectrolyte titration and the amount of DBCO groups present on HES-D

capsules was determined via an anthracene click reaction. Based on the amount of available groups, the amount of DBCO molecules and IL-2 molecules used for NC functionalization was calculated. Additionally, after each functionalization step the NC size and morphology was determined by dynamic light scattering.

Although the reproducibility of NC preparation was confirmed by physicochemical and biological investigations, the same NC batch was used for the whole study.

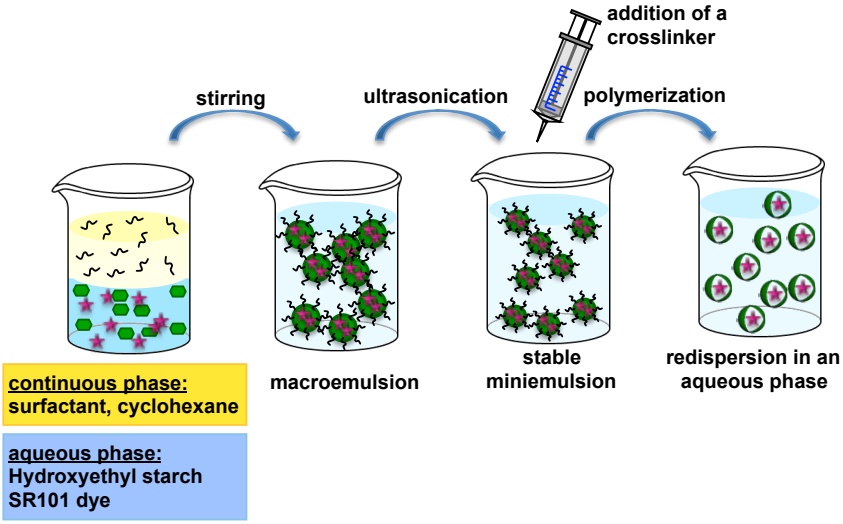

Figure 23. Generation of HES nanocapsules by miniemulsion polymerization. The continuous phase containing the surfactant and cyclohexane was mixed with an aqueous phase containing hydroxyethyl starch (HES) and the fluorescent dye sulforhodamine 101 (SR101). Stirring resulted in the formation of small macrodroplets. The generation of smaller minidroplets was induced by ultrasonication. 2,4-toluene diisocyanate (TDI) was added to the suspension for crosslinking of HES. After polymerization, the capsules were washed and redispersed in an aqueous solution. Adapted from Baier et al., 2010.[103]

5.1.2 Characterization of Nanomaterials

Extensive characterization of nanomaterials regarding physical and chemical properties is imperative for their biological application *in vitro* and *in vivo*.[199,200] Especially nanomaterial size, size distribution and shape may already predict possible cellular uptake and biodistribution. In addition, the surface charge of nanomaterials expressed as “zeta potential” should be considered for cell uptake studies and is mandatory for nanotoxicity predictions.

5.1.2.1 Nanoparticle Size – Dynamic Light Scattering

Many investigations face the influence of nanoparticle size on cellular uptake, biodistribution to specific organs or tumors and *in vivo* clearance, but the optimal particle size is still highly discussed. Increased NP size impairs permeation efficacy of nanomaterials with nanoparticles possessing a size of below 100 nm show better penetration into tumors, unless larger nanomaterials are transported to the tumor via cells.[129,201,202] Further studies

highlighted that, in general, a particle size up to 500 nm is suitable for cellular uptake.[120,203,204]

Dynamic light scattering (DLS) (also referred to as photon correlation spectroscopy) for biomaterials that was first introduced by Berne and Pecora is a commonly used technique in polymer chemistry for assessing shape, size and molecular behavior of nanomaterials in a distinct solution.[205] In principle, if a laser light catches nanomaterials in solution, the light scatters in all directions and, as the laser emits light coherently, a fluctuation of the scattering intensity can be measured. The Brownian motion of particles or molecules in a suspension and their interference causes light scattering with different intensities. Based on the light intensity the Brownian motion, the diffusion coefficient, of the particles can be determined and by usage of the diffusion coefficient the particle size can be calculated.[205]

5.1.2.2 Nanoparticle Charge – Measurement of Zeta Potential

Nanoparticle charge plays a tremendous role in the bioapplication of nanomaterials. Most cells reveal a negatively charged membrane, which highly affects cell uptake of charged nanomaterials. The zeta potential (ζ-potential) is no definite charge of the nanomaterial, but the electrostatic potential of the layer of absorbed ions to the nanoparticle surface in a defined solution.[206] In solution, charged nanoparticles bind ions of opposite charge present in the dispersed medium in order to neutralize their electrostatic potential and compose a firm layer of electrons. In a second layer loosely attached ions are adsorbed. Due to particle diffusion in the dispersed medium ions from the second layer may detach and induce an electrostatic potential of the particle, the so-called zeta potential. The basic principle for measurement is electrophoresis during which charged particles move within an electric field. The measured velocity of the particles across the dispersed medium is a measure of the zeta potential.[206]

5.1.2.3 Nanoparticle Morphology – Scanning Electron Microscopy

Biomaterials revealing a size in the nanometer range are inadequately analyzed with light microscopy due to the limited resolution of around 200 nm. Electron microscopy (EM) applying electrons that feature shorter wavelengths compared with photons enables the precise assessment of nanostructures due to a resolution of around 0.2 nm. During EM, an electron beam interacts with electrons in the determined specimen and due to electrostatic forces some electrons will be scattered. The scattered electrons are collected and processed for an image of the sample. A major disadvantage of electron microscopy is that it has to be performed under high vacuum at room temperature as gas molecules may interfere with the

electron beam and the emitted electrons, but on the other hand nanometer sized structures can be determined.[207]

The two types of electron microscopy, transmission electron microscopy (TEM) and scanning electron microscopy (SEM), largely differ in their image processing.[208] For TEM analysis ultra-thin slices of the specimen are required as the analysis is based on the "transmission" of the electric beam through the specimen. Transmitted electrons are collected for image processing. In contrast, SEM allows the analysis of specimens through which the electric beam cannot pass. Energy from the electron beam is transmitted to the specimen which then emits electrons and imaging is processed by scanning of the sample.[208]

5.1.2.4 Measuring Endotoxin Level

Pathogen-associated molecular patterns (PAMPs) are recognized by Toll-like receptors (TLRs) that are primarily expressed by macrophages and dendritic cells (DCs).[11] Endotoxin, a lipopolysaccharide (LPS) present in the outer membrane of gram-negative bacteria may induce DC maturation upon interaction with TLRs present on the cell surface.[13]

In order to exclude elevated levels of LPSs in the nanoparticle dispersion, a Limulus Amebocyte Lysate (LAL) PYROGENT™ Plus Single Test that detects endotoxin levels above 0.06 endotoxin units per ml (EU/ml) was performed. The Food and Drug Administration (FDA) limit for endotoxins in medical applications is 5 EU/kg. The most sensitive endotoxin single test Kit from Lonza with a sensitivity of 0.06 EU/ml was taken for measuring the endotoxin level in the NP supernatants. For LAL testing 0.25 ml of the NP supernatant was added to the Limulus Amebocyte lysate. For positive control, 0.25 ml endotoxin-free water was added to the positive sample control, whereas for the negative control 0.25 ml endotoxin free water was applied in a vial lysate. All vials were incubated for 60 min at 37 °C and afterwards, the vials were carefully turned upside down. A positive detection of endotoxin is characterized by coagulation of the liquid into a firm gel.

5.2 Experimental Methods

5.2.1 Preparation of Human Cells

5.2.1.1 Isolation of Human Peripheral Blood Mononuclear Cells

Buffy Coats from 500 ml peripheral blood of healthy volunteers were obtained with the approval of the local ethic committee of Rhineland-Palatine. Blood was diluted 1:2 with Dulbecco's phosphate buffered saline (DPBS) (without $CaCl_2$/$MgCl_2$, at RT), layered on top of 15 ml Biocoll Separation Solution in a 50 ml falcon, and spun at 400xg for 30 min without

break at 20 °C. Peripheral blood mononuclear cells (PBMCs) were taken from white interphase and washed at least three times with ice-cold phosphate buffered saline (PBS) [1:10 dilution of 10x PBS (402 g NaCl, 78 g NaH_2PO_4 x $2H_2O$), at pH 7] at 400xg for 8 min. In general, living cells were counted using a Neubauer Chamber and distinguished from dead cells through counterstaining with trypan blue (1:10 diluted in PBS) that passes through the membrane of dead cells. For preparation of autologous serum the yellow phase above the lymphocyte interphase was collected, heat-inactivated for 30 min at 56 °C and spun twice for 5 min at 2500xg to get rid of aggregated proteins.

5.2.1.2 Human Monocyte-Derived Immature and Mature Dendritic Cells

Human PBMCs were seeded at $1.5x10^7$ cells per well in 6-well plates (3 ml/well) in RPMI 1640 medium supplemented with 1% heat-inactivated serum and incubated for 45 min at 37 °C. Non-adherent cells were removed by washing the adherent cells twice with pre-warmed (37 °C) PBS (containing 1% autologous serum). Adherent monocytes were cultured in Iscove's Modified Dulbecco's Medium (MDM) supplemented with 2.5% heat-inactivated autologous serum, 400 U/ml granulocyte-macrophage colony stimulating factor (GM-CSF) and 150 U/ml IL-4 at 37 °C. On day 3 of culture, one ml culture medium per well was renewed with fresh Iscove's MDM supplemented with 2.5% autologous serum, 800 U/ml GM-CSF and 150 U/ml IL-4. Immature dendritic cells (iDCs) were obtained on day 5 or 6 of culture by placing the cell culture plates on ice for 10 min for harvesting loosely attached and iDCs in suspension. Human iDCs were either directly applied in experiments or further cultured in Iscove's MDM supplemented with 2.5% autologous serum, 400 U/ml GM-CSF and 150 U/ml IL-4 for two days. Mature dendritic cells (mDCs) were generated by culturing iDCs obtained on day 5 or day 6 of culture for another two days in Iscove's MDM supplemented with 2.5% autologous serum, 400 U/ml GM-CSF, 150 U/ml IL-4, 2.5 ng/ml IL-1β, 2.5 ng/ml tumor necrosis factor alpha (TNF-α), 25 U/ml IL-6 and 0.5 µg/ml Prostaglandin E2 (PGE_2). The cytokines IL-1β, TNF-α, IL-6 and PGE_2 represent the "maturation cytokine cocktail" for terminal differentiation of iDCs into mDCs. Following the generation of monocyte-derived DCs from PBMCs, iDCs and mDCs were phenotypically characterized by flow cytometry (see section 5.2.2).

5.2.1.3 Isolation of Human $CD4^+$ T Cells

PBMC-derived human $CD4^+$ cells were labeled with magnetic anti-CD4 MicroBeads at 4 µl beads per $1x10^7$ PBMCs in 16 µl MACS buffer [PBS supplemented with 0.5% human albumin and 3 mM ethylenediaminetetraacetic acid (EDTA)] for 15 min gently shaking at 4 °C. Labeled cells were spun at 300xg for 10 min, resuspended in 1.5 ml MACS buffer and

applied on a sterile LS column (capacity of $2x10^9$ total cells) that was washed before twice with 3 ml MACS buffer on a MidiMACS™ Separator. The cell-loaded column was washed three times with 3 ml MACS buffer for removal of the unlabeled cell fraction. Enriched $CD4^+$ cells in the column were eluted by removal of the column from the MidiMACS™ Separator and labeled cells were washed out from the column with four times 5 ml MACS buffer blew through the column with a plunger. $CD4^+$ enriched cells were washed with PBS and resuspended in X-VIVO™ 20 medium. After isolation $CD4^+$ purity was checked by flow cytometry (see section 5.2.2).

5.2.1.4 Generation and Stimulation of CellTrace™ Violet-Labeled $CD4^+CD25^{high}$ T Cells

Purified $CD4^+$ T cells from PBMCs were stained with CellTrace™ Violet in order to visualize IL-2-induced proliferation. According to manufacturer's instructions CellTrace™ Violet was dissolved in 20 µl DMSO for a stock concentration of 5 mM. $1\text{-}10x10^7$ $CD4^+$ T cells dissolved in 10 ml PBS were stained with CellTrace™ Violet at a final concentration of 0.5 µM for 20 min at 37 °C, 40 ml X-VIVO™ 20 medium was added and the cell suspension was incubated for another 5 min at RT. The stained cells were washed twice with X-VIVO™ 20 medium at 400xg for 8 min. For activation of CellTrace™ Violet-positive $CD4^+$ T cells, T cells were seeded at $2x10^6$ cells/well in a 12-well plate and stimulated with soluble 1 µg/ml anti-CD3 mAb (OKT3) and 0.5 µg/ml anti-CD28 mAb in 1 ml X-VIVO™ 20 medium for 16 h at 37 °C. $CD4^+CD25^{high}$ T cells were harvested and washed twice with PBS for removal of anti-CD3 and anti-CD28 mAb. CellTrace™ Violet staining and T cell activation for CD25 upregulation were checked by flow cytometry (see section 5.2.2).

5.2.2 Flow Cytometry Analysis

5.2.2.1 Cell Surface Marker Analysis of Immature and Mature Dendritic Cells

Before applying iDCs (day 5 or 6) or mDCs (day 7 or 8) in experiments, the cell surface marker expression of DCs was determined to ensure proper DC differentiation and exclude DC contamination with other PBMC-derived lymphocytes. Therefore, $1x10^5$ DCs were stained with unlabeled anti-human mAbs against CD14, CD19, CD80, CD83, CD86 and HLA-DR for 20 min at 4 °C. All markers, except HLA-DR, were detected with the secondary Ab anti-mouse-PE for 15 min at 4 °C. Anti-HLA-DR Ab was detected with a secondary anti-rat-FITC mAbs for 15 min at 4 °C. HLA-DR staining was performed in combination with each surface marker and single staining was performed for control. Isotype controls, rat IgG2aκ and mouse IgG2aκ, were detected with anti-rat-FITC and anti-mouse-PE secondary Abs,

respectively. Expression of cell surface molecules on DCs was measured using a BD™ LSR II flow cytometer.

5.2.2.2 Phenotypic Analysis of Nanoparticle-Loaded Dendritic Cells

The extracellular phenotype of SEMA or VBPA NP-loaded iDCs and mDCs was analyzed by flow cytometry to determine if NP internalization may have an influence on DC maturation. Human iDCs (day 5) were treated with SEMA- and VBPA-functionalized PS NPs for 24 h and were cultured for another two days in Iscove's MDM supplemented with 2.5% autologous serum, 400 U/ml GM-CSF and 150 U/ml IL-4 to retain the cells immature or in Iscove's MDM additionally containing the "maturation cytokine cocktail" (2.5 ng/ml IL-1β, 2.5 ng/ml TNF-α, 25 U/ml IL-6 and 0.5 µg/ml PGE_2) for terminal mDC differentiation. The cells were harvested after 10 min on ice, washed with MACS buffer and stained with PE-labeled mAbs against CD80, CD83, CD86, CCR7, B7-DC, B7-H2 and HLA-DR for 20 min at 4 °C. Unstained cells were taken as a control. Cell surface marker-stained NP-loaded DCs were measured using a BD™ LSR II flow cytometer.

In a separate staining the NP-treated cells were stained with the Annexin V Apoptosis Detection Kit APC (1:20 dilution in a total volume of 20 µl per staining) for 10 min at RT. Cells were washed twice with 1x Binding buffer before they were measured on a BD™ LSR II flow cytometer (data not shown).

5.2.2.3 Intracellular and Extracellular Characterization of $CD4^+CD25^{high}$ T Cells

In order to examine $CD4^+$ T cell purity after isolation from PBMCs and the CD25 expression level before and after $CD4^+$ T cell activation, $1x10^5$ cells/staining of isolated $CD4^+$ cells were separately stained with anti-CD4-FITC (1:30), anti-CD8-FITC and anti-CD25-PE mAbs in 20 µl MACS buffer. The isotope control mouse IgG2b-PE mAb was taken for gating $CD25^+$ cells. $CD4^+$ T cell characterization was examined using a BD™ LSR II flow cytometer after $CD4^+$ T cell isolation from human PBMCs and after stimulation of T cells with anti-CD3 and anti-CD28 mAbs.

Expression levels of the IL-2R, including the subunits CD25, CD122, and CD132, was measured using flow cytometry analysis after $CD4^+$ T cell activation by CD3/CD28 stimulation. To discriminate between $Foxp3^+$ and $Foxp3^-$ T cells, T cells were additionally stained with anti-human-Foxp3 mAbs. For this purpose, $1x10^6$ cells/staining $CD4^+CD25^{high}$ T cells were stained with anti-CD4-FITC (1:4), anti-CD25-Pe-Cy5, anti-CD122-APC and anti-CD132-PE mAbs for 20 min at 4 °C. Single stainings with anti-CD4-FITC (1:4), anti-CD25-Pe-Cy5, anti-CD4-APC, anti-CD4-PE and anti-human-CD25-V450 were performed for compensation. Additionally, the isotype control mouse IgG1κ-PE-Cy5 was included. After

extracellular surface marker staining, the cells were washed with PBS twice before they were fixed and permeabilized with 200 µl 1x Fixation/Permeabilization solution (from the Foxp3 Staining Buffer Set) for 30 min at 4 °C. Cells were harvested at 400xg and washed with 200 µl 1x Permeabilization Buffer (from the Foxp3 Staining Buffer Set). The cells were incubated with anti-human-Foxp3-eFluor450 diluted in 1x Permeabilization Buffer for 30 min at 4 °C. Afterwards, cells were washed twice with 1x Permeabilization Buffer and resuspended in MACS buffer for FACS analysis on a BD™ LSR II flow cytometer.

5.2.2.4 Fixable Viability Dye Staining

The basic principle of Fixable Viability Dyes is that viable cells possess an intact plasma membrane through which the dyes cannot penetrate. In contrast, in dead cells with a damaged membrane the Fixable Viability Dyes interact with amine groups of extracellular and intracellular proteins. As a positive control for the Fixable Viability Dye, a small aliquot of cells was exposed to 65 °C for 5 min, followed by 2 min on ice and afterwards, was mixed in a 1:1 ratio with viable cells. If the staining works properly, around 50% of measured cells should be positive for the Viability Dye.

For discrimination between dead and living cells, cells were washed with PBS, harvested at 400xg for 8 min and stained with the Fixable Viability Dye eFluor®780, which was 1:1000 diluted in PBS, for 30 min at 4 °C. Another two washing steps with PBS were performed before the cells were further stained or directly analyzed via flow cytometry on a BD LSRFortessa™ cell analyzer.

5.2.2.5 CellTrace™ Violet Proliferation Dye Analysis

Cell proliferation was assessed with the proliferation dye CellTrace™ Violet. CellTrace™ Violet is a non-fluorescent ester molecule that can penetrate plasma membrane. Within the cell, cellular esterases activate the molecule into a fluorescent dye and an active succinimydyl ester within the molecule covalently interacts with amine groups of cellular proteins.[125] Due to covalent linkage of the dye to cellular proteins, the fluorescent dye will be equally passed into daughter cells during cell division.

Analysis of the fluorescence intensity was performed with the flow cytometry software FlowJo (TreeStar Inc., USA). By plotting the proliferation dye against the counted cells, highly proliferating cells show several histogram peaks. Each peak within the histogram depicts one cell generation with the parenteral population showing the highest fluorescence intensity. Based on mathematical modelling, the software FlowJo computes the amount of division

peaks and a division index representing the average division number of each analyzed cell including undivided cells.[126]

5.2.3 Nanomaterial Uptake Studies

5.2.3.1 SEMA- and VBPA-Functionalized Nanoparticle Uptake by Human Immature and Mature Dendritic Cells

Human iDCs (day 5) and mDCs (day 7) were seeded at $1x10^6$ cells/well (3 ml/well) in 6-well plates in Iscove's MDM supplemented with 2.5% autologous serum, 400 U/ml GM-CSF and 150 U/ml IL-4 and Iscove's MDM containing 2.5% autologous serum, 400 U/ml GM-CSF, 150 U/ml IL-4, 2.5 ng/ml IL-1β, 2.5 ng/ml TNF-α, 25 U/ml IL-6 and 0.5 µg/ml PGE_2, respectively. The uptake of 25, 75 and 150 µg/ml unfunctionalized PS and SEMA- and VBPA-functionalized PS NPs by iDCs and mDCs was examined 2, 4, 18 and 24 h after NP addition to the cells. After the indicated time points, the cells were resuspended and 300 µl aliquots of the culture were taken for flow cytometry analysis. The cells were washed with MACS buffer and analyzed on a BD FACSCalibur™.

5.2.3.2 HES-D-IL-2 Nanocapsule Uptake by $CD4^+CD25^{high}$ T Cells

CellTrace™ Violet-stained $CD4^+CD25^{high}$ T cells, that were stimulated with anti-CD3 and anti-CD28 mAbs, were disseminated at $1x10^6$ cells/ml in 48-well plates with 0.75 ml/well X-VIVO™ 20 medium (2 wells per sample). HES, HES-D, HES-D-IL-2 and HES-D-IL-2^{low} NCs were applied on the T cells at concentrations of 12.5, 25, 75 and 150 µg/ml directly after seeding. Additionally, HES-D NCs were applied either with or without 50 U/ml soluble IL-2 (Proleukin). $CD4^+CD25^{high}$ T cells cultured either with or without 50 U/ml IL-2 (Proleukin) provided control samples. 24, 48, 72 and 96 h after NC addition, cells were resuspended and 330 µl aliquots were taken for flow cytometry analysis. The cells were washed with PBS at 400xg for 5 min and stained with the Fixable Viability Dye eFluor780 (1:1000 diluted with PBS) for 30 min at 4 °C, followed by another PBS wash and fixation of the cells with 4% paraformaldehyde (PFA) for 10 min at 4 °C. Fixed cells were washed twice with PBS and measured on a BD LSRFortessa™ cell analyzer.

5.2.4 Confocal Laser Scanning Microscopy

5.2.4.1 Confocal Laser Scanning Microscopy of SEMA- and VBPA-Functionalized Polystyrene Nanoparticle Uptake

Human iDCs (day 5) and mDCs (day 7) were seeded at $1.5x10^5$ cells/dish in µ-Dish$^{35mm, low}$ in 800 µl Iscove's MDM. SEMA- and VBPA-functionalized PS NPs were applied on the cells at 75 µg/ml and incubated for 24 h at 37 °C. Free NPs that were neither endocytosed nor associated with the cell membrane were washed out with PBS. 800 µl PBS was added and the cells were stained with 5 µg/ml CellMask™ Orange Plasma membrane stain and 2.5 µg/ml DRAQ5® for staining DNA for 20 min at 37 °C. Images were taken with a confocal LSM (Leica, TCS SP5X) and images were adapted with the Leica confocal software (LCS) (Leica, Germany).

5.2.4.2 Confocal Laser Scanning Microscopy of HES-D-IL-2 Nanocapsules

Anti-CD3 and anti-CD28 mAb-stimulated $CD4^+CD25^{high}$ T cells (CellTrace™ Violet unstained) were disseminated at $2x10^5$ cells/well in 8-well Nunc™ Lab-Tek™ Chambers in 200 µl/well X-VIVO™ 20 medium. T cells were incubated with HES-D and HES-D-IL-2 capsules at a concentration of 75 µg/ml and incubated at 37 °C. After 24, 48, 72 and 96 h, cell membranes were stained with 1 µg/ml CellMask™ Deep Red Plasma membrane stain for 20 min at 37 °C. Additionally, cell nuclei were labeled with 1 µg/ml Hoechst 33342 for 10 min at 37 °C. Confocal uptake pictures were obtained by a LSM 710 NLO (Carl Zeiss, Germany) and images were processed with the software ZEN 2009 (Carl Zeiss, Germany). CLSM experiments were performed with the technical assistance of [redacted] from the core facility for laser scanning microscopy of the FZI Mainz.

For lysosome staining, $CD4^+CD25^{high}$ T cells (stimulated with anti-CD3 and anti-CD28 mAbs; CellTrace™ Violet unstained) were seeded at $1x10^6$ cells/dish in µ-Dish$^{35mm, low}$ in 800 µl X-VIVO™ 20 medium. HES-D-IL-2 NCs were applied on the cells for 24 h at a concentration of 75 µg/ml. Before microscopy, cell membranes and lysosomes were stained with 1 µg/ml CellMask™ Deep Red Plasma membrane stain and 50 nM LysoTracker® Green DND-26 for staining of acidic vesicles for 20 min and 30 min, respectively. CLSM images were taken with Leica microscopy (TCS SP5X) and images were formatted using the lite version of the Leica confocal software (LCS) (Leica, Germany). CLSM microscopy was conducted with the technical assistance of [redacted] from the Max Planck Institute for Polymer Research in Mainz.

5.2.5 [^{3}H]-Thymidine Incorporation Assay

Proliferating cells must undergo DNA replication during S phase of cell cycle so that the exact copy of DNA can be passed to the daughter cell. If the radioactive nucleotide [^{3}H]-thymidine is present during cell division, it will be incorporated into DNA by matching the base adenosine.

Cells cultured in 96-well plates were pulsed with 1 µCi [^{3}H]-thymidine for 16-18 h at 37 °C. Afterwards, the cells were harvested with a Semiautomatic cell harvester (Skatronas, Skatron) and mixed with double-distilled water for cell bursting. Cell fragments and DNA were floated on a glassfiber filter membrane (Printed Filtermat A, glass fibre filter, PerkinElmer), embedded in a sample bag for a Betaplate™ (PerkinElmer) and radioactivity was measured utilizing a liquid scintillation counter (1205 Betaplate; LKB Wallac). [^{3}H]-thymidine incorporation is expressed as counts per minute (cpm) representing the proliferation rate. Percentage of proliferation was calculated by dividing cpm from the sample of interest with cpm obtained from the control group.

Proliferation [%] = [cpm (sample) / cpm (control)] * 100%

5.2.6 Mixed Leukocyte Reaction of T Cells and Nanoparticle-Loaded Dendritic Cells

Immature DCs (day 5) were incubated with SEMA- and VBPA-functionalized NPs at a concentration of 75 µg/ml for 24 h at 37 °C. Free NPs were washed out with PBS from the culture and the cells were additionally cultured for another two days with GM-CSF and IL-4 to retain the cells immature, whereas the other half of the cells was cultured with the "maturation cytokine cocktail" to induce terminal differentiation of the NP-treated iDCs. Before DCs were applied in a mixed leukocyte reaction, viable cells were counted with a Neubauer Chamber in a trypan blue exclusion assay. NP-loaded iDCs or mDCs were seeded at 0.25x10^4 DCs/well in a 96-well plate in X-VIVO™ 20 medium supplemented with 0.5% DC-derived autologous serum and 2 U/ml IL-2 (Proleukin). Human allogeneic CD4$^+$ T cells were added at a 10:1 ratio (0.25x10^5 TCs/well) and the culture was incubated for 3 days at 37 °C. Proliferation was measured by addition of [^{3}H]-thymidine (1 µCi) incorporation for 18 h.

In order to determine the cytokine secretion of T cells that were treated with NP-loaded DCs, another co-culture with higher cell numbers was prepared. Thus, a co-culture of NP-loaded DCs (3x10^5 DCs/well) and allogeneic CD4$^+$ T cells (3x10^6 TCs/well) in X-VIVO™ 20 medium supplemented with 0.5% DC-derived autologous serum and 2 U/ml IL-2 (Proleukin) in 6-well plates (3 ml/well) was assembled. After three days of culture 1.5 ml medium was collected for cytokine measurements and 1.5 ml fresh X-VIVO™ 20 medium supplemented with 0.5% DC-derived serum and 2 U/ml IL-2 (Proleukin) was added to the cultures.

5.2.7 Human Cytokine Analysis by Enzyme-Linked Immunosorbent Assay

5.2.7.1 Co-Culture of SEMA and VBPA Nanoparticle-Loaded Dendritic Cells and T Cells

Supernatants of NP-loaded DCs and co-cultures of NP-loaded DCs with $CD4^+$ T cells were obtained at different time points for the analysis of distinct cytokines associated with DC activation.

Human iDCs (day 5) were seeded at $1x10^6$ cells/well (3 ml/well) in 6-well plates in Iscove's MDM supplemented with 2.5% autologous serum, 400 U/ml GM-CSF and 150 U/ml IL-4. Immature DCs were stimulated with SEMA- and VBPA-functionalized NPs at a concentration of 75 µg/ml and 1 ml supernatants were taken after 24 h culture at 37 °C. The amounts of human IL-6, TNF-α and IL-10, IL-12p40 and IL-12p70 cytokines present in the supernatants were measured by enzyme-linked immunosorbent assay (ELISA). Untreated iDCs were taken as control.

In addition, supernatants derived from co-cultures of $CD4^+$ T cells and NP-loaded DCs were analyzed by ELISA measurements. In brief, NP-loaded DCs were co-cultured with allogeneic $CD4^+$ T cells in a 1:10 ratio (see section 5.2.6). After three days of co-culture supernatants were taken for ELISA. The supernatants from the co-culture of NP-loaded DCs and $CD4^+$ T cells were analyzed for the presence of IL-5, IL-10, IL-13 and interferon gamma (IFN-γ).

ELISA measurements were performed according to manufacturer's instructions. Unspecific binding was prevented by incubation either with 1-5% Albumin Fraction V or 10% FBS regarding to manufacturer's instructions. After each incubation, except after blocking unspecific binding sites, the wells were washed with PBS containing 0.05% Tween® 20. ELISA Kits from BD Bioscience included a Streptavidin-horseradish peroxidase conjugate enzyme reagent, whereas ELISA Kits from Immunotools, including ELISAs for IL-6, IL-10, IL-13, IFN-γ and TNF-α, were incubated with Streptavidine conjugated to Poly-Horse Radish Peroxidase (Poly-HRP) that was not included in the Kit at a dilution of 1:3000 for 30 min at 4 °C. Absorbance was detected at 450 nm with a reference wavelength of 570 nm in a microplate reader (Model 450, Bio-Rad Laboratories).

5.2.7.2 IL-2 Amounts on HES-D-IL-2 Nanocapsules

It is of major interest to determine the amount of ligand molecules present on the capsule surface. Testing the functionality of IL-2 in CTLL-2 proliferation assays, the amount of functional IL-2 can already be roughly estimated (see section 5.2.8). Besides, IL-2 ELISA measurements of the capsule suspension can be performed. However, it has to be considered that not all IL-2 molecules can be measured due to the sandwich arrangement in

an ELISA. Thus, the “relative” amount of IL-2 obtained by ELISA can rather be used for comparison with the amount of IL-2 in the capsule supernatant and among nanocapsules which differed in their amount of linked IL-2. As described above, after linking IL-2 to the capsule surface, the capsule suspension was dialyzed against 0.9% NaCl saline to get rid of dispensable amounts of IL-2 in the supernatant. Dialysis was followed by two centrifugation steps and the supernatant of each centrifugation step was measured for the abundance of IL-2.

To measure the IL-2 level on HES-D-IL-2 capsules, a small aliquot of constantly stirring capsules was taken. Additionally, the two supernatants, HES-D-IL-2 SN1 and HES-D-IL-2 SN2 obtained from the two centrifugation steps during NC purification, were determined for the amount of IL-2. Human IL-2 was measured with an ELISA Kit according to manufacturer’s instructions.

5.2.8 CTLL-2 Proliferation Assay

IL-2-dependent growing murine CTLL-2 T lymphocytes were cultured in RPMI1640 medium supplemented with 2 mM L-glutamine, 50 µM β-mercaptoethanol, 10% fetal bovine serum (FBS) and 50 U/ml IL-2 (Proleukin). Cells were split every 2-3 days and seeded at a concentration of $1x10^5$ cells/ml in a total volume of 3 ml per well in a 6-well plate. CTLL-2 cells were not IL-2 stimulated for at least 48 h and washed twice with PBS before experimental set up. For removal of dead cells, CTLL-2 cells were washed with PBS and spun at 150xg for 10 min at 4 °C.

CTLL-2 lymphocytes were seeded at $3x10^3$ cells/well in a 96-well plate (200 µl medium per well) in RPMI1640 medium supplemented with 2 mM L-glutamine, 50 µM β-mercaptoethanol, 10% fetal bovine serum (FBS). Penicillin-Streptomycin was added to the cell culture at a final concentration of 100 U/ml. To determine IL-2-dependent CTLL-2 growth, the cells were stimulated with IL-2 (Proleukin) at decreasing concentrations (1:2 dilutions) between 20 ng/ml and 0.0098 ng/ml. Since the CTLL-2 maintenance culture received different IL-2 (Proleukin) than the IL-2 that was bound to the capsule surface (Cell Sciences), both unfunctionalized IL-2 cytokines were applied in the assay as control. The stimulated cells were cultured for 48 h at 37 °C. Proliferation was measured by addition of 1 µCi [^{3}H]-thymidine for 18 h at 37 °C.

To measure the biological activity of azide-functionalized IL-2 (IL-2-N_3) the functionalized cytokine was additionally titrated on CTLL-2 cells. HES-D, HES-D-IL-2 and HES-D-IL-2^{low} NCs were titrated on CTLL-2 cells at different concentrations (75, 25, 12.5, 10, 1, 0.1, 0.01 and 0.001 µg/ml). The two supernatants obtained after dialysis during capsule purification

were additionally titrated on CTLL-2 cells. As the capsule supernatant and capsule suspension were dispersed in the same volume, the supernatants were applied with the same µl-volume as the respective capsule suspension.

5.2.9 Application of HES-D-IL-2 Nanocapsules *In Vivo*

HES-D-IL-2 NCs (300 µg in 150 µl 0.9% NaCl saline) were injected intravenously at approximately $1.5x10^{12}$ NCs/mouse into the tail of five to eight week old wild type C57BL/6 mice. Control mice received 0.9% NaCl saline alone. Mice were euthanized 24 h after injection by carbon dioxide inhalation, followed by dissection of auricular, cervical and inguinal lymph nodes, spleen and liver in Hank's Buffered Balanced Solution (HBBS) medium. Regarding lymph nodes and spleen, a single cell suspension was prepared by pressing the cells through a sterile 70-µm nylon cell strainer and cells were harvested at 400xg for 10 min at 4 °C. Besides, liver cells were mechanically separated by utilizing a scalpel and digested with 1 mg/ml collagenase type IV and 0.02 mg/ml Deoxyribonuclease I (DNaseI) in HBBS medium for 30 min shaking at 37 °C. Afterwards, liver cells were further separated by a sterile 70 µm nylon cell strainer and harvested at 400xg for 10 min at 4 °C. Lymphocytes, splenocytes and liver cells were washed with PBS and incubated with 1 ml ACK (ammonium-chloride-potassium) lysing buffer for 3 min at RT for removal of erythrocytes. Splenocytes and liver cells were not stained for flow cytometry analysis.

Lymphocytes were labeled with 1 µg anti-mouse CD16/CD32 Fc Block per $1x10^7$ cells for 20 min at 4 °C to inhibit unspecific binding of fluorescence-labeled antibodies to Fc receptors. The cells were washed with PBS and harvested at 400xg for 10 min at 4 °C, followed by staining the cells with the Fixable Viability Dye eFluor® 780 (1:1000 diluted in PBS) for 30 min at 4 °C. Cells were washed with FACS buffer (PBS containing 0.5% FBS and 1 mM EDTA) before cell surface molecule staining. $1x10^7$ cells were taken for each staining. In order to determine the capsule uptake into T cells, cells were stained with anti-mouse-CD4-PerCP-Cy5.5 and anti-mouse-CD25-APC mAbs for 30 min at 4 °C. For uptake of NCs by APCs, cell samples were separately stained with anti-mouse-B220-FITC, anti-mouse-CD11c-APC and anti-mouse-F4/80-PerCP-Cy5.5 mAbs. For controls, unstained lymphocytes were taken. Single stainings for compensation were performed with anti-mouse-CD4-PerCP-Cy5.5, anti-mouse-CD90.2(Thy-1.2)-APC and anti-mouse-CD90.2(Thy-1.2)-FITC mAbs. To increase the total cell number, each staining was performed twice and the cells were combined for flow cytometry analysis. Samples were measured using a BD LSRFortessa™ cell analyzer.

5.2.10 Statistical Analysis

Statistical analysis was performed by using GraphPad Prism 5 for Windows and GraphPad Prism 6 for Mac. For comparison of two samples that were linked together, a paired student t-test was performed.

For calculation of the half maximal effective concentration (EC_{50}) value, IL-2 concentration was converted into Log10. By using a nonlinear regression analysis with log(agonist) vs. response (three parameters), the EC_{50} values were calculated.

5.3 Theory of Methods

5.3.1 Mixed Leukocyte Reaction of Dendritic Cells and Allogeneic T Cells

5.3.1.1 Dendritic Cell Maturation

Antigen-presenting DCs play an outstanding role during initiation of an immune response by linking the innate and adaptive immune system.[10] Immature DCs express a pattern of immune receptors on their surface, so-called pattern recognition receptors (PRRs), including Toll-like receptors (TLRs), that recognize pathogen-associated molecular patterns (PAMPs) and damage-associated molecular patterns (DAMPs), and cytokine receptors through which signaling iDC maturation and migration to secondary lymphoid organs is induced.[11,209] Encountered foreign antigens, the proteins get processed by DCs and presented via major histocompatibility complex (MHC) molecules on the cell surface.[14,16] Humans display a variety of different MHC proteins, called human leukocyte antigen (HLA). DC maturation, which is induced upon antigen, cytokine or T cell stimulation, comprises elevated expression levels of MHC molecules and the upregulation of co-stimulatory surface molecules, including CD80 (B7-1), CD86 (B7-2) and CD40.[9]

5.3.1.2 T Cell Stimulation

For T cell activation *in vitro* and *in vivo* two signals are required simultaneously.[9] The first signal is antigen-specific and is transmitted through interaction of the TCR with peptide-loaded MHC molecules on antigen presenting cells (APCs). In a second signal, the co-stimulatory molecules present on the APC surface (CD80 and CD86) interact with surface molecules on T cells (CD28). This second signal is indispensable for a proper T cell activation.[9] Following activation, APC-derived cytokines determine T cell differentiation.[19,21]

A conclusive technique in immunology to assay T cell responses is a mixed leukocyte reaction (MLR) by measuring T cell proliferation.[14,210] Based on the broad HLA isotype

diversity, primary T cells mixed with allogeneic DCs get activated and proliferate. T cell proliferation is measured via a [^{3}H]-thymidine incorporation assay. Moreover, T cell stimulation can be triggered by monoclonal antibodies against CD3 that resembles the signaling subunit of the TCR and the co-stimulatory molecule CD28. T cell proliferation can be further enhanced by adding the cytokine IL-2 to the cultures.[62]

5.3.2 Enzyme-Linked Immunosorbent Assay

An enzyme-linked immunosorbent assay (ELISA) was first described by Engvall and Perlmann in 1971, but radioactivity was early replaced by peroxidase-conjugated antibodies and the assay was gradually altered.[211] In brief, in a sandwich ELISA, which was conducted in the present study, the antibody against the target antigen, so-called capture antibody, is coated on a 96-well plate. Before the suspension containing the antigen of interest is added to the well and the antigen interacts with the antibody, unspecific binding sites are blocked with serum. A second, peroxidase-linked antibody, the so-called detection antibody, against the antigen is applied on the antibody-antigen complex. The two antibodies must detect different epitopes on the antigen to impede competitive binding. Each sample or standard is examined as duplicate and the mean absorbance at concentration zero of the standard is subtracted from each sample.

For calculation of protein concentration a standard curve of the protein of interest has to be generated on the same plate. Thus, the mean absorbance (y-axis) is plotted against the concentration (x-axis) and curve fitting is performed. If the mean absorbance of the protein of interest is not in the range of the standard curve, the sample has to be diluted and afterwards the calculated concentration has to be multiplied with the dilution factor.

5.3.3 Flow Cytometry

Fluorescence is the emission of light with higher wavelengths from excited fluorochromes. Fluorescent molecules get excited by photon adsorption and adopt a higher energy state that returns into its resting energy state through the emission of light.[212]
The ability to assess cell size, granularity, cell membrane proteins and intracellular proteins at a single cell levels renders this technique crucial for molecular cell analysis in immunology.

For single cell analysis, the cells are separated in a fluid stream, the so-called continuous laminar flow. Through the excitement of a cell with a monochromatic laser beam, the cell emits light in all directions that is collected by distinct filters and dichroic mirrors.[212] The emitted light is collected and measured by photomultiplier tubes for analysis. By means of the “Forward Scatter (FSC)” the size of cells can be detected for preliminary discrimination

between dead and living cells, whereas the “Sideward Scatter (SSC)” can be utilized to make predications about the granularity of a cell. In line with the SSC distinct other filters collect the fluorescence from the excited cell.[212] Cell membrane proteins or intracellular proteins can be detected by measuring the fluorescence intensity of the fluorochrome-labeled antibodies.

During the detection of more than one fluorochrome at the same time, the emission spectra of the distinct dyes may overlap. In order to minimize spectral overlap the fluorochromes have to be compensated against each other, which can be achieved through single stainings.

For data analysis the FSC channel is blot against the SSC channel in order to gate for the cell population of interest. The population of interest is further selected for the discrimination of doublets by plotting the weight against area channel (FSC-W vs. FSC-A and SSC-W vs. SSC-A) and thus, detect disproportions between cell size and cell signal. The singlets with distinct fluorescence intensities are displayed in histograms or dot plots and gated for fluorescently positive and negative cells expressed as percentage of positive cells. In addition to percentages, the mean fluorescence intensity (MFI) of a fluorescent dye from a parenteral population can be used for comparative analysis.

In this thesis either a BD™ LSRII flow cytometer equipped with a Blue Argon laser (488 nm), HeNe Red diode laser (633 nm), Violet laser (405 nm) and a UV laser (325 nm) or a BD LSRFortessa™ containing an additional Yellow Green laser (561 nm) was used. The various fluorochromes applied in the present study are listed in Table 4 with their excitation and peak emission.

Table 4. Fluorescent dyes used for flow cytometry.

Fluorochrome	Abbreviation	Excitation maximum [nm]	Peak emission [nm]	Laser line [nm]	Filter
Annexin V-Allophycocyanine	Annexin V-APC	650	660	633 (LSR)	660/20
Allophycocyanine	APC	650	660	640 (Fortessa) 633 (LSR)	670/30 660/20
CellTrace™ Violet	-	405	450	405 (Fortessa) 405 (LSR)	450/50 440/40
eFluor450 / V450	eFluor450	405	450	405 (LSR)	440/40
Fluoresceinisothiocyanate	FITC	495	519	488 (Fortessa) 488 (LSR)	530/30 530/30
Fixable Viability Dye eFluor® 780	eFluor780	633	780	640 (Fortessa) 633 (LSR)	780/60 780/60
R-Phycoerythrin	PE	480; 565	578	633 (LSR)	575/26
R-Phycoerythrin-Cyanine 5	PE-Cy5	480; 565; 650	670	633 (LSR)	695/40
Peridinin chlorophyll-Cyanine	PerCP-Cy5.5	480	695	488 (Fortessa)	710/50

Fluorochrome	Abbreviation	Excitation maximum [nm]	Peak emission [nm]	Laser line [nm]	Filter
5.5					
N-(2,6-diisopropylphenyl)perylene-3,4-dicarbonacidimid	PMI	488	525	488 (LSR)	530/30
Sulforhodamine 101	SR101	580	605	561 (Fortessa)	610/20

5.3.4 Confocal Laser Scanning Microscopy

Nanoparticle uptake by cells assessed with flow cytometry analysis does not differentiate between intracellular particle uptake and mere association with the cell membrane. Confocal laser scanning microscopy (cLSM) enables the pointwise "scanning" of a single focal plane from three-dimensional specimens due to optical sectioning.[213] Due to distinct filtering techniques out-of-focus light is subtracted from the focal plane and thus, allows discriminating between intracellular and extracellular particle localization. In contrast to conventional light microscopy, not the whole specimen is illuminated at the same time, but one region after another resulting in further reduction of light scattering.[213] Beyond that, optical sectioning from three-dimensional specimen enables to mount a 3D reconstruction of the analyzed specimen in the z-axis.

In the present work, nanomaterial uptake by living cells was assessed. For precise determination of intracellular or extracellular localization of the biomaterials, cell nucleus and cell membrane were additionally stained. Fluorescent dyes that were used for confocal microscopy are listed in Table 5.

Table 5. Fluorochromes used for confocal laser scanning microscopy.

Fluorochrome	Excitation maximum [nm]	Peak emission [nm]	Laser detection
CellMask™ Deep Red Plasma membrane stain	649	666	Helium-Neon laser (633 nm) (Leica) Helium-Neon laser (633 nm) (Zeiss)
CellMask™ Orange Plasma membrane stain	554	567	DPSS laser (561 nm) (Leica)
DRAQ5®	647	681	Helium-Neon laser (633 nm) (Leica)
Hoechst 33342 nucleic acid stain	343	483	Argon-UV (405 nm) (Zeiss)
LysoTracker® Green DND-26	504	511	Argon laser (496 nm) (Leica)
PMI	488	525	Argon laser (488 nm) (Leica)
SR101	580	605	DPSS laser (561 nm) (Leica) Helium-Neon laser (543 nm) (Zeiss)

6 Appendix

6.1 Reagents and Materials

Table 6. Reagents

Reagent	Company	Cat #	Conc used	Application
2-Mercaptoethanol	Sigma	M-7522	50 µM	Cell culture
ACK Lysing Buffer, BioWhittaker	Lonza	10-548E	Stock	Erythrolysis
Albumin Fraktion V	Roth	8076.2	1-5%	ELISA
Annexin V Apoptosis Detection Kit APC	eBioscience	88-8007-74	1:20	Flow cytometry
Anti-human-B7DC-PE mAb (clone: MIH18; IgG1κ; mouse)	eBioscience	12-5888-41	1:2	NP-loaded DCs, flow cytometry
Anti-human-B7H2-PE mAb (clone: MIH12; IgG1κ; mouse)	eBioscience	12-5889-71	1:4	NP-loaded DCs, flow cytometry
Anti-human-CCR7-PE mAb (clone: 150503; IgG2a; mouse)	R&D Systems	FAB197P	1:2	NP-loaded DCs, flow cytometry
Anti-human-CD122-APC mAb (clone: TU27; IgG1κ; mouse)	BioLegend	339008	1:4	IL-2R staining, flow cytometry
Anti-human-CD132-PE mAb (clone: TUGh4; IgG2bκ; rat)	BD Pharmingen	555898	1:4	IL-2R staining, flow cytometry
Anti-human-CD14 mAb (clone: RMO52; IgG2aκ, mouse)	Beckman Coulter	IM0643	5 µg/ml	DC maturation, flow cytometry
Anti-human-CD19 mAb (clone: J4-119; IgG1; mouse)	Beckman Coulter	IM1313	5 µg/ml	DC maturation, flow cytometry
Anti-human-CD25-PE mAb (clone 4E3; IgG2b, mouse)	Miltenyi Biotec	130-091-024	1:5	$CD4^+$ T cell characterization
Anti-human-CD25-PE-Cy5 mAb (clone M-A251; IgG1κ; mouse)	BD Pharmingen	555433	1:2	IL-2R staining, flow cytometry
Anti-human-CD25-V450 mAb (clone: M-A251; IgG1; mouse)	BD Bioscience	560355	1:20	IL-2R staining, flow cytometry
Anti-human-CD273 (B7-DC)-PE mAb (clone MIH18; IgG1κ, mouse)	eBioscience	12-5888	1:2	NP-loaded DCs, flow cytometry

Reagent	Company	Cat #	Conc used	Application
Anti-human-CD275 (B7-H2)-PE mAb (clone MIH12; IgG1κ, mouse)	eBioscience	14-5889	1:4	NP-loaded DCs, flow cytometry
Anti-human-CD28 mAb (clone: CD28.2; IgG1κ; mouse)	BD Pharmingen	555725	0.5-2 µg/ml	T cell stimulation
Anti-human-CD3 mAb (clone: OKT3)	Lab made	-	1 µg/ml	T cell stimulation
Anti-human-CD4 microbeads	Miltenyi Biotec	120-000-440	1:5	T cell isolation
Anti-human-CD4-APC mAb (clone: RPA-T4; IgG1; mouse)	BD Pharmingen	555349	1:20	IL-2R staining, flow cytometry
Anti-human-CD4-FITC mAb (clone: 13B8.2; IgG1; mouse)	Beckman Coulter	A07750	1:4	IL-2R staining, flow cytometry
Anti-human-CD4-FITC mAb (clone: 13B8.2; IgG1; mouse)	Beckman Coulter	A07750	1:30	$CD4^+$ T cell characterization
Anti-human-CD4-PE mAb (clone: EDU-2; IgG2a; mouse)	Immunotools	21270084	1:10	IL-2R staining, flow cytometry
Anti-human-CD8-FITC mAb (clone: B9.11; IgG1; mouse)	Beckman Coulter	A07756	1:30	$CD4^+$ T cell characterization
Anti-human-CD80 mAb (clone: MAB104; IgG1; mouse)	Beckman Coulter	IM1449	5 µg/ml	DC maturation, flow cytometry
Anti-human-CD80-PE mAb (clone: MAB104; IgG1; mouse)	Beckman Coulter	IM1853U	1:2	NP-loaded DCs, flow cytometry
Anti-human-CD83 mAb (clone: HB15a; IgG2bκ; mouse)	Beckman Coulter	IM2069	5 µg/ml	DC maturation, flow cytometry
Anti-human-CD83-PE mAb (clone: HB15e; IgG1κ; mouse)	BD Pharmingen	12-0839	1:2	NP-loaded DCs, flow cytometry
Anti-human-CD86 mAb (clone: BU63; IgG1; mouse)	AbD Serotec	MCA1118	5 µg/ml	DC maturation, flow cytometry
Anti-human-CD86-PE mAb (clone: IT2.2; IgG2bκ; mouse)	eBioscience	12-0869	1:10	NP-loaded DCs, flow cytometry

Reagent	Company	Cat #	Conc used	Application
Anti-human-Foxp3-eFluor®450 mAb (clone: 236A/E7; IgG1κ; mouse)	eBioscience	48-4777	1:10	IL-2R staining, flow cytometry
Anti-human-HLA-DR-PE mAb (clone: MEM-12; IgG1κ, mouse)	Immunotools	21278994	1:5	NP-loaded DCs, flow cytometry
Anti-human-MHCII-HLA-DR mAb (clone: YD1/63.4.10; IgG2a; rat)	Thermo Scientific	MA1-70113	5 µg/ml	DC maturation, flow cytometry
Anti-mouse-CD11c-APC mAb (clone: N418; Armenian hamster IgG)	eBioscience	17-0114-82	1:100	Murine cells *ex vivo*
Anti-mouse-CD16/32 (clone: 93; IgG2aλ; rat)	eBioscience	14-0161-85	1 µg per $1x10^7$ cells	Murine cells *ex vivo*
Anti-mouse-CD25-APC mAb (clone: PC61.5; IgG1λ; rat)	eBioscience	17-0251-81	1:50	Murine cells *ex vivo*
Anti-mouse-CD4-PerCP-Cy5.5 mAb (clone: RM4-5; IgG2aκ; rat)	eBioscience	45-0042-82	1:200	Murine cells *ex vivo*
Anti-mouse-CD90.2(Thy-1.2)-APC mAb (clone: 53-2.1; IgG2aκ; rat)	eBioscience	17-0902-81	1:400	Murine cells *ex vivo*
Anti-mouse-CD90.2(Thy-1.2)-FITC mAb (clone: 53-2.1; IgG2aκ; rat)	eBioscience	11-0902-82	1:200	Murine cells *ex vivo*
Anti-mouse-F4/80-PerCP-Cy5.5 mAb (clone: BM8; IgG2aκ; rat)	eBioscience	45-4801-80	1:1000	Murine cells *ex vivo*
Anti-mouse/human-CD45R/B220-FITC mAb (clone: RA3-6B2; IgG2aκ; rat)	BioLegend	103206	1:1000	Murine cells *ex vivo*
Biocoll Separation Solution	Biochrom AG	L6115	Stock	PBMC isolation
CellMask™ Deep Red Plasma membrane stain	Molecular Probes	C10046	1 µg/ml	cLSM
CellMask™ Orange Plasma membrane stain	Molecular Probes	C10045	5 µg/ml	cLSM

Reagent	Company	Cat #	Conc used	Application
CellTrace™ Violet Cell Proliferation Kit	Molecular Probes	C34557	0.5 µM	T cell proliferation
Collagenase, Type IV	CellSystems	LS004188	1 mg/ml	Murine cells *ex vivo*
Deoxyribonuclease I	CellSystems	LS002138	0.02 mg/ml	Murine cells *ex vivo*
Dimethyl sulfoxide (DMSO) Hybri-Max®	Sigma	D2650	Stock	
DRAQ5®	Cell Signaling Technology	4084L	2.5 µg/ml	cLSM
Dulbecco's Phosphate Buffered Saline (DPBS)	Gibco by life technologies	14190-094	1x	PBMC isolation
Fetal Bovine Serum (FBS)	PAA Laboratories	A15-151	0.5-10%	Cell culture, ELISA
Fixable Viability Dye eFluor® 780	eBioscience	65-0865-14	1:1000	Flow cytometry
Foxp3 Staining Buffer Set	eBioscience	00-5523-00	-	Foxp3 staining
Granulocyte-macrophage colony stimulating factor (GM-CSF) (recombinant human); Leukine® lyophilized LEUKINE 250 mcg	Sanofi-aventis	NDC-0024-5843-05	400 U/ml	iDC and mDC culture
Hank's Balanced Salt Solution	Sigma-Aldrich	H6648	-	Murine cells *ex vivo*
Hoechst 33342	Invitrogen	H3570	1 µg/ml	cLSM
Human-Albumin 20%	CSL Behring	E4044411B	0.5%	MACS Buffer
Interferon gamma (IFN-γ) ELISA (matched pair for ELSIA)	Immunotools	21333538	-	MLR
Interleukin-10 (high sensitivity human ELISA Set)	Immunotools	31330109	-	DC maturation, MLR
Interleukin-12 (p40) ELISA (BD OptEIA™ Set Human IL-12 (p40))	BD Bioscience	555171	-	DC maturation
Interleukin-12p70 ELISA (BD OptEIA™ Set Human IL-12 (p79))	BD Bioscience	555183	-	DC maturation
Interleukin-13 ELISA (matched pair for ELISA)	Immunotools	21339138	-	MLR

Reagent	Company	Cat #	Conc used	Application
Interleukin-1β (recombinant human)	Miltenyi Biotec	130-093-898	2.5 ng/ml	mDC culture
Interleukin-2 ELISA (BD OptEIA™ Set Human IL-2)	BD Bioscience	555190	-	HES-D-IL-2
Interleukin-2® (recombinant, human)	Cell Sciences	CRI100C	-	HES-D-IL-2
Interleukin-4	Immunotools	11340047	150 U/ml	iDC and mDC
Interleukin-5 ELISA (BD OptEIA™ Set Human IL-5)	BD Bioscience	555202	-	MLR
Interleukin-6 (recombinant human)	Strathmann Biotec	hIL6-25	25 U/ml	mDC culture
Interleukin-6 ELISA (human)	Immunotools	31670069	-	DC maturation
Iscove's Modified Dulbecco's Medium (MDM)	PAA Laboratories	E15-819	-	DC culture
Isotype control: mouse IgG1-FITC (clone: 679.1Mc7)	Beckman Coulter	A07795	1:30	$CD4^+$ T cell characterization
Isotype control: mouse IgG1κ (clone: MOPC-21)	BD Pharmingen	554680	1:10	NP-loaded DCs, flow cytometry
Isotype control: mouse IgG1κ-PE-Cy5 (clone: MOPC-21)	BD Pharmingen	555750	1:10	$CD4^+$ T cell characterization
Isotype control: mouse IgG2aκ (clone: G115-178)	BD Pharmingen	554648	1:10	NP-loaded DCs, flow cytometry
Isotype control: mouse IgG2aκ (clone: MOPC-173)	BD Pharmingen	554126	1:50	DC maturation, flow cytometry
Isotype control: mouse IgG2b-PE (clone: IS6-11E5.11)	Miltenyi Biotec	130-092-215	1:10	$CD4^+$ T cell characterization
Isotype control: rat IgG2aκ (clone: R35-95)	BD Pharmingen	553927	1:50	DC maturation, flow cytometry
L-Glutamine (200 mM)	PAA Laboratories	M11-004	2 mM	Cell culture
Limulus Amebocyte Lysate PYROGENT Plus Single test Kit	Lonza	N289-06	-	Endotoxin
LysoTracker® Green DND-26	Molecular Probes	L7526	50 nM	cLSM

Reagent	Company	Cat #	Conc used	Application
Paraformaldehye extra pure	Merck	104005	4%	Cell fixation
Penicillin-Streptomycin (10,000 U/ml)	Gibco by Life Technologies	15140-122	100 U/ml	Cell culture
Proleukin® 18 x 10^6 IU (Aldesleukin)	Chiron	UA0556B/10	0-200 IU/ml	T cell stimulation
Prostaglandin E_2 (PGE_2)	Cayman Chemical	14010	0.5 µg/ml	DC maturation
RPMI 1640, BioWhittaker®	Lonza	BE12-167F	-	iDC and mDC
Saline (sterile solution of sodium chloride (NaCl, 0.9%)	B.Braun	0375B14	Stock	Nanocapsules
Secondary antibody: FITC Goat anti-rat IgG (clone: Poly4054)	BioLegend	405404	1:80	DC maturation, flow cytometry
Secondary antibody: PE F(ab')2 Fragment Donkey anti-mouse IgG	Jackson ImmunoResearch	715-116-151	1:100	DC maturation, flow cytometry
Streptavidine conjugated to Poly-Horse Radish Peroxidase (Poly-HRP)	ImmunoTools	31334248	1:3000	ELISA from Immunotools
Thymidine, specific activity 20Ci(740GBq), 5mCi	PerkinElmer	NET027X005MC	1 µCi	Proliferation assay
Trypan Blue Solution (0.4%)	Sigma	T8154	0.04%	Cell counting
Tumor Necrosis Factor alpha (TNF-α) (high sensitivity human ELISA Set)	Immunotools	31333019	-	DC maturation
Tumor Necrosis Factor alpha (TNF)-α (recombinant human)	Miltenyi Biotec	130-094-024	2.5 ng/ml	mDC culture
Tween® 20	Sigma-Aldrich	P1379	0.05%	ELISA
X-VIVO™ 20 Medium	Lonza	BE04-448Q	-	T cell culture

Table 7. Materials

Material	Company	Cat #	Application
70-µm Falcon™ Cell Strainers	Fisher Scientific	352350	Murine cell isolation
Disposable dental needle, 0.5x25 mm	B. Braun Medical AG	9186158	^{3}H-thymidine assay
Injekt®-F, Single-use syringes, 1 ml	B. Braun Medical AG	9166017V	^{3}H-thymidine assay
LS column	Miltenyi Biotec	130-042-401	T cell isolation
MidiMACS™ Separator (LS)	Miltenyi Biotec	130-042-301	T cell isolation
Nunc™ Lab-Tek™ Chambered Coverglass, 8-well	Thermo Scientific	155411	cLSM
Printed Filtermat A, glass fibre filter	PerkinElmer	1205-401	^{3}H-thymidine assay
Sample Bag for Betaplate™	PerkinElmer	1205-411	^{3}H-thymidine assay
µ-Dish $^{35mm, low}$	ibidi	80131	cLSM

6.2 List of Abbreviations

Ab	Antibody
ACK	Ammonium-Chloride-Potassium
APC	Antigen-presenting cell (in the context of cells)
APC	Allophycocyanine (in the context of fluorescent dyes)
APC-Cy	Allophycocyanine-Cyanine 7
BSA	Bovine serum albumin
CCR7	C-C chemokine receptor type 7
CD	Cluster of differentiation
CLSM	Confocal laser scanning microscopy
cpm	Counts per minute
CTCL	Cutaneous T cell lymphoma
CTL	Cytotoxic T lymphocyte
CTLA-4	Cytotoxic T-lymphocyte antigen
CTLL-2	Cytotoxic T cell line
DAMP	Damage-associated molecular patterns
DBCO	Dibenzylcyclooctyne
DC	Dendritic cell
DEREG	*De*pletion of *reg*ulatory T cells
DLS	Dynamic light scattering
DMSO	Dimethyl sulfoxide
DNA	Deoxyribonucleic acid
DNase	Deoxyribonuclease
DPBS	Dulbecco's phosphate buffered saline
EC_{50}	Half maximal effective concentration
EDTA	Ethylenediaminetetraacetic acid
ELISA	Enzyme-linked immunosorbent assay
EM	Electron microscopy
EPR-Effect	Enhanced permeability and retention effect
EU/ml	Endotoxin units per milliliter
FACS	Fluorescence activated cell sorter; flow cytometry

FBS	Fetal bovine serum
FDA	Food and Drug Administration (USA)
FITC	Fluoresceinisothiocyanate
Foxp3	Forkhead box P3
FRET	Fluorescence resonance energy transfer
FSC	Forward scatter
g	Gravity
GM-CSF	Granulocyte-macrophage colony stimulating factor
HBBS	Hank's buffered balanced saline
HES	Hydroxylethyl starch
HES-D	Dibenzylcyclooctyne-functionalized HES nanocapsules
HES-D-IL-2	Interleukin 2-functionalized HES-D nanocapsules
HLA	Human leukocyte antigen
ICOS	Inducible co-stimulator
iDC	Immature dendritic cell
IFN-γ	Interferon-gamma
IgG	Immunoglobulin G
IL	Interleukin
IL-2R	Interleukin-2 receptor
iNOS	Inducible nitric oxide synthase
iTreg	Induced regulatory T cell
kDa	Kilo Dalton
LAL	Limulus amebocyte lysate
LCS	Leica confocal software
LPS	Lipopolysaccharide
LSM	Laser scanning microscopy
mAb	Monoclonal antibody
mDC	Mature dendritic cell
MDM	Modified Dulbecco's Medium
MDSC	Myeloid-derived suppressor cell
MFI	Mean fluorescence intensity

MHC	Major histocompatibility complex
MLR	Mixed leukocyte reaction
NC	Nanocapsule
NK cell	Natural killer cell
NK T cell	Natural killer T cell
nMFI	Normalized mean fluorescence intensity
NP	Nanoparticle
nTreg	Natural regulatory T cell
OVA	Ovalbumin
P(E/B-*b*-EO)	Poly((ethylene-co-butylene)-b-(ethylene oxide))
PAMP	Pathogen-associated molecular patterns
PBMC	Peripheral blood mononuclear cell
PBS	Phosphate buffered saline
PE	R-Phycoerythrin
PE-Cy	R-Phycoerythrin-Cyanine
PEG	Poly(ethylene glycol)
PEO	Poly(ethylene oxide)
PerCP-Cy5.5	Peridinin chlorophyll-Cyanine 5.5
PFA	Paraformaldehyde
PGE_2	Prostaglandin E2
PLGA	Poly(lactic-co-glycolic acid)
PMI	*N*-(2,6-diisopropylphenyl)perylene-3,4-dicarbonacidimid
PRR	Pattern recognition receptor
PS	Polystyrene
RNA	Ribonucleic acid
ROS	Radical oxygen species
rSD	Relative standard deviation
RT	Room temperature
SD	Standard deviation
SDS	Sodium dodecyl sulfate
SEM	Scanning electron microscopy

SEM	Standard error of the mean
SEMA	2-sulfoethyl methacrylate
siRNA	Small interfering nucleic acid
SOCS	Suppressor of cytokine signaling
SR101	Sulforhodamie 101
SSC	Side scatter
STAT	Signal transducer and activator of transcription
TAA	Tumor-associated antigen
TC	T cell
TCR	T cell receptor
TDI	2,4-toluene diisocyanate
Teff	T effector cell
TEM	Transmission electron microscopy
Th1 / Th2	T helper type 1 or type 2 cell
TLR	Toll-like receptor
TNF-α	Tumor necrosis factor alpha
Tr1	Type 1 regulatory T cell
Treg	Regulatory T cell
V59	2,2-azobis(2-methylbutyronitrile)
VBPA	Vinyl-benzylphosphonic acid
VEGF	Vascular endothelial growth factor
µCi	Microcurie

6.3 References

1 Strebhardt, K. & Ullrich, A. Paul Ehrlich's magic bullet concept: 100 years of progress. *Nat Rev Cancer*. **2008**. 8, 473-480.

2 Hanahan, D. & Weinberg, R. A. The hallmarks of cancer. *Cell*. **2000**. 100, 57-70.

3 Hanahan, D. & Weinberg, R. A. Hallmarks of cancer: the next generation. *Cell*. **2011**. 144, 646-674.

4 Schreiber, R. D., Old, L. J. & Smyth, M. J. Cancer immunoediting: integrating immunity's roles in cancer suppression and promotion. *Science*. **2011**. 331, 1565-1570.

5 Dunn, G. P., Old, L. J. & Schreiber, R. D. The three Es of cancer immunoediting. *Annu Rev Immunol*. **2004**. 22, 329-360.

6 Fridman, W. H., Pages, F., Sautes-Fridman, C. & Galon, J. The immune contexture in human tumours: impact on clinical outcome. *Nat Rev Cancer*. **2012**. 12, 298-306.

7 Hoebe, K., Janssen, E. & Beutler, B. The interface between innate and adaptive immunity. *Nat Immunol*. **2004**. 5, 971-974.

8 Janeway, C. A., Jr. & Medzhitov, R. Innate immune recognition. *Annu Rev Immunol*. **2002**. 20, 197-216.

9 Banchereau, J. *et al.* Immunobiology of dendritic cells. *Annu Rev Immunol*. **2000**. 18, 767-811.

10 Steinman, R. M. & Hemmi, H. Dendritic cells: translating innate to adaptive immunity. *Curr Top Microbiol Immunol*. **2006**. 311, 17-58.

11 Akira, S., Takeda, K. & Kaisho, T. Toll-like receptors: critical proteins linking innate and acquired immunity. *Nat Immunol*. **2001**. 2, 675-680.

12 Gabrilovich, D. I., Ostrand-Rosenberg, S. & Bronte, V. Coordinated regulation of myeloid cells by tumours. *Nat Rev Immunol*. **2012**. 12, 253-268.

13 Takeda, K. & Akira, S. Toll-like receptors in innate immunity. *Int Immunol*. **2005**. 17, 1-14.

14 Banchereau, J. & Steinman, R. M. Dendritic cells and the control of immunity. *Nature*. **1998**. 392, 245-252.

15 Liu, Y. J. Dendritic cell subsets and lineages, and their functions in innate and adaptive immunity. *Cell*. **2001**. 106, 259-262.

16 Guermonprez, P., Valladeau, J., Zitvogel, L., Thery, C. & Amigorena, S. Antigen presentation and T cell stimulation by dendritic cells. *Annu Rev Immunol*. **2002**. 20, 621-667.

17 Joffre, O. P., Segura, E., Savina, A. & Amigorena, S. Cross-presentation by dendritic cells. *Nat Rev Immunol*. **2012**. 12, 557-569.

18 Wagner, D. H., Jr. Re-shaping the T cell repertoire: TCR editing and TCR revision for good and for bad. *Clin Immunol*. **2007**. 123, 1-6.

19 Weninger, W., Manjunath, N. & von Andrian, U. H. Migration and differentiation of CD8+ T cells. *Immunol Rev*. **2002**. 186, 221-233.

20 Barry, M. & Bleackley, R. C. Cytotoxic T lymphocytes: all roads lead to death. *Nat Rev Immunol*. **2002**. 2, 401-409.

21 Langenkamp, A., Messi, M., Lanzavecchia, A. & Sallusto, F. Kinetics of dendritic cell activation: impact on priming of TH1, TH2 and nonpolarized T cells. *Nat Immunol*. **2000**. 1, 311-316.

22 Murphy, K. M. & Reiner, S. L. The lineage decisions of helper T cells. *Nat Rev Immunol*. **2002**. 2, 933-944.

23 Sakaguchi, S., Yamaguchi, T., Nomura, T. & Ono, M. Regulatory T cells and immune tolerance. *Cell*. **2008**. 133, 775-787.

24 Weaver, C. T., Hatton, R. D., Mangan, P. R. & Harrington, L. E. IL-17 family cytokines and the expanding diversity of effector T cell lineages. *Annu Rev Immunol*. **2007**. 25, 821-852.

25 Steinman, R. M., Hawiger, D. & Nussenzweig, M. C. Tolerogenic dendritic cells. *Annu Rev Immunol*. **2003**. 21, 685-711.

26 Allan, S. E. *et al.* CD4+ T-regulatory cells: toward therapy for human diseases. *Immunol Rev*. **2008**. 223, 391-421.

27 Nemazee, D. Receptor editing in lymphocyte development and central tolerance. *Nat Rev Immunol*. **2006**. 6, 728-740.

28 Mays, L. E. & Chen, Y. H. Maintaining immunological tolerance with Foxp3. *Cell Res*. **2007**. 17, 904-918.

29 Sakaguchi, S., Miyara, M., Costantino, C. M. & Hafler, D. A. FOXP3+ regulatory T cells in the human immune system. *Nat Rev Immunol*. **2010**. 10, 490-500.

30 Tang, Q. & Bluestone, J. A. The Foxp3+ regulatory T cell: a jack of all trades, master of regulation. *Nat Immunol*. **2008**. 9, 239-244.

31 Saraiva, M. & O'Garra, A. The regulation of IL-10 production by immune cells. *Nat Rev Immunol*. **2010**. 10, 170-181.

32 Sakaguchi, S. Naturally arising Foxp3-expressing CD25+CD4+ regulatory T cells in immunological tolerance to self and non-self. *Nat Immunol*. **2005**. 6, 345-352.

33 Roncarolo, M. G. *et al.* Interleukin-10-secreting type 1 regulatory T cells in rodents and humans. *Immunol Rev*. **2006**. 212, 28-50.

34 Jonuleit, H., Schmitt, E., Schuler, G., Knop, J. & Enk, A. H. Induction of interleukin 10-producing, nonproliferating CD4(+) T cells with regulatory properties by repetitive stimulation with allogeneic immature human dendritic cells. *J Exp Med*. **2000**. 192, 1213-1222.

35 Dhodapkar, M. V., Steinman, R. M., Krasovsky, J., Munz, C. & Bhardwaj, N. Antigen-specific inhibition of effector T cell function in humans after injection of immature dendritic cells. *J Exp Med*. **2001**. 193, 233-238.

36 Chaput, N., Conforti, R., Viaud, S., Spatz, A. & Zitvogel, L. The Janus face of dendritic cells in cancer. *Oncogene*. **2008**. 27, 5920-5931.

37 Steinbrink, K., Mahnke, K., Grabbe, S., Enk, A. H. & Jonuleit, H. Myeloid dendritic cell: From sentinel of immunity to key player of peripheral tolerance? *Hum Immunol*. **2009**. 70, 289-293.

38 Steinman, R. M. & Nussenzweig, M. C. Avoiding horror autotoxicus: the importance of dendritic cells in peripheral T cell tolerance. *Proc Natl Acad Sci U S A*. **2002**. 99, 351-358.

39 Sakaguchi, S. *et al.* Foxp3+ CD25+ CD4+ natural regulatory T cells in dominant self-tolerance and autoimmune disease. *Immunol Rev*. **2006**. 212, 8-27.

40 Zou, W. Regulatory T cells, tumour immunity and immunotherapy. *Nat Rev Immunol*. **2006**. 6, 295-307.

41 Sato, T. *et al.* Interleukin 10 in the tumor microenvironment: a target for anticancer immunotherapy. *Immunol Res*. **2011**. 51, 170-182.

42 Dummer, W. *et al.* Elevated serum levels of interleukin-10 in patients with metastatic malignant melanoma. *Melanoma Res*. **1995**. 5, 67-68.

43 Moore, K. W., de Waal Malefyt, R., Coffman, R. L. & O'Garra, A. Interleukin-10 and the interleukin-10 receptor. *Annu Rev Immunol*. **2001**. 19, 683-765.

44 Dummer, W. *et al.* Interleukin-10 production in malignant melanoma: preferential detection of IL-10-secreting tumor cells in metastatic lesions. *Int J Cancer*. **1996**. 66, 607-610.

45 Kim, J. *et al.* IL-10 production in cutaneous basal and squamous cell carcinomas. A mechanism for evading the local T cell immune response. *J Immunol*. **1995**. 155, 2240-2247.

46 Chaudhry, A. *et al.* Interleukin-10 signaling in regulatory T cells is required for suppression of Th17 cell-mediated inflammation. *Immunity*. **2011**. 34, 566-578.

47 Wong, S. C. *et al.* Macrophage polarization to a unique phenotype driven by B cells. *Eur J Immunol*. **2010**. 40, 2296-2307.

48 Steinbrink, K., Wolfl, M., Jonuleit, H., Knop, J. & Enk, A. H. Induction of tolerance by IL-10-treated dendritic cells. *J Immunol*. **1997**. 159, 4772-4780.

49 Steinbrink, K. *et al.* Interleukin-10-treated human dendritic cells induce a melanoma-antigen-specific anergy in CD8(+) T cells resulting in a failure to lyse tumor cells. *Blood*. **1999**. 93, 1634-1642.

50 Adler, H. S. & Steinbrink, K. MAP kinase p38 and its relation to T cell anergy and suppressor function of regulatory T cells. *Cell Cycle*. **2008**. 7, 169-170.

51 Driesen, J., Popov, A. & Schultze, J. L. CD25 as an immune regulatory molecule expressed on myeloid dendritic cells. *Immunobiology*. **2008**. 213, 849-858.

52 Ostrand-Rosenberg, S. & Sinha, P. Myeloid-derived suppressor cells: linking inflammation and cancer. *J Immunol*. **2009**. 182, 4499-4506.

53 Gabrilovich, D. I. & Nagaraj, S. Myeloid-derived suppressor cells as regulators of the immune system. *Nat Rev Immunol*. **2009**. 9, 162-174.

54 Fujimura, T., Mahnke, K. & Enk, A. H. Myeloid derived suppressor cells and their role in tolerance induction in cancer. *J Dermatol Sci*. **2010**. 59, 1-6.

55 Rech, A. J. *et al.* CD25 blockade depletes and selectively reprograms regulatory T cells in concert with immunotherapy in cancer patients. *Sci Transl Med*. **2012**. 4, 134ra162.

56 Klages, K. *et al.* Selective depletion of Foxp3+ regulatory T cells improves effective therapeutic vaccination against established melanoma. *Cancer Res*. **2010**. 70, 7788-7799.

57 Bacha, P. *et al.* Interleukin 2 receptor-targeted cytotoxicity. Interleukin 2 receptor-mediated action of a diphtheria toxin-related interleukin 2 fusion protein. *J Exp Med*. **1988**. 167, 612-622.

58 Mahnke, K. *et al.* Depletion of CD4+CD25+ human regulatory T cells in vivo: kinetics of Treg depletion and alterations in immune functions in vivo and in vitro. *Int J Cancer*. **2007**. 120, 2723-2733.

59 Rasku, M. A. *et al.* Transient T cell depletion causes regression of melanoma metastases. *J Transl Med*. **2008**. 6, 12.

60 Telang, S. *et al.* Phase II trial of the regulatory T cell-depleting agent, denileukin diftitox, in patients with unresectable stage IV melanoma. *BMC Cancer*. **2011**. 11, 515.

61 Malek, T. R. & Castro, I. Interleukin-2 receptor signaling: at the interface between tolerance and immunity. *Immunity*. **2010**. 33, 153-165.

62 Malek, T. R. The biology of interleukin-2. *Annu Rev Immunol*. **2008**. 26, 453-479.

63 Boyman, O. & Sprent, J. The role of interleukin-2 during homeostasis and activation of the immune system. *Nat Rev Immunol*. **2012**. 12, 180-190.

64 Liao, W., Lin, J. X. & Leonard, W. J. Interleukin-2 at the crossroads of effector responses, tolerance, and immunotherapy. *Immunity*. **2013**. 38, 13-25.

65 Fujii, M. *et al.* High-affinity receptor-mediated internalization and degradation of interleukin 2 in human T cells. *J Exp Med*. **1986**. 163, 550-562.

66 Duprez, V., Ferrer, M. & Dautry-Varsat, A. High-affinity interleukin 2 receptor alpha and beta chains are internalized and remain associated inside the cells after interleukin 2 endocytosis. *J Biol Chem*. **1992**. 267, 18639-18643.

67 Nakarai, T. *et al.* Interleukin 2 receptor gamma chain expression on resting and activated lymphoid cells. *J Exp Med*. **1994**. 180, 241-251.

68 Suzuki, H. *et al.* Deregulated T cell activation and autoimmunity in mice lacking interleukin-2 receptor beta. *Science*. **1995**. 268, 1472-1476.

69 Nelson, B. H., Lord, J. D. & Greenberg, P. D. Cytoplasmic domains of the interleukin-2 receptor beta and gamma chains mediate the signal for T-cell proliferation. *Nature*. **1994**. 369, 333-336.

70 Sadlack, B. *et al.* Ulcerative colitis-like disease in mice with a disrupted interleukin-2 gene. *Cell*. **1993**. 75, 253-261.

71 Willerford, D. M. *et al.* Interleukin-2 receptor alpha chain regulates the size and content of the peripheral lymphoid compartment. *Immunity*. **1995**. 3, 521-530.

72 Cheng, G., Yu, A., Dee, M. J. & Malek, T. R. IL-2R signaling is essential for functional maturation of regulatory T cells during thymic development. *J Immunol*. **2013**. 190, 1567-1575.

73 Liao, W., Lin, J. X. & Leonard, W. J. IL-2 family cytokines: new insights into the complex roles of IL-2 as a broad regulator of T helper cell differentiation. *Curr Opin Immunol*. **2011**. 23, 598-604.

74 Yu, A., Zhu, L., Altman, N. H. & Malek, T. R. A low interleukin-2 receptor signaling threshold supports the development and homeostasis of T regulatory cells. *Immunity*. **2009**. 30, 204-217.

75 Okita, R. *et al.* Targeting of CD4+CD25high cells while preserving CD4+CD25low cells with low-dose chimeric anti-CD25 antibody in adoptive immunotherapy of cancer. *Int J Oncol*. **2009**. 34, 563-572.

76 Boyman, O., Kovar, M., Rubinstein, M. P., Surh, C. D. & Sprent, J. Selective stimulation of T cell subsets with antibody-cytokine immune complexes. *Science*. **2006**. 311, 1924-1927.

77 Webster, K. E. *et al.* In vivo expansion of T reg cells with IL-2-mAb complexes: induction of resistance to EAE and long-term acceptance of islet allografts without immunosuppression. *J Exp Med*. **2009**. 206, 751-760.

78 Klapper, J. A. *et al.* High-dose interleukin-2 for the treatment of metastatic renal cell carcinoma : a retrospective analysis of response and survival in patients treated in the surgery branch at the National Cancer Institute between 1986 and 2006. *Cancer*. **2008**. 113, 293-301.

79 Grinberg-Bleyer, Y. *et al.* IL-2 reverses established type 1 diabetes in NOD mice by a local effect on pancreatic regulatory T cells. *J Exp Med*. **2010**. 207, 1871-1878.

80 Koreth, J. *et al.* Interleukin-2 and regulatory T cells in graft-versus-host disease. *N Engl J Med*. **2011**. 365, 2055-2066.

81 Rosenberg, S. A. & Lotze, M. T. Cancer immunotherapy using interleukin-2 and interleukin-2-activated lymphocytes. *Annu Rev Immunol*. **1986**. 4, 681-709.

82 Bluestone, J. A. The yin and yang of interleukin-2-mediated immunotherapy. *N Engl J Med*. **2011**. 365, 2129-2131.

83 Danese, S. & Mantovani, A. Inflammatory bowel disease and intestinal cancer: a paradigm of the Yin-Yang interplay between inflammation and cancer. *Oncogene*. **2010**. 29, 3313-3323.

84 Blankenstein, T., Coulie, P. G., Gilboa, E. & Jaffee, E. M. The determinants of tumour immunogenicity. *Nat Rev Cancer*. **2012**. 12, 307-313.

85 Pardoll, D. M. The blockade of immune checkpoints in cancer immunotherapy. *Nat Rev Cancer*. **2012**. 12, 252-264.

86 Kwek, S. S., Cha, E. & Fong, L. Unmasking the immune recognition of prostate cancer with CTLA4 blockade. *Nat Rev Cancer*. **2012**. 12, 289-297.

87 Scott, A. M., Wolchok, J. D. & Old, L. J. Antibody therapy of cancer. *Nat Rev Cancer*. **2012**. 12, 278-287.

88 Sorensen, M. R. & Thomsen, A. R. Virus-based immunotherapy of cancer: what do we know and where are we going? *APMIS*. **2007**. 115, 1177-1193.

89 Restifo, N. P., Dudley, M. E. & Rosenberg, S. A. Adoptive immunotherapy for cancer: harnessing the T cell response. *Nat Rev Immunol*. **2012**. 12, 269-281.

90 Steinman, R. M. & Banchereau, J. Taking dendritic cells into medicine. *Nature*. **2007**. 449, 419-426.

91 Schuler, G., Schuler-Thurner, B. & Steinman, R. M. The use of dendritic cells in cancer immunotherapy. *Curr Opin Immunol*. **2003**. 15, 138-147.

92 Palucka, K. & Banchereau, J. Cancer immunotherapy via dendritic cells. *Nat Rev Cancer*. **2012**. 12, 265-277.

93 Kantoff, P. W. *et al.* Sipuleucel-T immunotherapy for castration-resistant prostate cancer. *N Engl J Med*. **2010**. 363, 411-422.

94 Bertrand, N., Wu, J., Xu, X., Kamaly, N. & Farokhzad, O. C. Cancer nanotechnology: The impact of passive and active targeting in the era of modern cancer biology. *Adv Drug Deliv Rev*. **2014**. 66C, 2-25.

95 Moon, J. J., Huang, B. & Irvine, D. J. Engineering nano- and microparticles to tune immunity. *Adv Mater*. **2012**. 24, 3724-3746.

96 Paulo, C. S., Pires das Neves, R. & Ferreira, L. S. Nanoparticles for intracellular-targeted drug delivery. *Nanotechnology*. **2011**. 22, 494002.

97 Baier, G. *et al.* BSA adsorption on differently charged polystyrene nanoparticles using isothermal titration calorimetry and the influence on cellular uptake. *Macromol Biosci*. **2011**. 11, 628-638.

98 Tenzer, S. *et al.* Rapid formation of plasma protein corona critically affects nanoparticle pathophysiology. *Nat Nanotechnol*. **2013**. 8, 772-781.

99 Veronese, F. M. & Mero, A. The impact of PEGylation on biological therapies. *BioDrugs*. **2008**. 22, 315-329.

100 Petros, R. A. & DeSimone, J. M. Strategies in the design of nanoparticles for therapeutic applications. *Nat Rev Drug Discov*. **2010**. 9, 615-627.

101 Abuchowski, A., van Es, T., Palczuk, N. C. & Davis, F. F. Alteration of immunological properties of bovine serum albumin by covalent attachment of polyethylene glycol. *J Biol Chem*. **1977**. 252, 3578-3581.

102 Besheer, A. *et al.* Characterization of PLGA nanospheres stabilized with amphiphilic polymers: hydrophobically modified hydroxyethyl starch vs pluronics. *Mol Pharm*. **2009**. 6, 407-415.

103 Baier, G., Musyanovych, A., Dass, M., Theisinger, S. & Landfester, K. Cross-linked starch capsules containing dsDNA prepared in inverse miniemulsion as "nanoreactors" for polymerase chain reaction. *Biomacromolecules*. **2010**. 11, 960-968.

104 Baier, G. *et al.* Suppressing unspecific cell uptake for targeted delivery using hydroxyethyl starch nanocapsules. *Biomacromolecules*. **2012**. 13, 2704-2715.

105 Maeda, H., Greish, K. & Fang, J. The EPR effect and polymeric drugs: A paradigm shift for cancer chemotherapy in the 21st century. *Polymer Therapeutics Ii: Polymers as Drugs, Conjugates and Gene Delivery Systems*. **2006**. 193, 103-121.

106 Park, J. *et al.* Combination delivery of TGF-beta inhibitor and IL-2 by nanoscale liposomal polymeric gels enhances tumour immunotherapy. *Nat Mater*. **2012**. 11, 895-905.

107 Allen, T. M. Ligand-targeted therapeutics in anticancer therapy. *Nat Rev Cancer*. **2002**. 2, 750-763.

108 Stephan, M. T., Moon, J. J., Um, S. H., Bershteyn, A. & Irvine, D. J. Therapeutic cell engineering with surface-conjugated synthetic nanoparticles. *Nat Med*. **2010**. 16, 1035-1041.

109 Swiggard, W. J., Mirza, A., Nussenzweig, M. C. & Steinman, R. M. DEC-205, a 205-kDa protein abundant on mouse dendritic cells and thymic epithelium that is detected by the monoclonal antibody NLDC-145: purification, characterization, and N-terminal amino acid sequence. *Cell Immunol*. **1995**. 165, 302-311.

110 Jiang, W. *et al.* The receptor DEC-205 expressed by dendritic cells and thymic epithelial cells is involved in antigen processing. *Nature*. **1995**. 375, 151-155.

111 Witmer-Pack, M. D., Swiggard, W. J., Mirza, A., Inaba, K. & Steinman, R. M. Tissue distribution of the DEC-205 protein that is detected by the monoclonal antibody NLDC-145. II. Expression in situ in lymphoid and nonlymphoid tissues. *Cell Immunol*. **1995**. 163, 157-162.

112 Kim, J. & Mooney, D. J. In Vivo Modulation of Dendritic Cells by Engineered Materials: Towards New Cancer Vaccines. *Nano Today*. **2011**. 6, 466-477.

113 Reddy, S. T., Swartz, M. A. & Hubbell, J. A. Targeting dendritic cells with biomaterials: developing the next generation of vaccines. *Trends Immunol*. **2006**. 27, 573-579.

114 Hamdy, S., Haddadi, A., Ghotbi, Z., Hung, R. W. & Lavasanifar, A. Part I: targeted particles for cancer immunotherapy. *Curr Drug Deliv*. **2011**. 8, 261-273.

115 Kwon, Y. J., James, E., Shastri, N. & Frechet, J. M. In vivo targeting of dendritic cells for activation of cellular immunity using vaccine carriers based on pH-responsive microparticles. *Proc Natl Acad Sci U S A*. **2005**. 102, 18264-18268.

116 Kwon, Y. J., Standley, S. M., Goodwin, A. P., Gillies, E. R. & Frechet, J. M. Directed antigen presentation using polymeric microparticulate carriers degradable at lysosomal pH for controlled immune responses. *Mol Pharm*. **2005**. 2, 83-91.

117 Miyata, K., Nishiyama, N. & Kataoka, K. Rational design of smart supramolecular assemblies for gene delivery: chemical challenges in the creation of artificial viruses. *Chem Soc Rev*. **2012**. 41, 2562-2574.

118 Davis, M. E. *et al.* Evidence of RNAi in humans from systemically administered siRNA via targeted nanoparticles. *Nature*. **2010**. 464, 1067-1070.

119 Dean, M., Fojo, T. & Bates, S. Tumour stem cells and drug resistance. *Nat Rev Cancer*. **2005**. 5, 275-284.

120 Foged, C., Brodin, B., Frokjaer, S. & Sundblad, A. Particle size and surface charge affect particle uptake by human dendritic cells in an in vitro model. *Int J Pharm*. **2005**. 298, 315-322.

121 Akagi, T., Baba, M. & Akashi, M. Biodegradable Nanoparticles as Vaccine Adjuvants and Delivery Systems: Regulation of Immune Responses by Nanoparticle-Based Vaccine. *Polymers in Nanomedicine*. **2012**. 247, 31-64.

122 Saadoun, D. *et al.* Regulatory T-cell responses to low-dose interleukin-2 in HCV-induced vasculitis. *N Engl J Med*. **2011**. 365, 2067-2077.

123 Frick, S. U. *et al.* Functionalized polystyrene nanoparticles trigger human dendritic cell maturation resulting in enhanced CD4+ T cell activation. *Macromol Biosci*. **2012**. 12, 1637-1647. Copyright Wiley-VCH Verlag GmbH & Co. KGaA. Reproduced with Permission.

124 Baecher-Allan, C., Brown, J. A., Freeman, G. J. & Hafler, D. A. CD4+CD25high regulatory cells in human peripheral blood. *J Immunol*. **2001**. 167, 1245-1253.

125 http://www.lifetechnologies.com/north-america/en/home/life-science/cell-analysis/flow-cytometry/cell-health-and-viability-assays-for-flow-cytometry/cell-proliferation-assays-for-flow-cytometry/celltrace-reagents-for-cell-proliferation.html.

126 http://www.flowjo.com/v9/html/proliferation.html.

127 Venkataraman, S. *et al.* The effects of polymeric nanostructure shape on drug delivery. *Adv Drug Deliv Rev*. **2011**. 63, 1228-1246.

128 Seong, S. Y. & Matzinger, P. Hydrophobicity: an ancient damage-associated molecular pattern that initiates innate immune responses. *Nat Rev Immunol*. **2004**. 4, 469-478.

129 Cabral, H. *et al.* Accumulation of sub-100 nm polymeric micelles in poorly permeable tumours depends on size. *Nat Nanotechnol*. **2011**. 6, 815-823.

130 Rejman, J., Oberle, V., Zuhorn, I. S. & Hoekstra, D. Size-dependent internalization of particles via the pathways of clathrin- and caveolae-mediated endocytosis. *Biochem J*. **2004**. 377, 159-169.

131 Johnston, H. J. *et al.* Evaluating the uptake and intracellular fate of polystyrene nanoparticles by primary and hepatocyte cell lines in vitro. *Toxicol Appl Pharmacol*. **2010**. 242, 66-78.

132 Bartneck, M. *et al.* Effects of nanoparticle surface-coupled peptides, functional endgroups, and charge on intracellular distribution and functionality of human primary reticuloendothelial cells. *Nanomedicine*. **2012**. 8, 1282-1292.

133 Liu, Y. *et al.* Intracellular dynamics of cationic and anionic polystyrene nanoparticles without direct interaction with mitotic spindle and chromosomes. *Biomaterials*. **2011**. 32, 8291-8303.

134 Chen, J. *et al.* Cationic nanoparticles induce nanoscale disruption in living cell plasma membranes. *J Phys Chem B*. **2009**. 113, 11179-11185.

135 Yoshida, M. & Babensee, J. E. Poly(lactic-co-glycolic acid) enhances maturation of human monocyte-derived dendritic cells. *J Biomed Mater Res A*. **2004**. 71, 45-54.

136 Yang, D. *et al.* [Gd@C(82)(OH)(22)](n) nanoparticles induce dendritic cell maturation and activate Th1 immune responses. *ACS Nano*. **2010**. 4, 1178-1186.

137 Paulis, L. E., Mandal, S., Kreutz, M. & Figdor, C. G. Dendritic cell-based nanovaccines for cancer immunotherapy. *Curr Opin Immunol*. **2013**. 25, 389-395.

138 Yao, S. *et al.* B7-h2 is a costimulatory ligand for CD28 in human. *Immunity*. **2011**. 34, 729-740.

139 Hutloff, A. *et al.* ICOS is an inducible T-cell co-stimulator structurally and functionally related to CD28. *Nature*. **1999**. 397, 263-266.

140 Blanco, P., Palucka, A. K., Pascual, V. & Banchereau, J. Dendritic cells and cytokines in human inflammatory and autoimmune diseases. *Cytokine Growth Factor Rev*. **2008**. 19, 41-52.

141 Jonuleit, H. *et al.* Pro-inflammatory cytokines and prostaglandins induce maturation of potent immunostimulatory dendritic cells under fetal calf serum-free conditions. *Eur J Immunol*. **1997**. 27, 3135-3142.

142 Hsieh, C. S. *et al.* Development of TH1 CD4+ T cells through IL-12 produced by Listeria-induced macrophages. *Science*. **1993**. 260, 547-549.

143 Trinchieri, G. Interleukin-12 and the regulation of innate resistance and adaptive immunity. *Nat Rev Immunol*. **2003**. 3, 133-146.

144 Broos, S. *et al.* Immunomodulatory nanoparticles as adjuvants and allergen-delivery system to human dendritic cells: Implications for specific immunotherapy. *Vaccine*. **2010**. 28, 5075-5085.

145 Conway, M. A., Madrigal-Estebas, L., McClean, S., Brayden, D. J. & Mills, K. H. Protection against Bordetella pertussis infection following parenteral or oral immunization with antigens entrapped in biodegradable particles: effect of formulation and route of immunization on induction of Th1 and Th2 cells. *Vaccine*. **2001**. 19, 1940-1950.

146 Cui, Z. & Mumper, R. J. Coating of cationized protein on engineered nanoparticles results in enhanced immune responses. *Int J Pharm*. **2002**. 238, 229-239.

147 Fujii, S. *et al.* Dendritic cell-based cancer immunotherapies. *Arch Immunol Ther Exp (Warsz)*. **2009**. 57, 189-198.

148 Heo, M. B., Cho, M. Y. & Lim, Y. T. Polymer nanoparticles for enhanced immune response: Combined delivery of tumor antigen and small interference RNA for immunosuppressive gene to dendritic cells. *Acta Biomater*. **2014**. 10, 2169-2176.

149 Rosalia, R. A. *et al.* Efficient ex vivo induction of T cells with potent anti-tumor activity by protein antigen encapsulated in nanoparticles. *Cancer Immunol Immunother*. **2013**. 62, 1161-1173.

150 Sokolova, V. *et al.* The use of calcium phosphate nanoparticles encapsulating Toll-like receptor ligands and the antigen hemagglutinin to induce dendritic cell maturation and T cell activation. *Biomaterials*. **2010**. 31, 5627-5633.

151 Caserta, S., Alessi, P., Guarnerio, J., Basso, V. & Mondino, A. Synthetic CD4+ T cell-targeted antigen-presenting cells elicit protective antitumor responses. *Cancer Res*. **2008**. 68, 3010-3018.

152 Macintyre, E. *et al.* The haemostatic effects of hydroxyethyl starch (HES) used as a volume expander. *Intensive Care Med*. **1985**. 11, 300-303.

153 Weissman, A. M. *et al.* Only high-affinity receptors for interleukin 2 mediate internalization of ligand. *Proc Natl Acad Sci U S A*. **1986**. 83, 1463-1466.

154 Letelier, M. E. *et al.* Possible mechanisms underlying copper-induced damage in biological membranes leading to cellular toxicity. *Chem Biol Interact*. **2005**. 151, 71-82.

155 Yu, S. S. *et al.* Macrophage-specific RNA interference targeting via "click", mannosylated polymeric micelles. *Mol Pharm*. **2013**. 10, 975-987.

156 Wang, C. F. *et al.* Copper-free azide-alkyne cycloaddition of targeting peptides to porous silicon nanoparticles for intracellular drug uptake. *Biomaterials*. **2014**. 35, 1257-1266.

157 Siebert, J. M., Baier, G., Musyanovych, A. & Landfester, K. Towards copper-free nanocapsules obtained by orthogonal interfacial "click" polymerization in miniemulsion. *Chem Commun (Camb)*. **2012**. 48, 5470-5472.

158 Hapuarachchige, S., Zhu, W., Kato, Y. & Artemov, D. Bioorthogonal, two-component delivery systems based on antibody and drug-loaded nanocarriers for enhanced internalization of nanotherapeutics. *Biomaterials*. **2014**. 35, 2346-2354.

159 Tsuji, T., Nakagawa, R., Sugimoto, N. & Fukuhara, K. Characterization of disulfide bonds in recombinant proteins: reduced human interleukin 2 in inclusion bodies and its oxidative refolding. *Biochemistry*. **1987**. 26, 3129-3134.

160 Kmieciak, M. *et al.* Human T cells express CD25 and Foxp3 upon activation and exhibit effector/memory phenotypes without any regulatory/suppressor function. *J Transl Med*. **2009**. 7, 89.

161 Taniguchi, T. & Minami, Y. The IL-2/IL-2 receptor system: a current overview. *Cell*. **1993**. 73, 5-8.

162 Lowenthal, J. W., MacDonald, H. R. & Iacopetta, B. J. Intracellular pathway of interleukin 2 following receptor-mediated endocytosis. *Eur J Immunol*. **1986**. 16, 1461-1463.

163 Kim, J. A., Aberg, C., Salvati, A. & Dawson, K. A. Role of cell cycle on the cellular uptake and dilution of nanoparticles in a cell population. *Nat Nanotechnol*. **2012**. 7, 62-68.

164 Duprez, V., Ferrer, M., Cornet, V., Olive, D. & Dautry-Varsat, A. Modulation of interleukin 2 internalization and interleukin 2-dependent cell growth by antireceptor antibodies. *J Biol Chem*. **1991**. 266, 1497-1501.

165 Lee, R. J. & Low, P. S. Delivery of liposomes into cultured KB cells via folate receptor-mediated endocytosis. *J Biol Chem*. **1994**. 269, 3198-3204.

166 Zhang, L. *et al.* Uptake of folate-conjugated albumin nanoparticles to the SKOV3 cells. *Int J Pharm*. **2004**. 287, 155-162.

167 Hed, J., Hallden, G., Johansson, S. G. & Larsson, P. The use of fluorescence quenching in flow cytofluorometry to measure the attachment and ingestion phases in phagocytosis in peripheral blood without prior cell separation. *J Immunol Methods*. **1987**. 101, 119-125.

168 Simons, E. R. Measurement of phagocytosis and of the phagosomal environment in polymorphonuclear phagocytes by flow cytometry. *Curr Protoc Cytom*. **2010**. Chapter 9, Unit9 31.

169 Bareford, L. M. & Swaan, P. W. Endocytic mechanisms for targeted drug delivery. *Adv Drug Deliv Rev*. **2007**. 59, 748-758.

170 Conner, S. D. & Schmid, S. L. Regulated portals of entry into the cell. *Nature*. **2003**. 422, 37-44.

171 Lamaze, C. *et al.* Interleukin 2 receptors and detergent-resistant membrane domains define a clathrin-independent endocytic pathway. *Mol Cell*. **2001**. 7, 661-671.

172 Evans, B. C. *et al.* Ex vivo red blood cell hemolysis assay for the evaluation of pH-responsive endosomolytic agents for cytosolic delivery of biomacromolecular drugs. *J Vis Exp*. **2013**, e50166.

173 Rejman, J., Bragonzi, A. & Conese, M. Role of clathrin- and caveolae-mediated endocytosis in gene transfer mediated by lipo- and polyplexes. *Mol Ther*. **2005**. 12, 468-474.

174 Hartemann, A. *et al.* Low-dose interleukin 2 in patients with type 1 diabetes: a phase 1/2 randomised, double-blind, placebo-controlled trial. *Lancet Diabetes Endocrinol*. **2013**. 1, 295-305.

175 Bandyopadhyay, A., Fine, R. L., Demento, S., Bockenstedt, L. K. & Fahmy, T. M. The impact of nanoparticle ligand density on dendritic-cell targeted vaccines. *Biomaterials*. **2011**. 32, 3094-3105.

176 Ogawara, K. *et al.* Hepatic uptake of polystyrene microspheres in rats: effect of particle size on intrahepatic distribution. *J Control Release*. **1999**. 59, 15-22.

177 Allen, T. M., Hansen, C., Martin, F., Redemann, C. & Yau-Young, A. Liposomes containing synthetic lipid derivatives of poly(ethylene glycol) show prolonged circulation half-lives in vivo. *Biochim Biophys Acta*. **1991**. 1066, 29-36.

178 Steenblock, E. R. & Fahmy, T. M. A comprehensive platform for ex vivo T-cell expansion based on biodegradable polymeric artificial antigen-presenting cells. *Mol Ther*. **2008**. 16, 765-772.

179 Yao, H. *et al.* Effective melanoma immunotherapy with interleukin-2 delivered by a novel polymeric nanoparticle. *Mol Cancer Ther*. **2011**. 10, 1082-1092.

180 Dinauer, N. *et al.* Selective targeting of antibody-conjugated nanoparticles to leukemic cells and primary T-lymphocytes. *Biomaterials*. **2005**. 26, 5898-5906.

181 Zheng, Y. *et al.* In vivo targeting of adoptively transferred T-cells with antibody- and cytokine-conjugated liposomes. *J Control Release*. **2013**. 172, 426-435.

182 Cavazzana-Calvo, M. *et al.* Attenuation of graft-versus-host disease and graft rejection by ex vivo immunotoxin elimination of alloreactive T cells in an H-2 haplotype disparate mouse combination. *Blood*. **1994**. 83, 288-298.

183 Fichter, M. *et al.* Nanocapsules generated out of a polymeric dexamethasone shell suppress the inflammatory response of liver macrophages. *Nanomedicine*. **2013**. 9, 1223-1234.

184 Kim, I. H. *et al.* FRET imaging of cells transfected with siRNA/liposome complexes. *Methods Mol Biol*. **2010**. 606, 439-455.

185 Hirsch, M., Strand, D. & Helm, M. Dye selection for live cell imaging of intact siRNA. *Biol Chem*. **2012**. 393, 23-35.

186 Becker, J. C. *et al.* Mouse models for melanoma: a personal perspective. *Exp Dermatol*. **2010**. 19, 157-164.

187 Dankort, D. *et al.* Braf(V600E) cooperates with Pten loss to induce metastatic melanoma. *Nat Genet*. **2009**. 41, 544-552.

188 Yu, H., Kortylewski, M. & Pardoll, D. Crosstalk between cancer and immune cells: role of STAT3 in the tumour microenvironment. *Nat Rev Immunol*. **2007**. 7, 41-51.

189 Liu, G. *et al.* Small interference RNA modulation of IL-10 in human monocyte-derived dendritic cells enhances the Th1 response. *Eur J Immunol*. **2004**. 34, 1680-1687.

190 Chhabra, A., Chakraborty, N. G. & Mukherji, B. Silencing of endogenous IL-10 in human dendritic cells leads to the generation of an improved CTL response against human melanoma associated antigenic epitope, MART-1 27-35. *Clin Immunol*. **2008**. 126, 251-259.

191 Jin, S. E., Jin, H. E. & Hong, S. S. Targeted delivery system of nanobiomaterials in anticancer therapy: from cells to clinics. *Biomed Res Int*. **2014**. 2014, 814208.

192 Davis, M. E., Chen, Z. G. & Shin, D. M. Nanoparticle therapeutics: an emerging treatment modality for cancer. *Nat Rev Drug Discov*. **2008**. 7, 771-782.

193 Landfester, K. Polyreactions in miniemulsions. *Macromolecular Rapid Communications*. **2001**. 22, 896-936.

194 Landfester, K. Synthesis of colloidal particles in miniemulsions. *Annual Review of Materials Research*. **2006**. 36, 231-279.

195 Landfester, K. & Musyanovych, A. Hydrogels in Miniemulsions. *Chemical Design of Responsive Microgels*. **2010**. 234, 39-63.

196 Ziegler, A., Landfester, K. & Musyanovych, A. Synthesis of phosphonate-functionalized polystyrene and poly(methyl methacrylate) particles and their kinetic behavior in miniemulsion polymerization. *Colloid Polym Sci*. **2009**. 287, 1261-1271.

197 Zeller, A. *et al.* Nanostructured coatings by adhesion of phosphonated polystyrene particles onto titanium surface for implant material applications. *ACS Appl Mater Interfaces*. **2010**. 2, 2421-2428.

198 Landfester, K. Miniemulsion polymerization and the structure of polymer and hybrid nanoparticles. *Angew Chem Int Ed Engl*. **2009**. 48, 4488-4507.

199 Powers, K. W. *et al.* Research strategies for safety evaluation of nanomaterials. Part VI. Characterization of nanoscale particles for toxicological evaluation. *Toxicol Sci*. **2006**. 90, 296-303.

200 Society, T. R. Nanoscience and nanotechnologies: opportunities and uncertainties. Report No. ISBN 0 85403 604 0, (London, 2004).

201 Yuan, F. *et al.* Vascular permeability in a human tumor xenograft: molecular size dependence and cutoff size. *Cancer Res*. **1995**. 55, 3752-3756.

202 Alexis, F., Pridgen, E., Molnar, L. K. & Farokhzad, O. C. Factors affecting the clearance and biodistribution of polymeric nanoparticles. *Mol Pharm*. **2008**. 5, 505-515.

203 Jung, T. *et al.* Biodegradable nanoparticles for oral delivery of peptides: is there a role for polymers to affect mucosal uptake? *Eur J Pharm Biopharm*. **2000**. 50, 147-160.

204 Xiang, S. D. *et al.* Pathogen recognition and development of particulate vaccines: does size matter? *Methods*. **2006**. 40, 1-9.

205 Berne, B. J., Pecora, R. *Dynamic Light Scattering - With Applications to Chemistry, Biology, and Physics*. (Dover Publications, 1976, 2000).

206 Clogston, J. D. & Patri, A. K. Zeta potential measurement. *Methods Mol Biol*. **2011**. 697, 63-70.

207 Klang, V., Valenta, C. & Matsko, N. B. Electron microscopy of pharmaceutical systems. *Micron*. **2013**. 44, 45-74.

208 Egerton, R. F. *Physical Principles of Electron Microscopy - An Introduction to TEM, SEM, and AEM*. (Springer, 2005).

209 Iwasaki, A. & Medzhitov, R. Toll-like receptor control of the adaptive immune responses. *Nat Immunol*. **2004**. 5, 987-995.

210 Steinman, R. M. & Witmer, M. D. Lymphoid dendritic cells are potent stimulators of the primary mixed leukocyte reaction in mice. *Proc Natl Acad Sci U S A*. **1978**. 75, 5132-5136.

211 Engvall, E. & Perlmann, P. Enzyme-linked immunosorbent assay (ELISA). Quantitative assay of immunoglobulin G. *Immunochemistry*. **1971**. 8, 871-874.

212 Brown, M. & Wittwer, C. Flow cytometry: principles and clinical applications in hematology. *Clin Chem*. **2000**. 46, 1221-1229.

213 Conchello, J. A. & Lichtman, J. W. Optical sectioning microscopy. *Nat Methods*. **2005**. 2, 920-931.